博士論文

Development of ultra-high strength zero-cement mortar

（超高強度ゼロセメントモルタルの開発）

廖 高宇

Contents

1. Introduction

1.1 Research background

Concrete is the most consumed material next to water in the world. In the production of Portland cement, which is the main component of concrete, there are some negative environmental impacts such as increased CO_2 emissions, large consumption of raw materials and energy, and emission of harmful environmental pollutants. In general, firing 1 ton cement clinker will generate 1 ton CO_2. So far, mixing Portland cement with waste by-products such as ground granulated blast-furnace slag and fly ash has greatly contributed to CO_2 reduction. However, further reductions in CO_2 emissions are required under the Paris Agreement, which came into effect in November 2016[(1)].

In recent years, a high alkali activated zero-cement materials—Geopolymer, which uses industrial by-products that can significantly reduce CO_2 emissions during manufacturing compared to Portland cement, is attracting attention from around the world as a CO_2 reduction measure. it has good early compressive strength, good chemical resistance, low permeability and excellent fire resistance behavior [(2)]. Some researchers [(3-4)] reported that its CO_2 emissions can be reduced by as high as 80%. The term "Geopolymer" was first defined by Davidovits in the 1970s as the products of alkali activation of calcined clays (especially metakaolin) [(5)]. However, the question "Can the Ca-rich system (eg. alkali-stimulated blast furnace slag fine powder) be used as a Geopolymer?" is discussed [(6)]. According to Japan Concrete Engineering Association, Geopolymer defined as "Raw materials based on amorphous aluminum silicate and hardened with at least one of aqueous solutions of alkali metal silicates, carbonates and hydroxides without using cement clinker [(7)] ".

In addition, there is also a special alkali activated material that uses CaO or $Ca(OH)_2$ as a low

alkali activator. It has a different reaction mechanism from Geopolymer and is also a promising candidate as an alternative to ordinary Portland cement.

At present, there is no uniform definition of such alkali-activated materials in various countries and organizations. ‘‘alkali-activated cements’’, ‘‘inorganic polymers’’, ‘‘geocements’’, ‘‘hydroceramics’’, ‘‘alkali-bonded ceramics’’ etc. are commonly used. These terms all describe materials synthesized utilizing the same chemistry.

In order to facilitate understanding and research, this thesis proposes the definition of zero-cement. The definition of zero-cement is that: "Does not use cement clinker, has the same performance as cement and is hardened using a raw material based on waste by-product and a small amount of alkali activator".

For easier understanding and differentiation, the alkali activated materials are divided into two categories: one type uses NaOH and Na_2SiO_3 with high alkalinity as alkali activator, which is called high alkali activated zero-cement, and another type uses CaO with low alkalinity as alkali activator, which is called low alkali activated zero-cement.

1.2 Research purpose

To develop ultra-high-strength zero-cement concrete, mortar should be the first step. It is important to strengthen the zero-cement matrix. Therefore, it was done with mortar, not concrete.

The purpose of this study is to conduct research on the following items:

(1) Development of ultra-high strength zero-cement mortar more than 100MPa.

(2) Elucidation of the influencing factors and mechanism of zero-cement mortar: to clarify the factors affecting the compressive strength of zero-cement mortar, study the reaction products and pore structure, and elucidate the mechanism of strength development of alkali activated

zero-cement mortar.

(3) Proposal of design method for ultra-high strength zero-cement mortar: a technology that enables the production of the ultra-high strength zero-cement mortar using different source materials is important. Proposing a design method for ultra-high strength zero-cement mortar by evaluating active constituent in raw materials such as fly ash, blast furnace slag, shirasu and metakaolin.

1.3 Research innovation

(1) Developed a low-alkali activated zero-cement mortar above 130MPa.

At 90℃ heat curing, as the amount of low-alkali activator increases, the compressive strength increases first and then decreases. When the amount of low-alkali activator is 80kg/m^3, the maximum compressive strength in 7 days reaching up to 136 MPa.

(2) Clarified the factors affecting the compressive strength of zero-cement mortar.

(3) First proposed the evaluation method of compressive strength for zero-cement mortar: “strength index”.

The strength and strength index have a high correlation, so it is effective to use the strength index to evaluate the compressive strength of the zero-cement mortar.

(4) Proposed a strength prediction model of zero-cement mortar.

Proposed zero-cement model can accurately expresses the strength development of zero-cement mortar. This equation is capable of explaining the strength change due to the change in the proportion of RCaO, RAl_2O_3 and $RSiO_2$ content, the relationship between the glass content/water ratio and strength in zero-cement mortar.

(5) Proposed a design method for ultra-high strength zero-cement mortar according to C/(A+S) molar ratio of zero-cement.

It is also possible to predict the strength development of zero-cement simply by C/(S+A) molar ratio. Regardless of high-alkali activation or low-alkali activation, the relative compressive strength of 7 days and 28 days has a high correlation with C/(S+A). From the overall trend, the greater the C/(S+A), the higher the relative compressive strength.

1.4 Research content

The aim of this thesis is to develop an ultra-high strength zero-cement mortar of more than 100 MPa and to elucidate of the influencing factors and mechanism of ultra-high strength zero-cement mortar, and to propose the design method of ultra-high-strength zero-cement mortar in order to reduce CO_2 emissions and provide theoretical basis and technical support for practical application. The contents of every chapter are as follows:

Chapter 1 is mainly for the research background, research purpose and research content, tried to build a foundation for the research of the whole thesis. Besides, the thesis structure will be also constructed by introducing the main research content of every chapters.

In Chapter 2 the potential for zero-cement to contribute towards significant reduction in CO_2 emissions is identified. The literatures about high-alkali systems and low-alkali systems are reviewed. It is clear that compressive strength development of zero-cement has not been studied in a methodical way, the mechanism of such zero-cement has not been fully elucidated, and the design method of zero-cement is lacking.

Chapter 3 are devoted to study the development of high alkali activated zero-cement mortar. For the compressive strength, how much influence do various factors have? Is it relevant? And can it make zero-cement? In order to confirm that, first, as a preliminary experiment, according to the Taguchi Method, it was confirmed that it could have a different effects in the presence of various factors. Then, in order to clarify the relationship between the chemical composition and

the compressive strength, the type and composition of the high-alkali activator was fixed, and only the powder ratio was changed. By measuring reaction products, pore structure, reaction rate and gel content, the relationship between compressive strength and pore structure & reaction product is clarified, and the mechanism of strength development of high-alkali-activated zero-cement mortar is also elucidated.

Chapter 4 are devoted to study the development of low alkali activated zero-cement mortar. Elucidate the relationship between influencing factors and compressive strength. Considering factors such as the amount of alkaline activator used and curing conditions, ratio of chemical components, W/B ratio, particle size distribution, type of raw material, etc. Besides, the strength index is proposed to evaluate the strength of zero-cement mortar.

Chapters 5 the design method of ultra-high-strength zero-cement mortar are proposed and verified. Based on the results of Chapters 3 and Chapters 4, predict the compressive strength with a similar design concept and design method, whether low alkali or high alkali. That is, if there is a need to achieve a certain design strength, it can derive the zero-cement mixing ratio according to the design method.

Chapters 6 are devoted to environmental performance evaluation. Since the purpose is to reduce CO_2 emissions, this chapter has confirmed the CO_2 emissions of ultra-high strength zero-cement mortar made in low-alkali and high-alkali conditions, compared to cement mortar made in normal conditions.

Finally, in Chapter 7 conclusions are drawn regarding the ultra-high-strength zero-cement mortar. Some recommendations are made, and directions for future research are identified.

The Fig.1.4.1 presents the thesis outline.

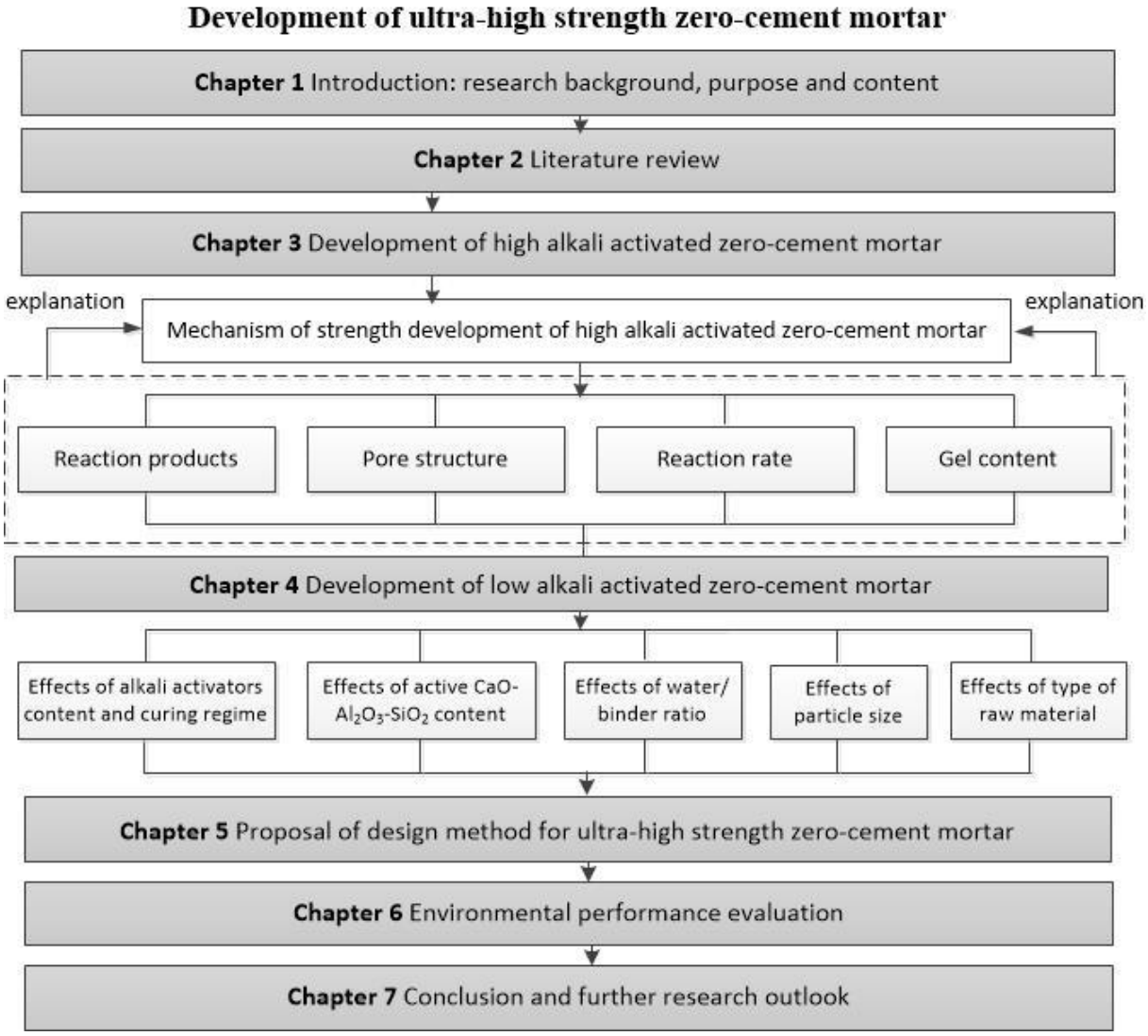

Fig.1.4.1 Thesis outline

References

(1) 一宮一夫:ジオポリマーの研究開発の現状.コンクリート工学 55,131-137 (2017).

(2) Singh B, Ishwarya G, Gupta M, Bhattacharyya S. Geopolymer concrete: A review of some recent developments. Constr Build Mater 2015;85:78-90.

(3) Van Deventer JSJ, Provis JL, Duxson P, Brice DG. Chemical research and climate change as drivers in the commercial adoption of alkali activated materials. Waste Biomass Valor 2010;1:145–55.

(4) Duxson P, Provis JL, Lukey GC, van Deventer JSJ. The role of inorganic polymer technology in development of 'green concrete'. Cem Concr Res 2007;37:1590–7.

(5) Davidovits, J.: Geopolymer Chemistry and Applications. Institut Geopolymer, Saint-Quentin, France (2008).

(6) J. Provis and J. van Deventer: "Alkali Activated Materials: State-of-the-Art Report", RILEM TC 224-

AAM,springer.
(7) 公益社団法人　日本コンクリート工学会：建設分野へのジオポリマー技術の適用に関する研究委員会報告書, pp.6-22, 2017.9.

2. Literature review

2.1 Introduction

In recent years, researchers have paid more and more attention to alkali activated materials, which uses industrial by-products that can significantly reduce CO_2 emissions during manufacturing compared to Portland cement, is attracting attention from around the world as a CO_2 reduction measure. Some researchers [1-2] reported that its CO_2 emissions can be reduced by as high as 80%. For easier understanding and differentiation, the alkali activated materials are divided into two categories: one type uses NaOH and Na_2SiO_3 with high alkalinity as alkali activator, which is called high alkali activated zero-cement, and another type uses CaO with low alkalinity as alkali activator, which is called low alkali activated zero-cement.

According to the existing literature, high alkali activated zero-cement can be divided into two systems [3], low-calcium systems and high-calcium systems. The main reaction product of high-calcium systems is CASH gel. The main reaction product of the low-calcium system is NASH gel. But the study of its mechanism has not been explained clearly. For the low alkali activated zero-cement, the main reaction product is CSH gel. For the low alkali activated zero-cement, the compressive strength is generally low, and there is little research on high strength.

The research progress is discussed below.

2.2 High alkali activated zero-cement

2.2.1 Introduction

There is a rough conclusion about the chemical reaction product of high alkali activated zero-cement (Geopolymer). According to the calcium content of the zero-cement binder, the high alkali activated zero-cement can be divided into two categories: one type the primary reaction product is N-A-S-(H)–type gel, which is called low-calcium alkali activation, and another type the primary reaction product is C-A-S-H–type gel, which is called high-calcium alkali

activation. So we can divide the alkali-activated materials into two systems, the low-calcium system and the high-calcium system. High-calcium systems react according to the left-hand (blue) pathway, the main product of the high-calcium system is CASH with the nature of secondary products determined by Mg content. When a small amount of magnesium is contained, crystalline zeolites are formed. When containing medium to high amounts of magnesium, layered double-hydroxide group are formed. Whereas low-calcium systems react according to the right-hand (green) pathway, The first of these gel types which is poor in calcium, is often represented as N-A-S-(H) [3].

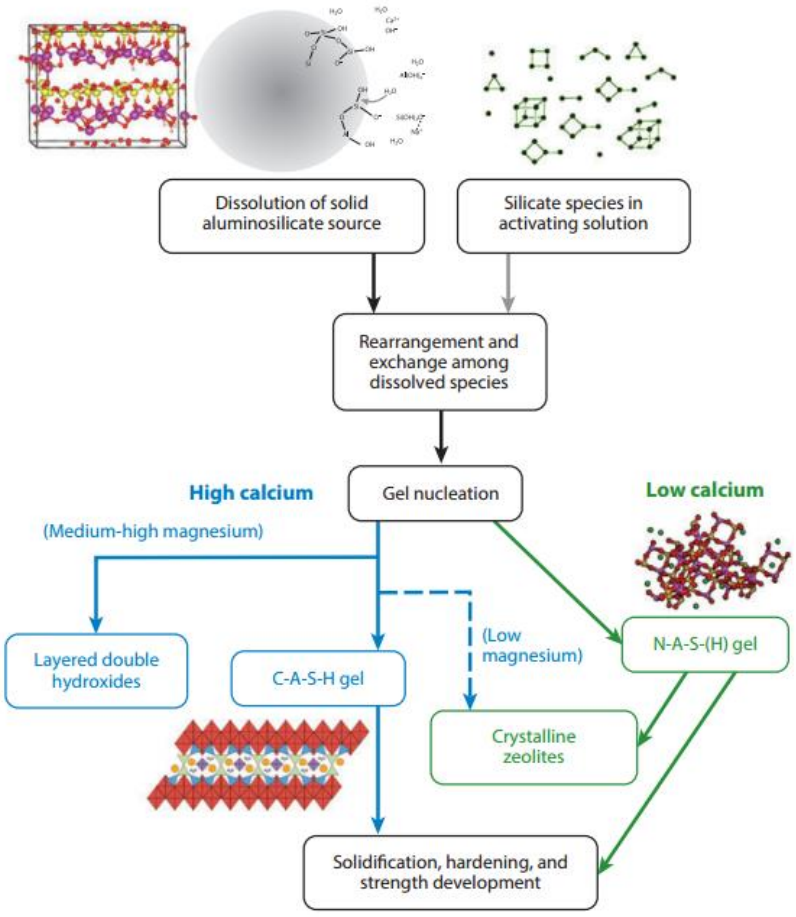

Fig.2.2.1 Process and reaction products of alkaline activation [3].

2.2.2 Low-calcium alkali activation

2.2.2.1 Effect of chemical activators

Chemical activators play a vital role in initiating alkali activation reactions. The concentration of chemical activators has a significant effect on the mechanical properties of alkali activated zero-cement. In general, strong alkali is necessary to increase the surface hydrolysis of aluminosilicate particles present in the raw materials, because the NaOH concentration determines the dissolution of Si and Al species, of which the leaching of silicon and aluminum mainly depends the concentration of NaOH and the leaching time [(4)].

Gorhan and Kurklu [(5)] studied the effect of concentrations of NaOH on the 7 days compressive strength of FA geopolymer mortar. The compressive strength results show that the optimal NaOH concentration is 6M. NaOH concentration is too high or too low will lead to a decrease in strength, too low the concentration will not enough to stimulate a strong chemical reaction, too high the concentration will cause premature coagulation of silica.

Somna et al. [(6)] also studied the effect of NaOH concentration (gradually increasing from 4.5M to 16.5M) on compressive strength of FA geopolymers. The results show that increasing the NaOH concentration from 4.5M to 9.5M, the compressive strength is significantly improved. Increasing the NaOH concentration from 9.5M to 14M, although the compressive strength also increased, but the degree is much smaller. As the NaOH concentration increases, the increase in compressive strength is mainly due to the higher degree of leaching of silica and alumina. The compressive strength began to decrease when the NaOH concentration was 16.5 M, it is mainly due to the excess hydroxide ions, which caused the premature precipitation of geopolymeric gels, resulting in lower strength.

Komljenovic et al. [(7)] studied the effect of alkali activator types on the mechanical properties of geopolymer mortar, using five different types of alkali activators: $Ca(OH)_2$, NaOH,

$NaOH+Na_2CO_3$, KOH and Na_2SiO_3 with various concentrations to make FA geopolymer mortar. According to the compressive strength results, the best alkali activator is Na_2SiO_3, followed by $Ca(OH)_2$, NaOH, $NaOH+Na_2CO_3$ and KOH. Regardless of which alkali activator is used, its compressive strength will generally increase with increasing activator concentration. The author also concluded that the optimal value of the Na_2SiO_3 modulus is 1.5.

Sukmak et al. [8] studied the effect of Na_2SiO_3/NaOH ratio and activator/FA ratios on the development of compressive strength of FA geopolymer bricks. The Na_2SiO_3/NaOH ratios used was 0.4, 0.7, 1.0, 1.5 and 2.3, while the activator/FA ratio used was 0.4, 0.5, 0.6 and 0.7. The bricks were placed at room temperature for 24 hours, and then cured in an oven at 75 ° C for 48 hours at high temperature. The results show that when the L/FA ratio less than 0.3 and greater than 0.8, the compressive strength is zero. The optimum Na_2SiO_3/NaOH ratio is 0.7, the optimum activator/FA ratio is 0.6.

Ridtirud et al. [9] studied the effect of different Na_2SiO_3/NaOH ratios on the compressive strength of FA geopolymer mortar. The authors concluded that the optimal Na_2SiO_3/NaOH ratio is 1.5. The increase in compressive strength is mainly due to the increase in Na content in the mixture, where Na^+ ions play a key role in the formation of geopolymers by acting as charge balance ions. Because excess sodium silicate hinders the evaporation of water and also destroys the formation of a three-dimensional network of aluminosilicate geopolymers. Therefore, the excess silicate reduces its compressive strength.

Guo et al. [10] studied the effect of modulus and alkali activator content on the compressive strength of CFA-based geopolymers. The results show that the optimal modulus and the content of alkali activator are 1.5 and 10%, respectively. However, Law et al. [11] showed that the best modulus for FA based geopolymer concrete is 1.0.

2.2.2.2 Effect of curing regime

Compared with OPC concrete, in order to obtain good compressive strength, geopolymers require heat treatment. Heat treatment is conducive to the dissolution and geological polymerization of aluminosilicate gel, thereby improving the early strength. However, depending on the raw material, the heat treatment method used must be appropriate. Exceeding a certain temperature and heat treatment time may hinder geopolymerization and adversely affect the mechanical properties of the geopolymer.

Ahmari S et al. [12] studied the effect of curing temperature on the compressive strength of geopolymer. The results show that the optimal curing temperature is 90 ℃ and the compressive strength is about 15 MPa. Too high the temperature will cause a rapid polycondensation process and too much geopolymeric gel to form prematurely. Similarly, it will cause rapid evaporation of the pore solution and may lead to incomplete geological polymerization, which ultimately leads to a reduction in compressive strength.

Ridtirud et al. [9] concluded that in the early stage of curing (7-28 days), a higher curing temperature (60°C) will lead to a rapid development of strength. But higher curing temperature has little effect on the strength after 28 days.

2.2.2.3 Effect of particle size

Nazariet al. [13] studied the effect of particle size distribution on the compressive strength of geopolymers. Generally, samples made with fine particles show the highest compressive strength.

Sata et al. [14] studied effect of three different particle size of bottom ash on the compressive strength of bottom ash-based geopolymer mortar. The results show that the finer the particle size of bottom ash, the higher the compressive strength of the mortar. Higher fineness BA and higher specific surface area can increase the rate of geopolymerization.

2.2.2.4 Effect of water content

Chindaprasirt P et al. [15] concluded that the presence of water in a geopolymer system only serves as a transport medium. In addition, the mixed water also provides processability for the geopolymer mortar just mixed, because it does not directly participate in the geopolymerization reaction. Ahmari [12] studied the effects of initial water content (8%, 10%, 12%, 14%, 16% and 18%) on the compressive strength of copper polymer tailings-based geopolymer bricks. The results show that the compressive strength of geopolymer bricks increases with the increase of initial water content. Mainly because of the role of water as a liquid medium in the process of geological polymerization.

2.2.2.5 Effect of forming pressure

For manufacturing building bricks, the forming pressure can push the entrapped air in the binder out of the matrix to achieve the best densification of intra- or inter-particles packing. Therefore, pressure forming methods [16] [17] can be used to make bricks with lower porosity and higher strength.

2.2.3 High-calcium alkali activation

Calcium has the effect of reducing permeability, so the presence of calcium can enhance many aspects of the durability of alkali activated materials, which is essential for extending the service life of concrete [3].The primary reaction product is C-A-S-H–type gel, which is called high-calcium alkali activation. Low-calcium alkali activation usually requires high temperature curing, but the addition of blast furnace slag that contain high calcium, can make it possible to manufacture ultra-high-strength alkali activated zero-cement under normal temperature conditions.

Some studies [18-20] concentrate on the alkali activated materials and target strength up to 80 MPa. And some researchers have obtained mortar strength up to 120 MPa [21]. Vladimir

Zivica[22] studied metabentonite Geopolymer activated with sodium hydroxide, prepared under the combination uniaxial compressive stress of 300MPa and low L/S ratio(0.08), the compressive strength up to 111 MPa. Li Yaling [23] studied fly ash-metakaolin alkali activated materials, which activated with sodium hydroxide and sodium silicate, prepared under the combination uniaxial compressive stress of 200MPa and low L/S ratio (0.15), the compressive strength up to 116 MPa.

Phoo-ngernkham T et al. [24] successfully manufactured over 170 MPa alkali activated materials by using fly ash and granular blast furnace slag. The results show that the reaction product and strength of the geopolymer depend on the type of raw materials and alkali activator. Using NaOH+Na_2SiO_3 solution and NaOH solution to activate granular blast furnace slag, a very high 28 days compressive strength was obtained, 171.7 and 173.0 MPa, respectively.

Khan M et al. [25] using 12 M NaOH and Na_2SiO_3 to activated fly ash and slag mixture. The alkaline liquid/binder ratio is 0.60. The results show that the compressive strength of the geopolymer depends mainly on the nature of the raw material selected for the alkali activation solution. By adding an appropriate amount of slag to the fly ash geopolymer, compressive strength greater than 100 MPa can be obtained.

Chi M et al. [26] used 4% and 6% sodium oxide (Na_2O) and mass ratio of SiO_2 to Na_2O of 1 as the activator. The effect of alkali activator on the compressive strength of fly ash-slag geopolymer was studied. The liquid/binder ratio is kept constant at 0.5. The experiment results show that the fly ash/slag ratio and the amount of Na_2O are two important factors that affect the bonding mechanism and properties of fly ash-slag mortars. With the increase of Na_2O dosage, the bonding mechanism and properties of fly ash-slag mortar are improved. Fly ash/slag ratio of 50/50 and Na_2O concentration of 6% are optimal.

Lolyd RR et al. [27] investigated the microstructure of alkali activated materials synthesized from

fly ash and mixtures of fly ash and blast furnace slag. The solid precursors were activated with 7%Na_2O and 7%SiO_2 at ambient temperature. Relatively high 28 days compressive strengths of more than 100 MPa was obtained.

All summarized as follows in Table.2.2.1. For the research of these above 100MPa high-strength alkali activated materials, the raw materials used are fly ash and slag, and the main alkali activator used are water glass and sodium hydroxide. The mixing ratio of the raw materials used, the composition and ratio of the alkaline solution used in these studies are different, but they all obtained a high compressive strength. Therefore, the relationship between compressive strength and various influencing factors needs further research, and the mechanism of the development of compressive strength needs to be clarified.

Table.2.2.1 Synthesis of ultra-high strength high alkali activated zero-cement materials.

author	Source material	type of specimen	Activator		Activator/ Binder	Water/ Binder	28 days Compressive strength (MPa)
			type	chemical composition			
Tanakorn Phoo-neernkham	FA50S50	paste	NS+NH, NS/NH ratio of 2.	9.3%Na_2O,11.5%SiO_2 (wt%)、10 M sodium hydroxide (NH) and sodium silicate (NS) with11.67% Na_2O, 28.66% SiO_2, and 59.67% H_2O	0.6	0.39	114.5
	GBFS						171.7
	GBFS		NS	7%Na_2O,17%SiO_2 (wt%)、		0.36	173
Khan M	FA50S50	mortar	NS+NH Na2SiO3/ NaOH ratio of 2.5.	12 M NaOH, Na_2SiO_3 solution (SiO_2 = 29.4%, Na2O = 14.7%, water 55.9%),	0.6	0.36	108
	FA60S40						106
Chi M	FA50S50	mortar	NS+NH Na2SiO3/ NaOH ratio of 5.39.	6%Na_2O and mass ratio of SiO_2 to Na_2O is 1. NaOH, Na_2SiO_3 solution (SiO_2 = 29.2%, Na_2O = 14.8%, water 56%),	0.5	0.38	110.6
	FA30S70						105.8
Lolyd RR	FA+GGBS	mortar	NS+NH	7%Na_2O,7%SiO_2 (wt%)、wt% is the percent by weight of binder	0.325	0.19	100
	GGBS				0.35	0.21	101

2.3 Low alkali activated zero-cement

The chemical activator has a significant effect on strength development of the alkali activated zero-cement. Therefore, the choice of alkali activator is crucial. Current typical alkali activators

are high alkali such as NaOH and Na_2SiO_3 [28]. Although the use of these highly alkaline activators can achieve high strength development, there are also many practical problems, such as high cost, dangerous chemical corrosion and quick setting time [29]. Besides, in highly alkaline environments, water reducer does not work.

Calcium hydroxide and calcium oxide are much less expensive than sodium hydroxide or sodium silicate. Also, it is not strongly corrosive and the water reducer will work. So there are potential alternatives as low alkali activators.

Min Sik Kim et al. [29] compared the effects of CaO and $Ca(OH)_2$ on slag-based zero-cement binder. The use of calcium oxide (CaO) shows great potential for activating granular blast furnace slag and produces higher mechanical strength than calcium hydroxide $Ca(OH)_2$. The main product is C–S–H, $Ca(OH)_2$ and a hydrotalcite-like phase.

Woo Sung Yum et al.[30] used $CaCl_2$ as a potential activator additive, CaO-activated GGBFS binder blended with fly ash (CAS 4:4:2), which is a new type and has a price competitive zero-cement ternary mixed materials can be widely used in concrete production. Although CAS has no clinker cement compound, the addition of $CaCl_2$ not only significantly accelerates the reaction of CAS binder, but also greatly improves the strength. In the early days, the presence of $CaCl_2$ significantly promoted the dissolution of the glass phase of GGBFS and fly ash, which led to an increase in the production of reaction products (such as CSH, hydrocalumite) and pore size refinement.

Yeonung Jeong et al. [31] used CaO to activate four different sources of blast furnace slag, and studied the influence of slag characteristics on strength development and reaction products. Research shows that the increase in strength is not determined by any single main material parameter of the slag, but by a combination of various favorable factors, such as higher calcium sulfate content, higher basicity (or chemical indexes) and smaller overall particle size

distribution.

Taku Matsuda et al. [32] reported that under the conditions of a water binder ratio of 16%, a unit water volume of 90kg/m^3, and a fine aggregate ratio of 55%, zero-cement mortar was produced by using silica fume, fly ash, and blast furnace slag fine powder as a binder and adding an expanding material. The concrete compressive strength exceeding 60N/mm^2 could be manufactured.

Zhao F et al. [33] obtained the best mix proportion for preparing granular blast furnace slag and grade C fly ash ecological zero-cement materials by factorial design method: slag, 70%; fly ash, 18%; activator, 12%. The 28 days compressive strength of zero-cement mortar is as high as 49 MPa. The hydration products are mainly ettringite and C–S–H gel.

Morsy MS et al. [34] developed a zero-cement mortar by using fly ash (FA), lime (L) and metakaolin. The mortar is used to produce environmentally friendly building materials without carbon dioxide emissions and has a variety of benefits effect. The mass ratio of FA: MK: L is 30:40:30 %. Anhydrite was added as a chemical activator in different proportions of 0, 2.5, 5, 7.5 and 10% by weight of the binder. The results show that adding 10% activator has a significant effect on compressive strength and flexural strength. After 28 days of hydration, the compressive strength and flexural strength were increased by 56% and 45% compared to the control mortar.

Şahin M et al. [35] studied the use of slag and high lime fly ash rich in free lime and sulfate to make zero-cement mortars. For the samples cured at 23 °C or 80 °C, the 28 days compressive strength exceeded 13 MPa and 20 MPa, respectively.

Sharma AK et al. [36] studied the effects of different proportions of fly ash and blast furnace slag on the compressive strength of zero-cement. It was found that the strength increased with the slag content. However, the sample composed of 30% and 40% slag and cured for 28 days

showed higher strength than the single material. In addition, adding 2% lime, the strength is also greatly improved.

For the low alkali activated zero-cement, the compressive strength is generally low, and there is little research on high strength.

2.4 Conclusions

For the high alkali activated zero-cement, compressive strength is mainly affected by factors such as chemical activators, curing regime, particle size distribution, water content and forming pressure. When manufacturing high alkali activated zero-cement, proper sodium hydroxide concentration and Na_2SiO_3/NaOH ratio are crucial. In general, manufacture of high-strength alkali activated zero-cement mortar using only fly ash as powder is possible, but high temperature curing is required; The finer the particle size of binder, the higher the compressive strength of the mortar. Appropriate water content is conducive to the increase of compressive strength, because the water is critical for the diffusion of dissolved Al_2O_3 and SiO_2 species; Pressure forming methods can be used to make bricks with lower porosity and higher strength. Low-calcium alkali activation usually requires high temperature curing, but the addition of blast furnace slag that contain high calcium, can make it possible to manufacture ultra-high-strength alkali activated zero-cement under normal temperature conditions. Besides, the compressive strength increases as the amount of blast furnace slag increases.

For the research of these above 100MPa high-strength alkali activated materials, the raw materials used are fly ash and slag, and the main alkali activator used are water glass and sodium hydroxide. The mixing ratio of the raw materials used, the composition and ratio of the alkaline solution used in these studies are different, but they all obtained a high compressive strength. Therefore, the relationship between compressive strength and various influencing factors needs

further research, and the mechanism of the development of compressive strength needs to be clarified.

For the low alkali activated zero-cement, the use of CaO shows great potential for activating waste by-product. The main product of low alkali activated zero-cement is C–S–H, $Ca(OH)_2$ and a hydrotalcite-like phase. $Ca(OH)_2$ and CaO are much less expensive than NaOH or Na_2SiO_3. Besides, it is not strongly corrosive and the water reducer will work. Therefore, uses CaO or $Ca(OH)_2$ as low alkali activator. It has a different reaction mechanism from high alkali activated zero-cement and it is a promising candidate as an alternative to ordinary Portland cement. For the low alkali activated zero-cement, the compressive strength is generally low, and there is little research on high strength.

References

(1) Van Deventer JSJ, Provis JL, Duxson P, Brice DG. Chemical research and climate change as drivers in the commercial adoption of alkali activated materials. Waste Biomass Valor 2010;1:145–55.

(2) Duxson P, Provis JL, Lukey GC, van Deventer JSJ. The role of inorganic polymer technology in development of ‘green concrete’. Cem Concr Res 2007;37:1590–7.

(3) Provis JL, Bernal SA. Geopolymers and Related Alkali-Activated Materials. Annual Review of Materials Research 2014;44(1):299-327.

(4) Panias D, Giannopoulou IP, Perraki T. Effect of synthesis parameters on the mechanical properties of fly ash-based geopolymers. Colloids Surf A 2007;301(1–3):246–54.

(5) Gorhan G, Kurklu G. The Influence of the NaOH solution on the properties of the fly ash–based geopolymer mortar cured at different temperatures. Composites B Eng 2013.

(6) Somna K, Jaturapitakkul C, Kajitvichyanukul P, Chindaprasirt P. NaOHactivated ground fly ash geopolymer cured at ambient temperature. Fuel 2011;90(6):2118–24.

(7) Komljenovic M, Bascarevic Z, Bradic V. Mechanical and microstructural properties of alkali-activated fly ash geopolymers. J Hazard Mater 2010;181(1–3):35–42.

(8) Sukmak P, Horpibulsuk S, Shen S-L. Strength development in clay-fly ash geopolymer. Constr Build Mater 2013;40:566–74.

(9) Ridtirud C, Chindaprasirt P, Pimraksa K. Factors affecting the shrinkage of fly ash geopolymers. Int J Miner Metall Mater 2011;18(1):100–4.

(10) Guo X, Shi H, Dick WA. Compressive strength and microstructural characteristics of class C fly ash geopolymer. Cem Concr Compos 2010;32(2):142–7.
(11) Law D, Adam A, Molyneaux T, Patnaikuni I, Wardhono A. Long term durability properties of class F fly ash geopolymer concrete. Mater Struct 2014:1–11.
(12) Ahmari S, Zhang L. Production of eco-friendly bricks from copper mine tailings through geopolymerization. Constr Build Mater 2012;29:323–31.
(13) Nazari A, Bagheri A, Riahi S. Properties of geopolymer with seeded fly ash and rice husk bark ash. Mater Sci Eng A 2011;528(24):7395–401.
(14) Sata V, Sathonsaowaphak A, Chindaprasirt P. Resistance of lignite bottom ash geopolymer mortar to sulfate and sulfuric acid attack. Cem Concr Compos 2012;34(5):700–8.
(15) Chindaprasirt P, Chareerat T, Sirivivatnanon V. Workability and strength of coarse high calcium fly ash geopolymer. Cem Concr Compos 2007;29:224–9.
(16) Zhao F-q, Zhao J, Liu H-j. Autoclaved brick from low-silicon tailings. Constr Build Mater 2009;23(1):538–41.
(17) Cheah CB, Noor Shazea AN, Part WK, Ramli M, Kwan WH. The high volume reuse of hybrid biomass ash as a primary binder in cementless mortar block. Am J Appl Sci 2014;11(8):1369–78.
(18) Hardjito D, Wallah SE, Sumajouw DMJ, Rangan BV. On the development of fly ash-based geopolymer concrete. ACI Mater J 2004;101:467–72.
(19) Diaz-Loya EI, Allouche EN, Vaidya S. Mechanical properties of fly ash-based geopolymer concrete. ACI Mater J 2011;108:300–6.
(20) Pan Z, Sanjayan JG, Rangan BV. Fracture properties of geopolymer paste and concrete. Mag Concr Res 2011;63:763–77.
(21) Atis, C. et al. Very high strength (120 MPa) class F fly ash geopolymer mortar activated at different NaOH amount, heat curing temperature and heat curing duration. Constr. Build. Mater. 96, 673-678 (2015).
(22) Živica, V., Palou, M., Kuzielová, E. & Žemlička, M. Super High Strength Metabentonite Based Geopolymer. Procedia Engineering 151, 133-140 (2016).
(23) 李亚林. 粉煤灰—偏高岭土复合基地质聚合物的结构与性能研究[D].西南科技大学,2017.
(24) Phoo-ngernkham T, Maegawa A, Mishima N, Hatanaka S, Chindaprasirt P. Effects of sodium hydroxide and sodium silicate solutions on compressive and shear bond strengths of FA–GBFS geopolymer. Constr Build Mater 2015;91:1-8.
(25) Khan M, Shaikh F, Hao Y, Hao H. Synthesis of high strength ambient cured geopolymer composite by using low calcium fly ash. Constr Build Mater 2016;125:809-820.
(26) Chi M, Huang R. Binding mechanism and properties of alkali-activated fly ash/slag mortars. Constr Build Mater 2013;40:291-298.
(27) Lloyd RR. The durability of inorganic polymer cements 2008.
(28) J.S. Van Deventer, J.L. Provis, P. Duxson, Technical and commercial progress in the adoption of geopolymer

cement, Miner. Eng. 29 (2012) 89–104.
(29) Kim MS, Jun Y, Lee C, Oh JE. Use of CaO as an activator for producing a price-competitive non-cement structural binder using ground granulated blast furnace slag. Cem Concr Res 2013;54:208-214.
(30) Yum WS, Jeong Y, Yoon S, Jeon D, Jun Y, Oh JE. Effects of CaCl 2 on hydration and properties of lime(CaO)-activated slag/fly ash binder. Cement and Concrete Composites 2017;84:111-123.
(31) Jeong Y, Park H, Jun Y, Jeong JH, Oh JE. Influence of slag characteristics on strength development and reaction products in a CaO-activated slag system. Cement and Concrete Composites 2016;72:155-167.
(32) 松田拓ほか : ポルトランドセメントを使用しない超低収縮・高強度コンクリート，日本建築学会大会学術講演梗概集，pp.1185-1186，2017
(33) Zhao F, Ni W, Wang H, Liu H. Activated fly ash/slag blended cement. Resources, Conservation & Recycling 2007;52(2):303-313.
(34) Morsy MS, Alsayed SH, Salloum YA. Development of eco-friendly binder using metakaolin-fly ash–lime-anhydrous gypsum. Constr Build Mater 2012;35:772-777.
(35) Şahin M, Mahyar M, Erdoğan ST. Mutual activation of blast furnace slag and a high-calcium fly ash rich in free lime and sulfates. Constr Build Mater 2016;126:466-475.
(36) Sharma AK, Sivapullaiah PV. Strength development in fly ash and slag mixtures with lime. Proceedings of the Institution of Civil Engineers - Ground Improvement 2016;169(3):194-205.

3. Development of high alkali activated zero-cement mortar

3.1 Introduction

Manufacture of high-strength alkali activated zero-cement mortar using only fly ash as raw material is possible, but high temperature curing is required. For example, Phoo-ngernkham et al. [(1)] use fly ash as powder, using an alkaline solution of 14mol/L NaOH, heat curing at 115°C for 24 hours, successfully manufactured 120MPa geopolymer. In addition, it is known to replace a part of fly ash with blast furnace slag in order to cure at room temperature [(2) (3) (4) (5) (6)], and the compressive strength increases as the amount of blast furnace slag increases.

From the literature review in the previous chapter, these above 100MPa high-strength alkali activated materials, the raw materials used are fly ash and slag, and the main alkali activator used are water glass and sodium hydroxide. The mixing ratio of the raw materials used, the composition and ratio of the alkaline solution used in these studies are different, but they all obtained a high compressive strength. Therefore, the relationship between compressive strength and various influencing factors needs further research, and the mechanism of the development of compressive strength also needs to be clarified.

This chapter are devoted to study the development of high alkali activated zero-cement mortar. For the compressive strength, how much influence do various factors have? Is it relevant? And can it make zero-cement? In order to confirm that, first, as a preliminary experiment, according to the Taguchi Method, it was confirmed that it could have a different effects in the presence of various factors.

Then, in order to clarify the relationship between the chemical composition ratio and the compressive strength, the type and composition of the high-alkali activator was fixed, and only the powder ratio was changed. By measuring reaction products, pore structure, reaction rate, and gel content, the relationship between compressive strength and pore structure＆reaction

product is clarified, and the mechanism of strength development of high-alkali-activated zero-cement mortar is also elucidated.

3.2 Factors affecting compressive strength of high alkali activated zero-cement mortar

3.2.1 Introduction

The aim of this study is to confirm that how much influence do various factors have? Is it relevant? And can it make zero-cement? In order to confirm that, first, as a preliminary experiment, according to the Taguchi Method, a parametric study was carried out to achieve this purpose. It include particle size of Slag, Na_2SiO_3/NaOH mass ratio, NaOH concentration (M/L), and Slag content [B×%] were chosen as the influencing parameters. Then summarize the main factor determining the compressive strength. Finally, propose an optimal combination of high alkali activated zero-cement mortar.

3.2.2 Materials and Experimental Methods

The Taguchi method can study the effects of various variables with a small number of experiments [7]. Taguchi method is a design method to study multi-factors and multi-levels. It selects some representative points from a comprehensive experiment based on orthogonality for experiment. These representative points have "uniformly dispersed and neatly arranged" feature. Taguchi method is a high-efficiency, fast and economical experimental design method. In addition, the Taguchi method also has the following advantages:

(1) Practically arrange the experiment according to the table, easy to use;

(2) The layout is balanced and the number of trials is less;

(3) The Taguchi method provides a method for analyzing the results, which are intuitive and easy to analyze.

(4) Because of its orthogonality, it is easy to analyze the main effects of various factors. However, it also has some disadvantages: the data analysis method provides a preferred value that can only be a certain combination of levels used in the experiment, and the preferred result will not exceed the range of the level taken; In addition, it cannot provide a clear direction for further experiments, it makes the experiment still very groping and not very accurate.

The Taguchi method has been widely used in other engineering applications, but the application to high alkali activated zero-cement mortar is very limited [8-11]. To manufacture more than 100MPa ultra-high alkali activated zero-cement mortar. A parametric study was carried out to achieve this purpose. It include type of Slag, Na_2SiO_3/NaOH mass ratio, NaOH concentration (M/L), alkali [B×%], and slag content [B×%]. Table.3.2.1 shows the materials used, Table.3.2.2 shows the factors and levels for the experiment. Table.3.2.3 illustrates L-16 array proposed by Taguchi method. Table.3.2.4 shows the parameters of the experiments.

Table.3.2.1 Materials used

	Material	Material characters	Symbol
Binder (B)	Fly ash TypeI	Density:2.4g/cm3, Specific surface area:5680cm2/g	FA
	Slag3000	Density:2.91g/cm3, Specific surface area:3100cm2/g	BF3000
	Slag4000	Density:2.91g/cm3, Specific surface area:4040cm2/g	BF4000
	Slag6000	Density:2.91g/cm3, Specific surface area:5860cm2/g	BF6000
	Slag8000	Density:2.90g/cm3, Specific surface area:8020cm2/g	BF8000
Alkali solution	NaOH	12mol/L	NH
	Sodium silicate	36.5%SiO2,18%Na2O	NS
Fine aggregate	sand	Surface dry density: 2.55g/cm3, water absorption:2%	S

Table.3.2.2 the factors and levels for the experiment

Level	(A)Type of Slag	(B)WG/NaOH mass ratio	(C)NaOH concentration (M/L)	(D)Slag content
1	8000	1	8	40
2	3000	1.5	10	50
3	6000	2	12	30
4	4000	0.5	14	20

Table.3.2.3 L-16 array proposed by Taguchi method

Series of experiment	A	B	C		D
1	1	1	1	1	1
2	1	2	2	2	2
3	1	3	3	3	3
4	1	4	4	4	4
5	2	1	2	3	4
6	2	2	1	4	3
7	2	3	4	1	2
8	2	4	3	2	1
9	3	1	3	4	2
10	3	2	4	3	1
11	3	3	1	2	4
12	3	4	2	1	3
13	4	1	4	2	3
14	4	2	3	1	4
15	4	3	2	4	1
16	4	4	1	3	2

Fly ash, granulated blast furnace slag used as binder, NaOH (NH) and $NaSiO_3$ (NS) as activator. The alkaline solution was prepared by mixing NS and NH at a mass ratio of 2: 1 before mixing, and storing for 24 hours in a 60°R.H. curing room at 20 ° C. At first, the powder and fine aggregate were dry-mixed for 3 min, and then add the alkali solution to the mixer, then mixed for additional 5 min. In the mortar mixture, sand/binder ratio were kept constant as 1.

Three prismatic specimens with 40 mm 40 mm 160 mm dimensions were prepared from fly ash, granulated blast furnace slag zero-cement mortar mixture for the strength measurements. After 28 days curing, measured the compressive strength. The reported compressive strengths are an average of six samples.

Table.3.2.4 the parameters of the experiments

Series of experiment	(A)Type of Slag	(B)WG/NaOH mass ratio	（C） NaOH concentration (M/L)	(D)Slag content
1	8000	1	8	40
2	8000	1.5	10	50
3	8000	2	12	30
4	8000	0.5	14	20
5	3000	1	10	20
6	3000	1.5	8	30
7	3000	2	14	50
8	3000	0.5	12	40
9	6000	1	12	50
10	6000	1.5	14	40
11	6000	2	8	20
12	6000	0.5	10	30
13	4000	1	14	30
14	4000	1.5	12	20
15	4000	2	10	40
16	4000	0.5	8	50

3.2.3 Influence of various factors on the compressive strength

Table.3.2.5 shows the Workability and 28 days compressive strength results. Table.3.2.6 shows the results of calculating the R value for each factor. The R value of Type of Slag, WG/NaOH mass ratio, NaOH concentration (M/L) and Slag content [B×%] are 23.55, 23.23, 31.43 and 24.3 respectively. NaOH concentration (M/L) have the highest contribution to compressive strength, and the contribution of the other factors is very close. According to Table.3.2.6, it is easy to get the Fig.3.2.1, which shows the significance of the

main effects of the considered factors on the 28 days compressive strength.

Several studies [12-13] show that the finer particle sizes of binder would result in the higher strength. Fig.3.2.1 illustrates the effect of different particle sizes of slag on compressive strength. As the specific surface area of the powder increases, the compressive strength decreases first and then increases. In general, the finer the powder, the faster the reaction and the highest compressive strength. However, as the specific surface area increases, the compressive strength will decrease once, which needs further research.

Table.3.2.5 Workability and 28 days compressive strength.

Series of experiment	(A)Slag	(B)WG/NaOH mass ratio	(C)NaOH concentration (M/L)	Alkali [B×%]	(D)Slag content [B×%]	0-hit flow(mm)	15-hit flow(mm)	Compressive strength (Mpa)
1	8000	1	8	0.5	40	142	176	97
2	8000	1.5	10		50	129	146	113.2
3	8000	2	12		30	124	130	91.9
4*	8000	0.5	14		20	100	102	49.1
5	3000	1	10		20	100	102	80.3
6	3000	1.5	8		30	182	202	74.9
7	3000	2	14		50	123	158	104.8
8	3000	0.5	12		40	189	210	45.7
9*	6000	1	12		50	100	105	49.6
10*	6000	1.5	14		40	100	102	53.1
11	6000	2	8		20	140	155	69.6
12	6000	0.5	10		30	180	218	84.7
13	4000	1	14		30	122	140	75.2
14	4000	1.5	12		20	100	102	50.8
15	4000	2	10		40	160	173	85.5
16	4000	0.5	8		50	168	196	79.4

Table.3.2.6 L-16 array proposed by Taguchi method

Series of experiment	A	B	C		D	Compressive strength (Mpa)
1	1	1	1	1	1	97
2	1	2	2	2	2	113.2
3	1	3	3	3	3	91.9
4	1	4	4	4	4	49.1
5	2	1	2	3	4	80.3
6	2	2	1	4	3	74.9
7	2	3	4	1	2	104.8
8	2	4	3	2	1	45.7
9	3	1	3	4	2	49.6
10	3	2	4	3	1	53.1
11	3	3	1	2	4	69.6
12	3	4	2	1	3	84.7
13	4	1	4	2	3	75.2
14	4	2	3	1	4	50.8
15	4	3	2	4	1	85.5
16	4	4	1	3	2	79.4
K1	351.2	302.1	320.9	337.3	281.3	
K2	305.7	292	363.7	303.7	347	
K3	257	351.8	238	304.7	326.7	
K4	290.9	258.9	282.2	259.1	249.8	
k1	87.8	75.5	80.2	84.3	70.3	
k2	76.4	73.0	90.9	75.9	86.8	
k3	64.3	88.0	59.5	76.2	81.7	
k4	72.7	64.7	70.6	64.8	62.5	
R	23.55	23.23	31.43	19.55	24.30	

The second factor affecting the strength is the WG/NaOH mass ratio. Some studies reported different conclusions [14] [15] [16] [17]. Fig.3.2.1 shows that the higher WG/NaOH mass ratio, the greater the strength, which may be related to the accelerated geopolymerisation reaction in higher WG/NaOH mass ratio and lead to higher strength.

Several studies [18-19] reported the optimal strength by utilizing appropriate NaOH concentration. In this study, the optimal NaOH concentration is 10M. The main role of NaOH is dissolving

Al_2O_3 and SiO_2 for geopolymerisation reactions. When the NaOH concentration is lower than 10M, as concentration of NaOH increase, the dissolution of silicate and alumina from the aluminosilicate source is increased, which results in higher strength [20-21]. When NaOH concentration over 10M, it will result low compressive strength. It is mainly due to the excessive hydroxide ions, which caused premature precipitation of geopolymeric gels, resulting in lower strength.

Fig.3.2.1 also shows the effect of (D) Slag content on strength. It is known to replace a part of fly ash with blast furnace slag in order to cure at room temperature, and the compressive strength increases as the amount of blast furnace slag increases[2] [3] [4][5][6]. In this study, more slag will result in higher compressive strength.

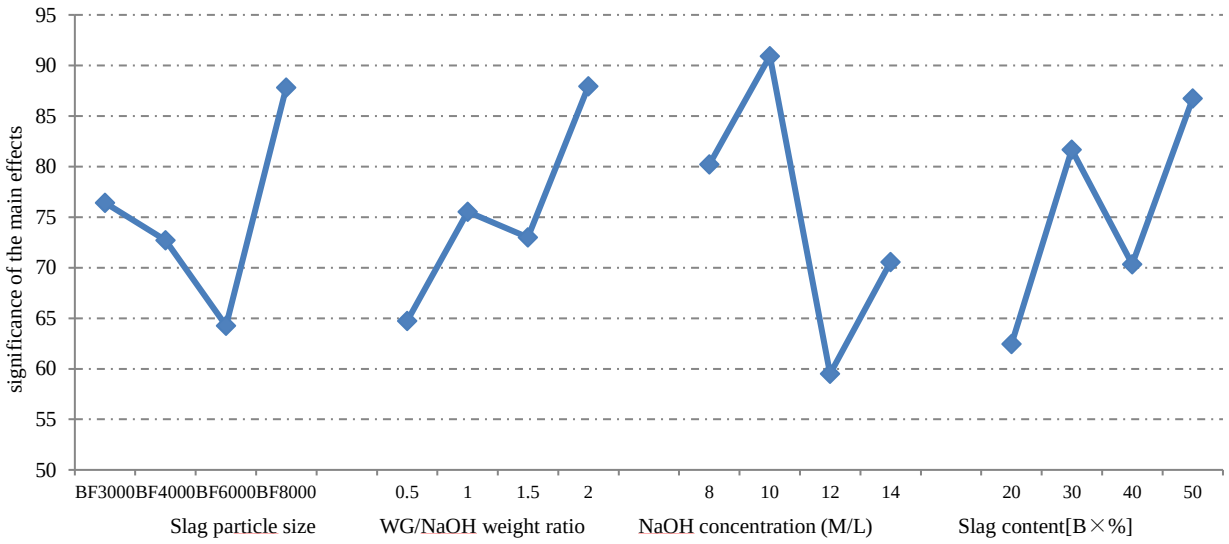

Fig.3.2.1 The significance of the main effects

Table.3.2.7 shows that the optimum combination is achieved by utilizing a specimen with 50 wt% Slag8000, NaOH concentration of 10 M and Silica modulus M＝2 reach up to compressive strength of 113.3 MPa.

Table.3.2.7 Percentage of participation and Optimum levels of the considered parameters

Parameter	(A)Slag	(B)WG/NaOH weight ratio	(C)NaOH concentration (M/L)	(D)Slag content
Percentage of participation (%)	23.0%	22.7%	30.7%	23.7%
Optimum Level	BF8000	2	10	50
Compressive strength	113.3Mpa			

3.2.4 Crystallization phenomenon

The modulus of a silicate solution is defined as the molar ratio SiO_2/Na_2O, high modulus solutions (modulus ≥2) are generally stable. Modulus solutions (modulus: 0.5−1.0) are particularly prone to crystallization [22]. Table.3.2.8 show the SiO_2/Na_2O molar ratio of each specimens. In this study, Specimen G4, G5, G8, G9, G10 and G13 alkaline solutions produced crystallization. Crystallization occurred in solutions of modulus 0.4−1.0. The chemical reaction equation show below.

$$Na_2O+SiO_2+H_2O \Rightarrow \begin{matrix} Na_2SiO_3\cdot 5H_2O \\ Na_2SiO_3\cdot 6H_2O \\ Na_2SiO_3\cdot 9H_2O \end{matrix}$$

Therefore, when preparing the alkali activator, the solutions of modulus should be avoided within the range of 0.4−1.0.

Table.3.2.8 SiO_2/Na_2O molar ratio of each specimens.

Sample designation	wt.% SiO_2	wt.% Na_2O	SiO_2/Na_2O molar ratio
G1	18.25	18.69	1.01
G2	21.90	20.10	1.13
G3	24.35	21.04	1.20
G4	12.15	26.41	0.48
G5	18.25	20.63	0.91
G6	21.90	18.55	1.22
G7	24.35	22.20	1.13
G8	12.15	24.09	0.52
G9	18.25	22.56	0.84
G10	21.90	23.05	0.98
G11	24.35	18.46	1.36
G12	12.15	21.50	0.58
G13	18.25	24.31	0.78
G14	21.90	21.65	1.05
G15	24.35	19.75	1.27
G16	12.15	18.92	0.66

3.3 Mechanism of strength development of high alkali activated zero-cement mortar

3.3.1 Introduction

Based on the results of section 3.2, the purpose of this section is to explore the mechanism of strength development of high alkali activated zero-cement.

In order to clarify the mechanism of strength development of high alkali activated zero-cement, the type and composition of the high-alkali activator was fixed, and only the powder ratio was changed. By measuring reaction products, pore structure, reaction rate, and gel content, the relationship between compressive strength and pore structure＆reaction product is clarified, and the mechanism of strength development of high-alkali-activated zero-cement mortar is also elucidated.

3.3.2 Materials and Experimental Methods

3.3.2.1 Factors and level of experiment

Table.3.3.1 shows the materials used. Table.3.3.2 and Table.3.3.3 show FA, BF chemical composition respectively. Fig.3.3.1 shows raw material XRD results. BF is basically amorphous, and FA is mainly composed of amorphous, quartz and mullite. Table.3.3.4 shows crystalline and amorphous content of FA.

Table.3.3.1 Materials used

	Material	Material characters	Symbol
Binder（B）	Fly ash Type I	Density:2.4g/cm^3, Specific surface area:5680cm^2/g	FA
	Slag4000	Density:2.91g/cm^3, Specific surface area:4040cm^2/g	BF
Alkali solution	NaOH	12mol/L	NH
	Sodium silicate	36.5%SiO_2,18%Na_2O	NS
Fine aggregate	sand	Surface dry density: 2.55g/cm^3, water absorption:2%	S

Table.3.3.2 FA chemical composition

SiO2	Al2O3	CaO	Fe2O3	MgO	P2O5	SO3	Na2O	K2O	TiO2	V2O5	Cr2O3	ZnO	SrO	ZrO2	BaO
64.80%	23.08%	2.50%	3.53%	1.14%	0.35%	0.70%	0.87%	1.30%	1.08%	0.06%	0.22%	0.03%	0.11%	0.06%	0.08%

Table.3.3.3 BF chemical composition

CaO	SiO2	Al2O3	MgO	SO3	Fe2O3	Cl	K2O	Na2O	TiO2	MnO	SrO	ZrO2	BaO
45.45%	32.23%	12.87%	5.69%	1.92%	0.33%	0.02%	0.35%	0.26%	0.52%	0.18%	0.05%	0.03%	0.07%

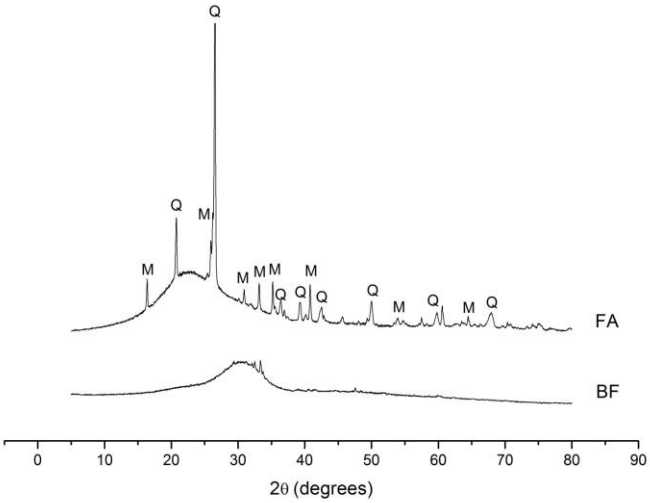

Q = Quartz (SiO_2), M = Mullite ($Al_{4.5}Si_{1.5}O_{9.75}$)

Fig.3.3.1 Raw material XRD

Table.3.3.4 Crystalline and amorphous content of FA

Crystalline phases (%)				Glassy phase (%)
Quartz （SiO_2）	Mullite （$Al_{4.5}Si_{1.5}O_{9.75}$）	Magnetite （Fe_3O_4）	Hematite (Fe_2O_3)	
10.31	9.68	0.46	0.13	79.41

Unlike ground granulated blast furnace slag, which comprised of near 100% amorphous phase, fly ash include some crystalline phases, such us quartz, mullite and magnetite, which cannot participate in reaction. Before designing the mix proportion, the contents of $RSiO_2$, RAl_2O_3 and RCaO in the fly ash must be calculated. The calculation method is as follows:

Step 1-Crystalline phases in the FA sample containing silica, alumina, or calcium oxide are identified by XRD (show in Table.3.3.4), these are Mullite and quartz (M and Q).

Step 2-The chemical composition of the crystalline phases is calculated. M contains 28.2 %SiO_2 and 71.8 % Al_2O_3. Q contains 100%SiO_2.

Step 3-The total content of non-reactive silica， alumina， and calcium oxide (labeled as $NRSiO_2$,$NRAl_2O_3$ and NRCaO) is calculated as follow:

$NRSiO_2$ = (Q* 100 + M* 28.2)/100 = (10.31 * 100 + 9.68* 28.2)/100 = 13.04%

$NRAl_2O_3$ = M* 71.8/100 =9.68* 71.8/100 =6.95%

NRCaO= 0%

Step 4-The non-reactive silica，alumina，and calcium oxide is subtracted from the total silica，alumina, and calcium oxide content (measured by XRF) to obtain the reactive components labeled as $RSiO_2$, RAl_2O_3 and RCaO:

$RSiO_2 = SiO_2 - NRSiO_2 = 58.21 – 13.04 = 45.17\%$

$RAl_2O_3 = Al_2O_3 - NRAl_2O_3 = 21.38 – 6.95 = 14.43\%$

RCaO= CaO - NRCaO = 4.72 - 0 = 4.72%

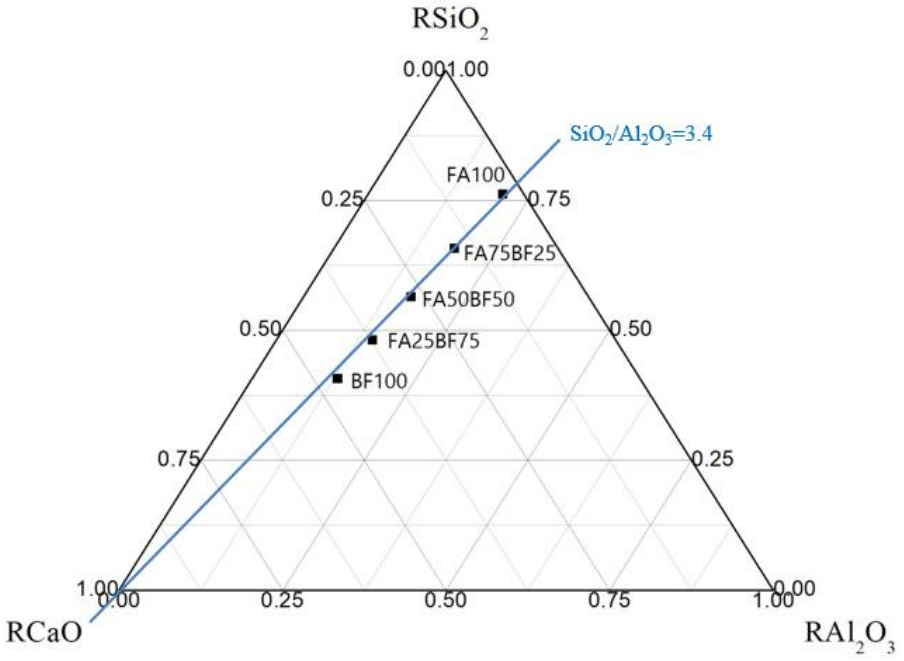

Fig.3.3.2 the RCaO-RAl_2O_3-$RSiO_2$ ternary diagram.

Fig.3.3.2 shows the RCaO-RAl_2O_3-$RSiO_2$ ternary diagram. There are 5 samples, the molar

ratios of $RSiO_2/RAl_2O_3$ are close to 3.4. Table.3.3.5 shows the factors and levels of this experiment. In this experiment, the mass ratio of the alkaline solution to the powder is 0.5, the sodium silicate solution (hereinafter, NS) and the sodium hydroxide aqueous solution (hereinafter, NH) are constant at a mass ratio of 2: 1, and change the mass ratio of blast furnace slag to fly ash. Chemical admixtures were not used because it does not work in high alkaline solutions.

Table.3.3.5 Factors and Levels of Experiment

No.	Symbol	Alkali solution [B×%]	Percentage of each material in powder (%)		NS/NH	H_2O/ Powder
			FA	BF		
1	FA100	0.5	100	0	2	0.26
2	FA75BF25		75	25		
3	FA50BF50		50	50		
4	FA25BF75		25	75		
5	BF100		0	100		

3.3.2.2 Mixture proportions

Table.3.3.6 shows the preparation of high alkali activated zero-cement mortar used in this experiment. The JIS type I fly ash and the blast furnace slag were used. For the alkaline solution, sodium silicate solution and 12mol/L sodium hydroxide aqueous solution were used. The mass ratio of fine aggregate sand to binder in mortar was 1: 1. The mass ratio of FA to BF was five levels of 100: 0, 75:25, 50:50, 25:75 and 0: 100.

Table.3.3.6 Mixture proportions

No.	Symbol	FA[kg/m^3]	BF[kg/m^3]	Sand[kg/m^3]	Alkali solution[kg/m^3]		
					NaOH	$NaSiO_3$	H_2O
1	FA100	863	0	863	50.3	158.2	222.9
2	FA75BF25	658	219	877	51.2	160.8	226.6
3	FA50BF50	445.5	445.5	891	52.0	163.4	230.2
4	FA25BF75	226.5	679.5	906	52.9	166.1	234.1
5	BF100	0	921	921	53.7	168.9	237.9

3.3.2.3 Mixing method

The alkaline solution was prepared by mixing NS and NH at a mass ratio of 2: 1 before mixing, and storing for 24 hours in a 60°R.H. curing room at 20 ° C. Using a mortar mixer, in order to make the powder and the fine aggregate uniform, the mixture was mixed for 3 minutes, then alkaline solution was added, and the mixture was mixed again for 5 minutes. In this experiment, the mixing amount of one batch was 2 L.

3.3.2.4 Experimental method

(1)Workability and compressive strength

Workability of mixtures was measured in terms of flow diameter as per JIS R 5201 "Physical test method for cement" and JIS A6207 "silica fume for concrete. The workability were conducted immediately, after mixing all the mixtures were tested twice.

As for curing, high alkali activated zero-cement mortar was mixed and then poured into the 40mm×40mm×160mm metal mold, vibrated for 2 minutes using a vibrating table, then sealed with a plastic film, the curing was performed at a temperature of 20°C, 60%RH. The compressive strength tests were conducted at the ages of 7 and 28 days using a universal testing machine. The reported compressive strengths are an average of six samples.

(2)Mercury intrusion porosimetry (MIP)

Pore structure analysis was performed by mercury intrusion porosimetry (MIP). The specimen crushed with a hammer, and a sample of about 5-10 mm square was immersed in ethanol for 48 hours to stop hydration. After that, the ethanol attached to the sample was evaporated in an environment of 60°C for 4 hours, stored in a vacuum chamber for more than 7 days, and measured.

(3) Percentage of water content

Select 3 pieces of dried samples with a weight of 1～2g, weigh them separately, and then immerse them in water, and weigh them again after 2h, 6h, 24h, 72h, 168h. Note that the initial sample mass is m_0, the mass after soaking is m_i, and the calculation equation of percentage of mass change (%) is: $P= 100\%*(m_i -m_0)/m_0$。 The percentage of mass change (%) is the average of three samples.

(4) Thermogravimetric (TG) analysis

Thermogravimetric (TG) analysis, in a TG differential thermal analysis instruments (MTC1000SA). Samples were crushed, approximately 20mg of ground sample powders was heated at 10°C/min from normal temperature to 1000°C in a nitrogen environment at 150 mL/min purge rate. In this experiment, thermogravimetric (TG) analysis was adopted to quantify the weight loss ratio(105℃-300℃) and CH contents.

(5) X-ray diffraction analysis (XRD)

X-ray diffraction (hereinafter referred to as XRD) was performed using an X-ray diffractometer. After grinding the hardened paste of each specimen, XRD analysis was performed. The X-ray diffraction measurement conditions were: tube voltage: 40 kV, tube current: 15 mA, measurement range: $2\theta = 5$ to 80 °, step angle: 0.02°, bead: 2deg/min.

(6) Unreacted rate of fly ash and slag

a. Unreacted fly ash content:

The selective dissolution method for analyzing alkali activated slag-fly ash blends was applied following the description of Puligilla et al. [23]. Samples were firstly ground and then dissolved in 1:20 HCl (vol%). Specifically, 1 g of reacted powder was added into 250 ml of HCl solutions, the mixture was then stirred for 3 h and filtered by using a 2 μm filter paper. The insoluble residues were washed with distilled water until a neutral pH is reached, then dried and stored until the analysis was carried out. The acid attack decomposes the original structure of slag and its reaction products, as well as the N-A-S-H type gels or other reacted phases, leaving behind the unreacted fly ash as the only insoluble residue.

b. Unreacted slag content:

In the single measurement method [24], the crushed sample is heat-treated and used for XRD measurement. In heating, the slag was completely crystallized and the decomposition of other minerals was considered to be minimal. The heating condition was 900 °C for 30 minutes, and after 30 minutes of heating, air cooling was performed. Three minerals (hereinafter referred to as slag minerals) of crystallized slag, Gehlenite (C_2AS), Akermanite (C_2MS_2), and Merwinite (C_3MS_2) were added. The total value of the three types of slag minerals determined was taken as the amount of unreacted slag in the sample.

3.3.3 Workability

Fig.3.3.3 shows the workability results of each specimen. As the substitution of blast furnace slag increase, the workability increase, but tended to decrease when the substitution rate exceeded 50%. The specimen FA50BF50 showed the best workability, with 0 falling movement workability being 159 mm and 15 falling movement workability being 173 mm. Giving each specimen 15 falling movements increased by only about 20 mm and show high viscosity .

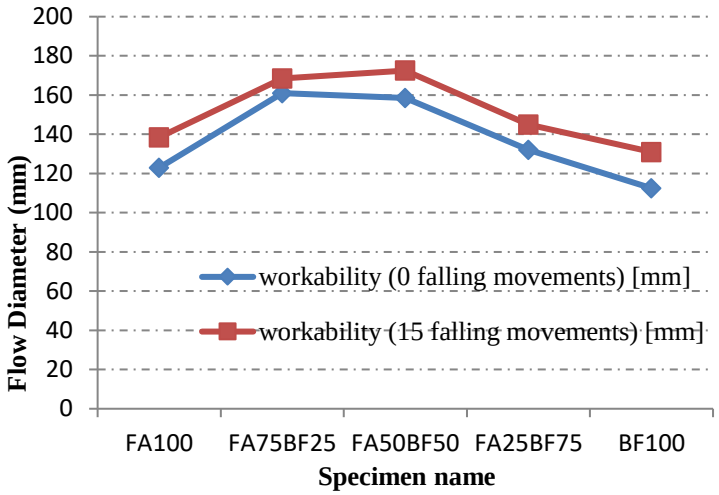

Fig.3.3.3 workability

3.3.4 Compressive strength

Fig.3.3.4 shows the results of compressive strength at 7 days and 28 days (20°C sealed curing). It was confirmed that the compressive strength of high alkali activated zero-cement mortar is greatly affected by the content of ground granulated blast furnace slag. At 7 days, the compressive strength tended to increase as the substitution rate of ground granulated blast furnace slag increased. The 7 days compressive strength of specimen FA100 without the addition of ground granulated blast furnace slag was only 7.6 MPa, and the 7 days compressive strength of specimen BF100 increased to 86 MPa.

In an alkaline environment, the high reactivity of the soluble aluminosilicate causes an increase in the silicon and aluminum content in the aqueous phase. These aluminosilicates make the polycondensation reaction more efficient and help to form a high quality matrix. Therefore, high compressive strength can be obtained [25]. The ground granulated blast furnace slag contains a large amount of reactive aluminosilicate, and the dissolution of ions from ground granulated blast furnace slag in an alkaline environment is much higher than that of fly ash. Aluminosilicate dissolves more with the increase of substitution rate of blast furnace slag. In addition, since the presence of calcium oxide in the ground granulated blast furnace slag rapidly

starts the hydration reaction, it is considered that the compressive strength at 7 days tends to increase as the amount of ground granulated blast furnace slag increases.

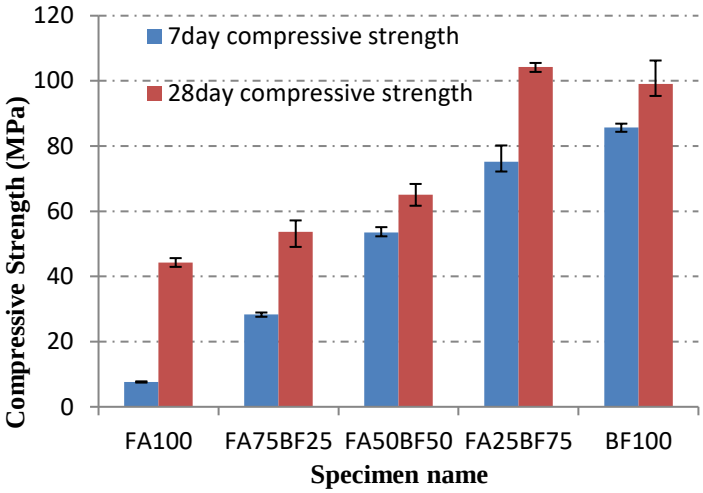

Fig.3.3.4 Compressive strength (20°C sealed curing)

The 28 days compressive strength was higher than 7 days compressive strength. The compressive strengths of the specimens FA100 and FA75BF25 increased by about 483% and 90%, respectively, and the others increased by less than 40%. Samantasinghar et al. [(26)] used fly ash, ground granulated blast furnace slag as powder, and used an 8 M NaOH solution as an alkaline solution, and an FA-GGBS mixture geopolymer with an alkaline solution to solid ratio of 0.35ml/g. For the GGBS100, the specimen showed the highest compressive strength at 7 days and 28 days, but at 90 days of age, it is reported that GGBS60 showed the highest compressive strength instead of the specimen GGBS100. In this study, the specimen FA25BF75 showed the highest strength instead of the specimen BF100 at 28 days, and the 28 days compressive strength is 104 MPa. The reason is considered that if the hydration reaction of ground granulated blast furnace slag continues for a long period of time, the hardened mortar will be continuously dewatered, which in turn causes shrinkage cracks and the compressive

strength decreases.

3.3.5 Pore size measurement

The cumulative pore volume distribution of each specimen is shown in Fig.3.3.5. Overall, the total pore volume tended to decrease as the substitution rate of slag increased. The total pore volume of the specimen FA100 and FA75BF25 with low substitution rate of the blast furnace slag at 7 days was about 0.080mL/g and 0.089mL/g, respectively. The solubility of fly ash is low, and the presence of partially dissolved hollow spheres is considered to have a relatively high total pore volume due to the formation of open pores. The total pore volume of the specimen FA50BF50 was a little small and became about 0.065mL/g. The total pore volume of the specimen BF100, which has the highest rate of displacement of the ground granulated blast furnace slag, shows a minimum value of about 0.050mL/g, and is considered to have the most densified microstructure.

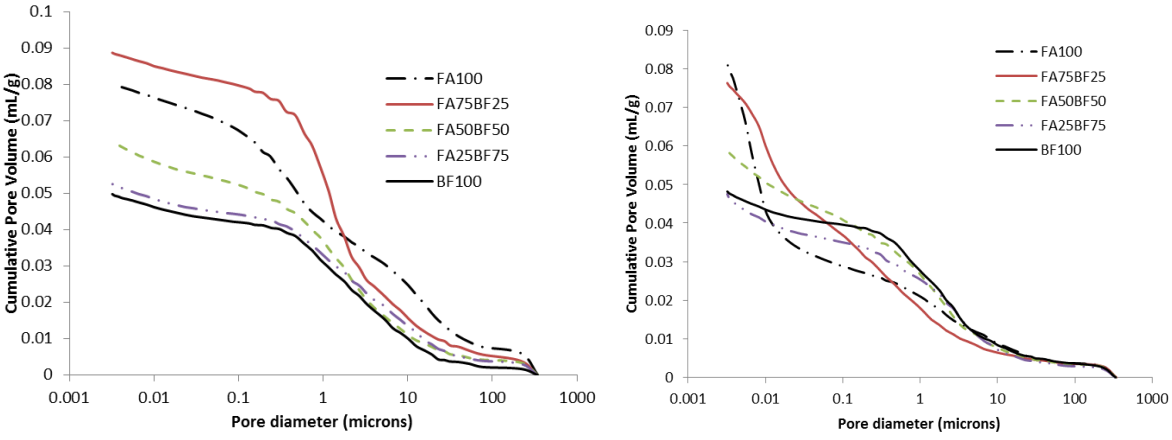

（a） （b）

Fig.3.3.5 Cumulative pore volume results for each specimen (a) 7 days, (b) 28 days

The total pore volume at 28 days also shows the same trend as at 7 days. The specimens FA100

and FA75BF25 with low substitution rate of the ground granulated blast furnace slag were about 0.081 mL/g and 0.076 mL/g, respectively, and the total pore volume of the specimen FA50BF50 was about 0.059 mL/g. specimen BF100 showed the lowest value at 0.048 mL/g, which is considered to be the most densified. In addition, compared with 7 days, the total pore volume of all specimens tended to decrease at 28 days.

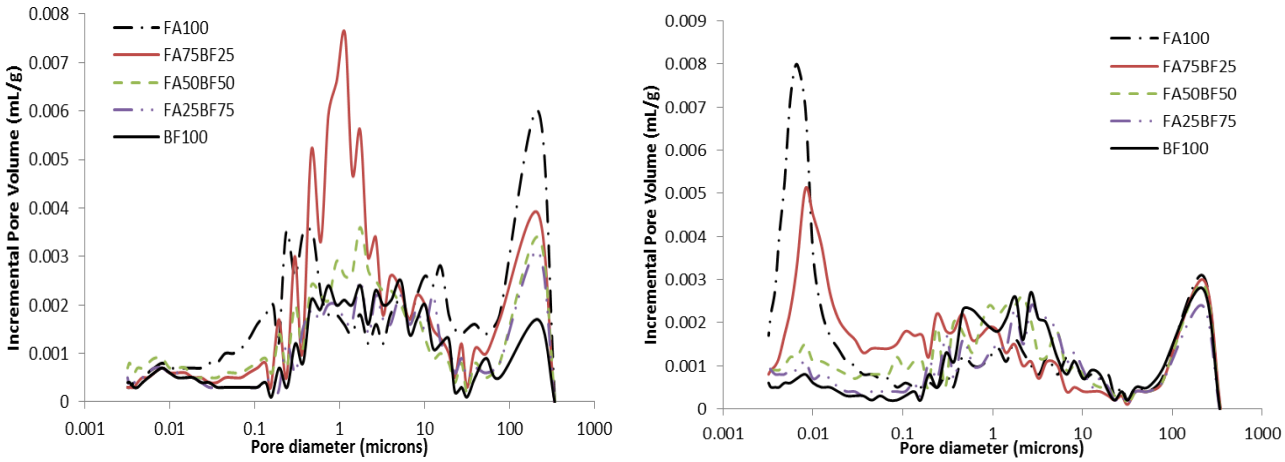

Fig.3.3.6 Result of incremental pore volume of each specimen (a) 7 days, (b) 28 days

Fig.3.3.6 shows the incremental pore volume distribution of the high alkali activated zero-cement mortar. At 7 days, the pore volume of large pore diameter (30μm to 340μm) tended to decrease as the substitution rate of ground granulated blast furnace slag increased. It is believed that the change in pore structure due to the substitution of ground granulated blast furnace slag contributed to the improvement of the compressive strength. The pore volume distribution of the specimen FA100 and FA75BF25 is concentrated on the small pore diameter (0.003μm to 0.05μm). From the results of compressive strength, the compressive strengths of the specimens FA100 and FA75BF25 increased by about 483% and 90% from 7 days, respectively. Consistent

with that, the shift from the large pore diameter to the smaller pore diameter is considered to have led to a significant increase in the compressive strength.

MIP can only measure the pore size between 3 nm and 340 μm, and cannot measure the total porosity. Therefore, saturated water content is used to express the total porosity. As can be seen from the Fig.3.3.7, contrary to the situation of Portland-cement, as the soaking time increases, the water content does not increase and stabilizes. Except for specimen FA25BF75 and FA50BF50 at 28 days, the water content of most samples increased first and then decreased. The main reason is that the specimen FA25BF75 and FA50BF50 reacted sufficiently, and the alkaline activators in the samples had already participated in the reaction to form the gel. The other specimen did not react sufficiently, and there were unreacted alkaline activators in it. After the sample was soaked in water, the sample first absorbed water, and then the alkaline activator in the sample was dissolved in water, therefore, percentage of mass change increase first, then decrease.

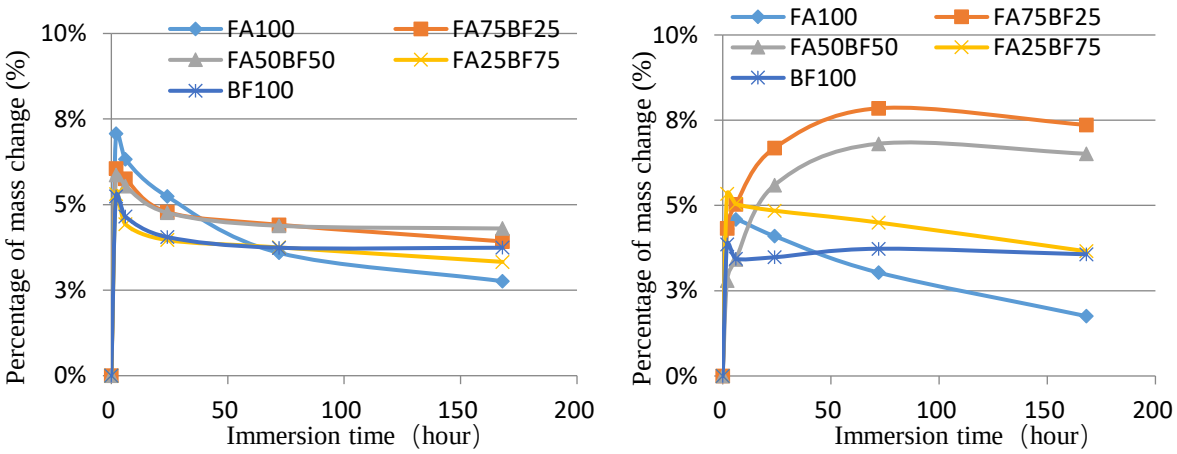

(a) 7days (a) 28days

Fig.3.3.7 Percentage of mass change (%) (a) 7days (b) 28days

For the OPC mortar, Many experiments have been conducted on the relationship between

cement mortar and pore volume strength, and the compressive strength has the highest correlation with the pore volume of more than 50 nm, and relationship between pore volume of more than 50 nm and compressive strength showed exponential approximation (1) [27] [28].

$$F_c = F_0 e^{-bP} \qquad (1)$$

Here, F_c: compressive strength (MPa),

F_0: Compressive strength when porosity is 0,

P: Pore volume (%)

b: Experimental constant.

Based on the literature [27] [28], the pore volume of zero-cement mortar was measured by MIP. In this study, there is no exponential approximate relationship between compressive strength and pore volume of over 50nm. As shown in Fig.3.3.8, relationship between pore volume of more than 50 nm and compressive strength showed a low correlation (R^2 = 0.4457). The main reason is that the main hydration products of cement are almost the same, but when the mixing ratio of BF to FA is different in zero-cement, the main products are changed, and different matrix are formed even in the same pore volume.

Since measuring the porosity with MIP while destroying the pores, there is a possibility that produce error. Therefore, when trying to predict strength more accurately, it is best to use water vapor adsorption method other than MIP to measure the porosity, the results will be more accurate.

In order to analysis the main reaction products of zero-cement, XRD experiments were also conducted below.

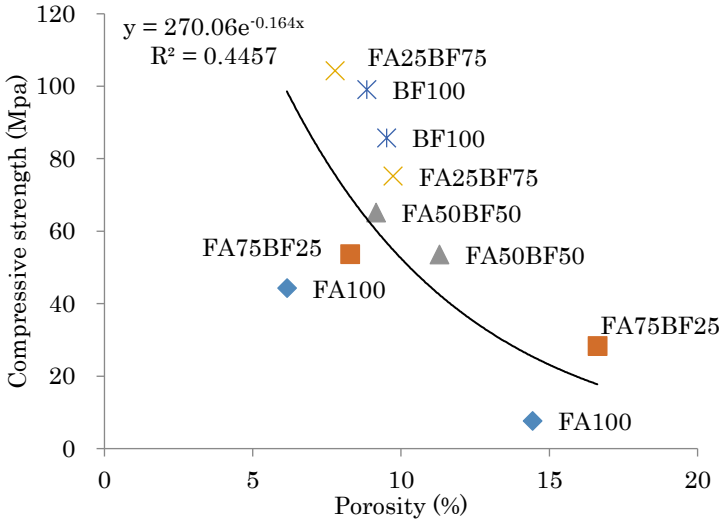

Fig.3.3.8 Relationship between pore volume of bigger than 50 nm and compressive strength

3.3.6 XRD analysis

The XRD results of zero-cement are shown in Fig.3.3.9. The 7days and 28days XRD diagrams showed the same trend. The specimen FA100 is composed of a glass phase indicated by a halo peak of 18 to 35°(2θ) and a crystal phase of quartz, mullite and magnetite. According to previous research results, the glass phase is NASH gel [29].

The specimen FA25BF75 is composed of a glass phase indicated by a halo peak of 28 to 35° (2θ), can be considered as CASH [30], which contributed to the increase of compressive strength, and the 28 days compressive strength became 104.2 MPa. The specimen BF100 showed a large amount of amorphous phase, and the 28 days compressive strength was 99 MPa.

During the condensation and hardening process of zero-cement containing high calcium, possible dissolution-precipitation reactions can be expressed as follows [31].

I. Dissolution of SiO_2, Al_2O_3 and CaO.

$SiO_2+Al_2O_3+OH^- \Rightarrow SiO_2(OH)_2^{2-}$ or $SiO(OH)_3^{-1} + Al(OH)_4^-$

$CaO+H_2O \Rightarrow Ca^{+2} +OH^-$

II. Precipitation reaction

$Ca^{+2} + SiO_2(OH)_2^{2-}$ or $SiO(OH)_3^{-1} + Al(OH)_4^- \Rightarrow$ CASH gel (1)

$Na^{+} + SiO_2(OH)_2^{2-}$ or $SiO(OH)_3^{-1} + Al(OH)_4^- \Rightarrow$ NASH gel (2)

The specimen FA100, which BF is not added, the main product is NASH gel because calcium is insufficient. The main products are different compared with other BF-added specimens, and the specimen FA100 deviates from the exponential relationship between the pore volume and compressive strength (Fig.3.3.8).

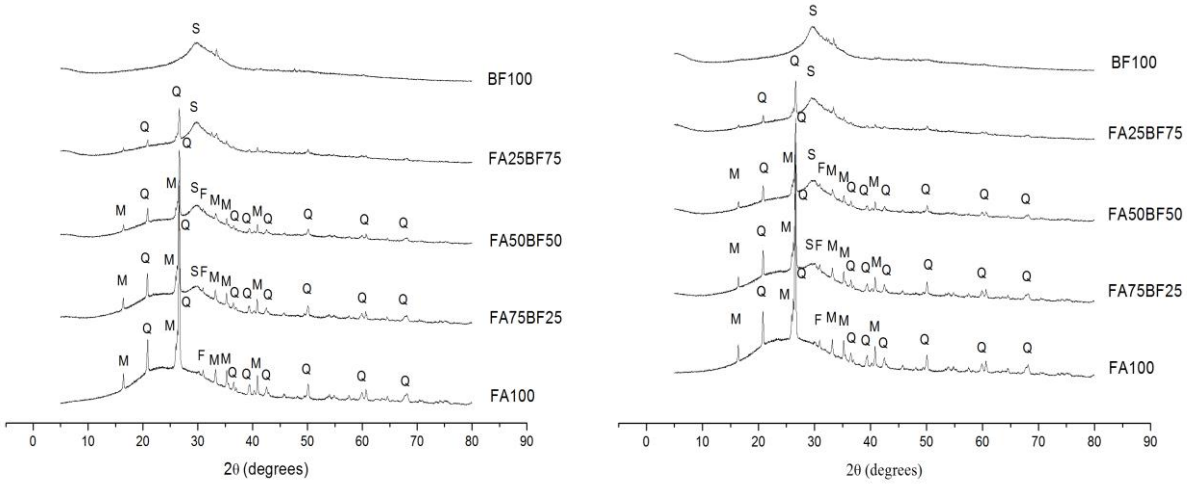

（a） （b）

Q = Quartz (SiO_2), M = Mullite ($Al_6Si_2O_{13}$), F=Magnetite (Fe_3O_4),

S=Calcium Silicate Hydrate

Fig.3.3.9 XRD of each specimen (a) 7 days, (b) 28 days

The reaction products of zero-cement is mainly amorphous phases, in order to clarify the relationship between the amount of gel produced and the compressive strength, the amount of gel formation needs to be measured.

3.3.7 Quantitative measurement of gel content

Total amorphous content is equal to gel content plus unreacted part of slag plus unreacted amorphous part of fly ash. If we can measure total amorphous content, unreacted part of slag and unreacted amorphous part of fly ash, then we can get the amount of gel formation. The equation is as follows:

Total amorphous content = Gel content + unreacted part of slag + unreacted amorphous part of fly ash

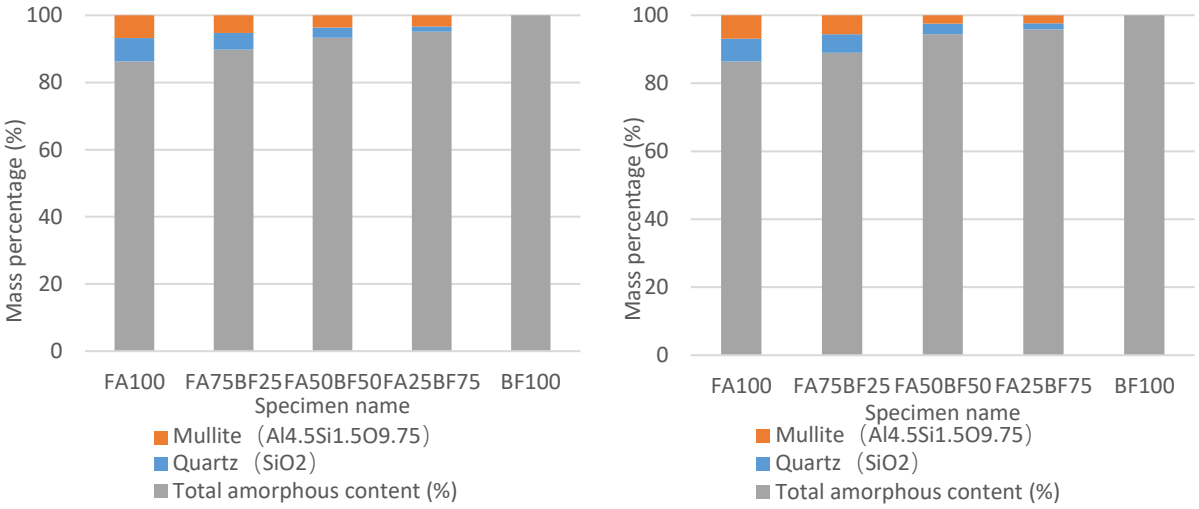

(a) 7days (b) 28days

Fig.3.3.10 Crystalline and total amorphous content of each specimen (a) 7days (b) 28days (Quantitative analysis by XRD-whole powder pattern fitting)

In order to obtain the gel amount of each specimen, it is necessary to measure the total amorphous content, unreacted part of slag and unreacted amorphous part of fly ash. The measurement results are as follows:

Fig.3.3.10 shows the results of crystalline and total amorphous content of each specimen at 7 days and 28 days, we can get this data from XRD quantitative analysis. Fig.3.3.11 shows the

results of unreacted fly ash and unreacted slag. It shows that the difference in the amount of unreacted slag and unreacted fly ash is not much different between 7 days and 28 days, which indicates that the reaction of the high alkali activated zero-cement is fast. As the curing age increases, the unreacted fly ash and slag decreases.

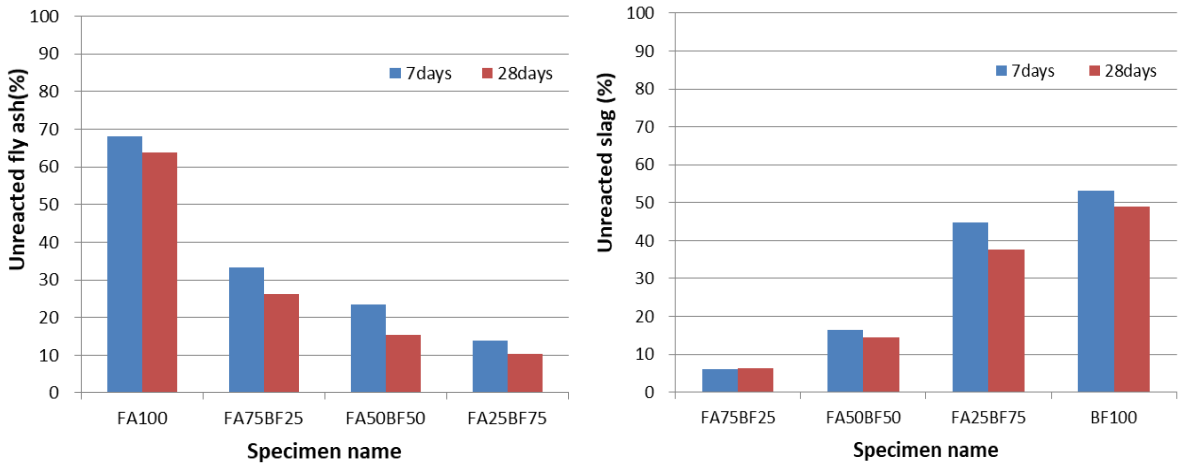

(a) (b)

Fig.3.3.11 (a) unreacted fly ash and (b) unreacted slag

Fig.3.3.12 shows the total mass percentage of reacted and unreacted FA&BF (%) at 7 days and 28 days. Overall, the 28 days mass percentage of reacted FA and reacted BF is greater than the 7 days mass percentage. 7 days and 28 days have the same change law, as the amount of BF used increases, the mass percentage of reacted BF increases. As the amount of FA used decreases, the mass percentage of reacted FA increases first and then decreases.

Fig.3.3.13 shows reaction degree of fly ash and slag (%) at 7days and 28days.The mixing ratio of FA and BF has an important influence on the reaction degree of raw materials. Overall, the 28 days reaction degree of FA and BF is greater than the 7 days reaction degree. As the amount of BF used increases, the reaction degree of FA increases first and then decreases. Gao X et

al.[32] demonstrates that the addition of slag into fly ash, the slag reactivity is reduced while the reaction degree of fly ash is increased and confirming an interaction between the precursors. FA-BF blended binder system leads to a more complicated chemistry, and usually presents coexisting N-A-S-H and C-(A)-S-H type gels. The results in this study shows similar tendency regarding the effect of slag-fly ash blends on the reaction degree.

While the reaction degree of BF shows a decreasing trend, as the amount of BF used increases. The main reason may be that excessive BF results in premature precipitation of CASH gel, which prevents the further dissolution of BF and lead to reducing the reaction degree of BF.

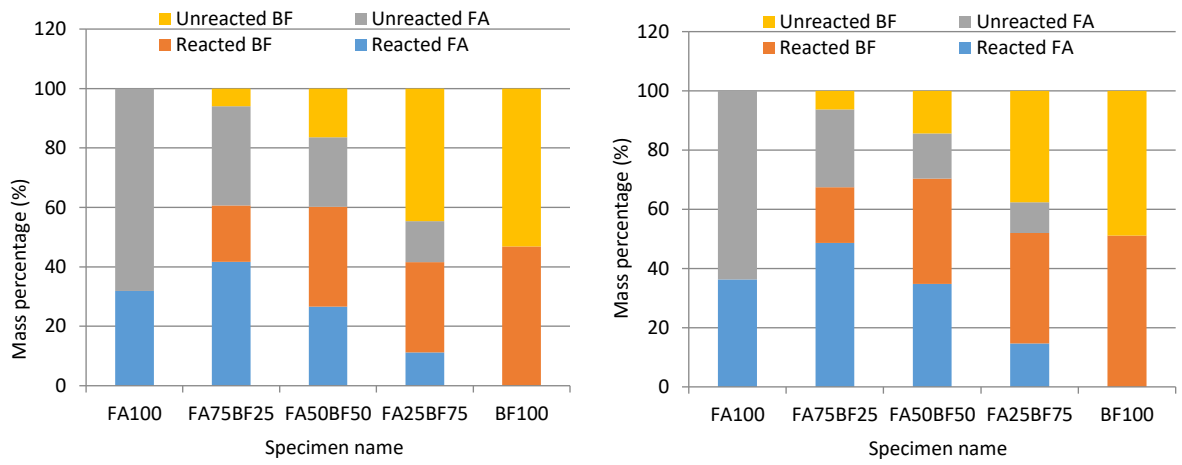

(a) (b)

Fig.3.3.12 Total mass percentage of reacted and unreacted FA&BF (%)

(a) 7days; (b) 28days

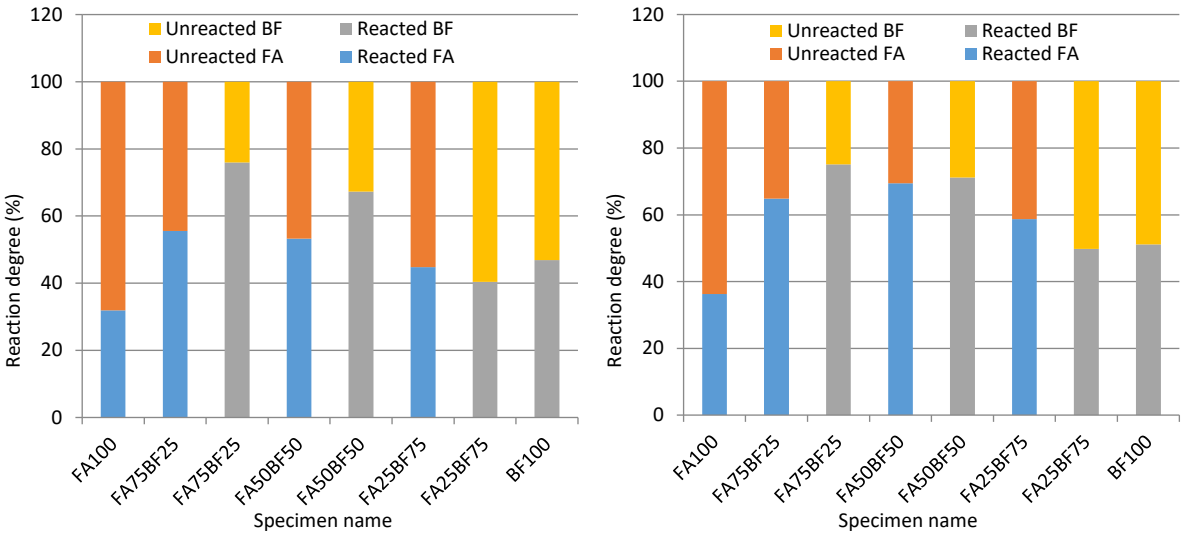

(a) (b)

Fig.3.3.13 Reaction degree of fly ash and slag (%) (a) 7days; (b) 28days

In order to get unreacted amorphous part of fly ash. It should subtract the crystal content of quartz and mullite from unreacted fly ash, Table.3.3.7 and Table.3.3.8 show the unreacted amorphous part of fly ash at 7days and 28days.

Table.3.3.7 Unreacted amorphous part of fly ash content (7days)

Unreacted fly ash (%)	Quartz (%)	Mullite (%)	Unreacted amorphous part of fly ash (%)
68.12	6.98	6.80	54.34
33.32	5.00	5.21	23.11
23.39	3.09	3.61	16.69
13.80	1.50	3.33	8.97
0.00	0.00	0.00	0.00

Table.3.3.8 Unreacted amorphous part of fly ash content (28days)

Unreacted fly ash (%)	Quartz (%)	Mullite (%)	Unreacted amorphous part of fly ash (%)
63.69	6.70	6.89	50.10
26.34	5.49	5.58	15.28
15.26	3.09	2.49	9.68
10.32	1.82	2.34	6.16
0.00	0.00	0.00	0.00

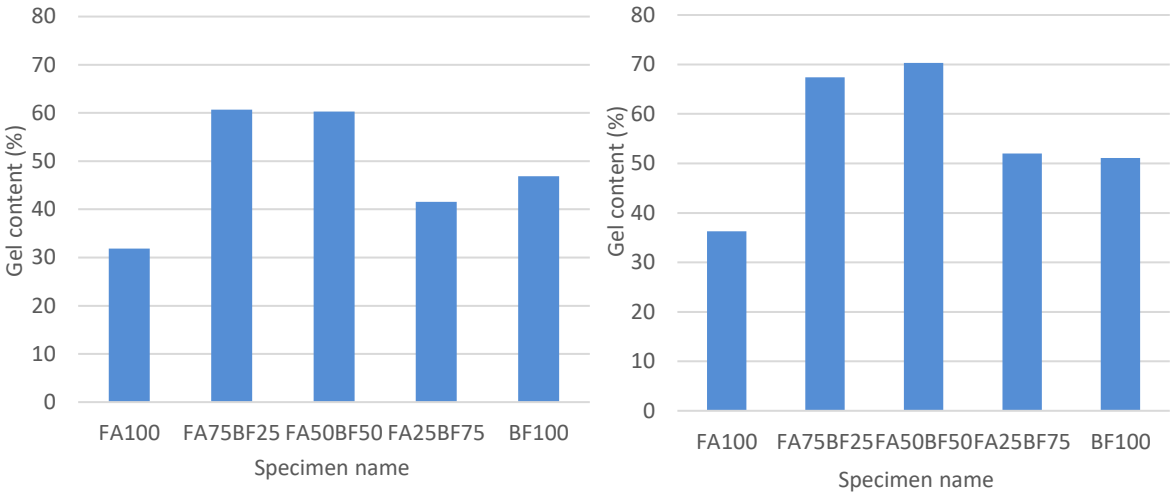

(a) 7days (b) 28days

Fig.3.3.14 Gel content of each specimen (a) 7days (b) 28days

From the previous measurement results, the gel content can be calculated. Fig.3.3.14 shows the results of gel content of each specimen at 7days and 28days. Specimen FA75BF25 and specimen FA50BF50 produced more gels, about 60% of the gels were generated in 7 days, and about 70% of the gels were generated in 28 days. This result is consistent with the water content. Except for specimen FA25BF75 and FA50BF50 at 28 days, the water content of most specimens increased first and then decreased. The main reason is that the specimen FA25BF75 and

FA50BF50 reacted sufficiently, and the alkaline activators in the samples had already participated in the reaction to form more gel. The other specimen did not react sufficiently, the presence of alkali activator did not participate in the reaction, so less gel was formed.

The Fig.3.3.15 shows the relationship between gel content and compressive strength. Specimen FA75BF25 and FA50BF50 had the highest gel content, but not the highest strength. The compressive strength of alkali-activated materials is not simply determined by the gel content. The type of gel also has a huge effect on the strength. It can be considered that the contribution of higher Ca/Si ratio type gels to strength is greater.

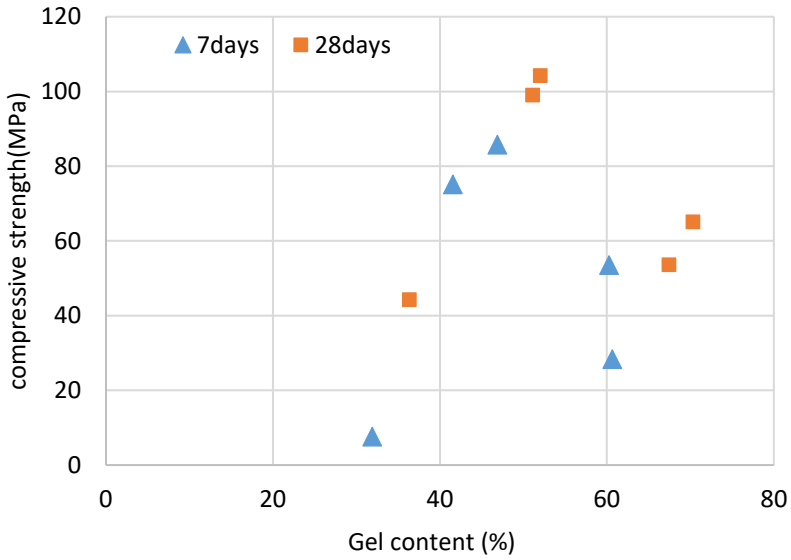

Fig.3.3.15 The relationship between gel content and compressive strength

3.3.8 TG analysis

Fig.3.3.16 and Fig.3.3.17 show the TGA and DTA curves of the hardened pastes for 7day and 28day curing. The mass loss temperature range of CH usually in 450°C~550°C, and the generated calcium carbonation have a broader temperature range between 550°C and 850°C. Zhang J et al. [33] reported that the solvent-exchanged samples have an obvious weight loss after

600 °C and keep losing weight until after 1000 °C. Isopropanol causes the least weight loss, followed by tetrahydrofuran and ethanol; acetone causes the largest weight loss. The reaction product, diacetone alcohol, (boiling point 166 °C) may adsorb on portlandite crystals; when heated in the TGA, the film may react with the surface of the portlandite to form calcium carbonate, which is decarbonated at higher temperature. Other solvents, such as ethanol and isopropanol, adsorption on portlandite crystals is possible.

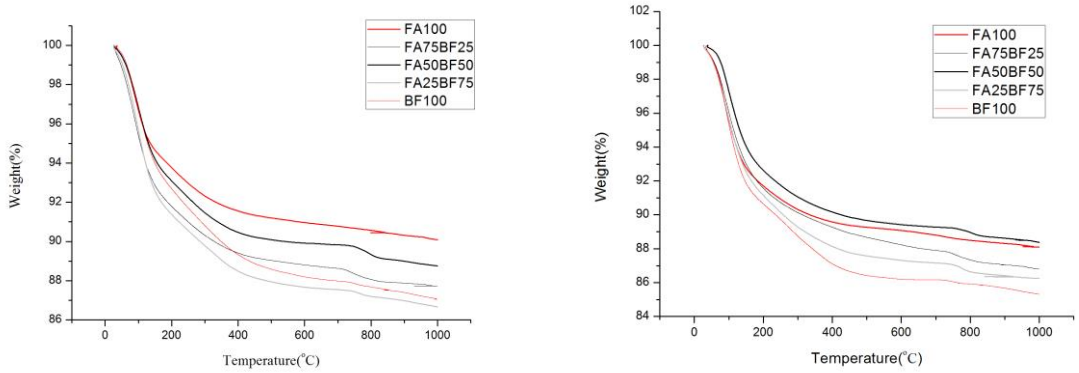

（a） （b）

Fig.3.3.16 Result of the TG analysis at (a) 7 days, (b) 28 days

DeJong MJ et al. [34] reported that the derivative of the mass loss clearly shows the primary range of C-S-H dehydration between 105 °C and 300 °C. Some studies [35-36] reported that the maximum weight loss peaks are found between 100 °C and 300 °C. the first peak is located around 110 °C, which is related to the removal of physically bound water present within the pores of binding gels, which are either N-A-S-H type gels or C-(A)-S-H gels. Kapeluszna E et al. [37] demonstrates that the C-(A)-S-H gel dehydration peak located around 110 ° C.

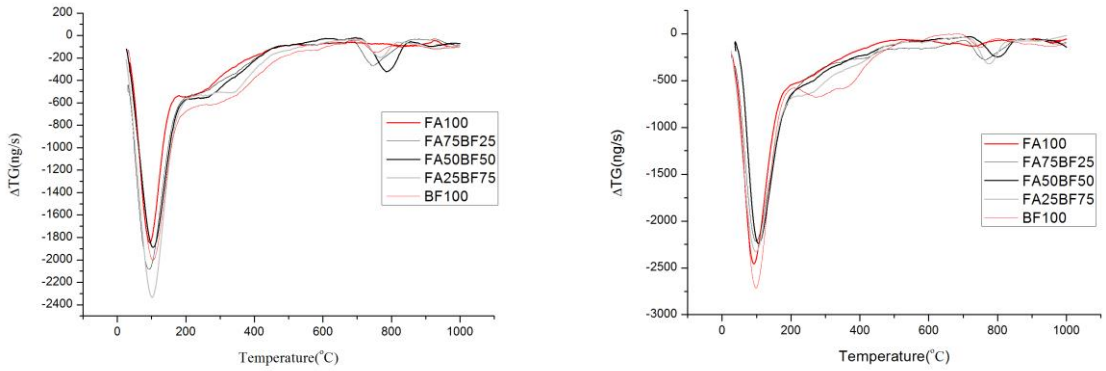

（a） （b）

Fig.3.3.17 Result of the DTG analysis at (a) 7 days, (b) 28 days

This study uses the weight loss ratio of 105 °C to 300 °C to indirectly characterize the bound water within the pores of N-A-S-H type gels or C-(A)-S-H gels.

The amount of weight loss ratio (W) (105℃-300℃) are expressed as% of the dry sample weight at 300 ℃ (W_{300}):

$$W = \frac{W_{105} - W_{300}}{W_{300}}$$

The bound water content is obtained by the difference between the weight losses of samples dried to 105 and at 1000°C, which is a widely used technique to assess the degree of Portland cement reaction. However, this method is not appropriate. The cement hydrates particularly C-S-H, ettringite and monosulfate–lose part of their chemically combined water below 105°C. In addition, the weight loss due to the decomposition of carbonates is included when the interval 105 to 1000°C is used [38]. In this study, the amount of hydrate water (H) are expressed as% of the dry sample weight at 550 ℃ (W_{550}) [39]:

$$H = \frac{W_{40} - W_{550}}{W_{550}}$$

Fig.3.3.18 show the relationship between bound water and compressive strength. Fig.3.3.19 show the relationship between weight loss ratio(105℃-300℃) and compressive strength. It shows that compressive strength have a good linear relationship with the weight loss ratio (W) (105℃-300℃) (R^2=0.8792).

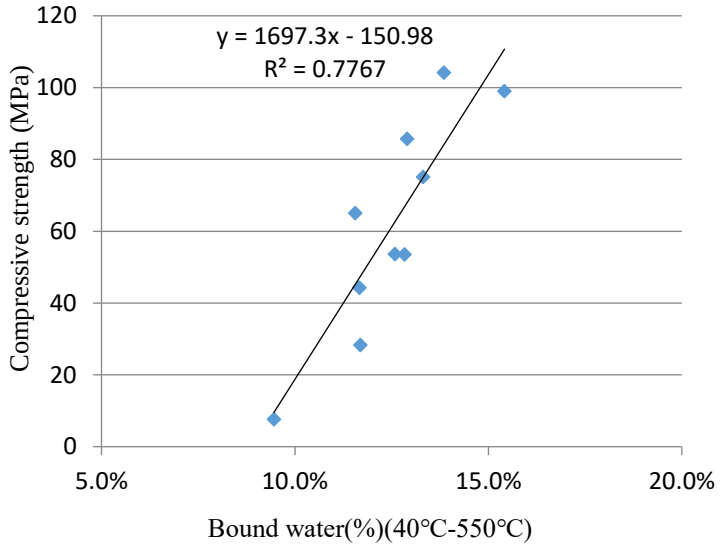

Fig.3.3.18 the relationship between bound water and compressive strength

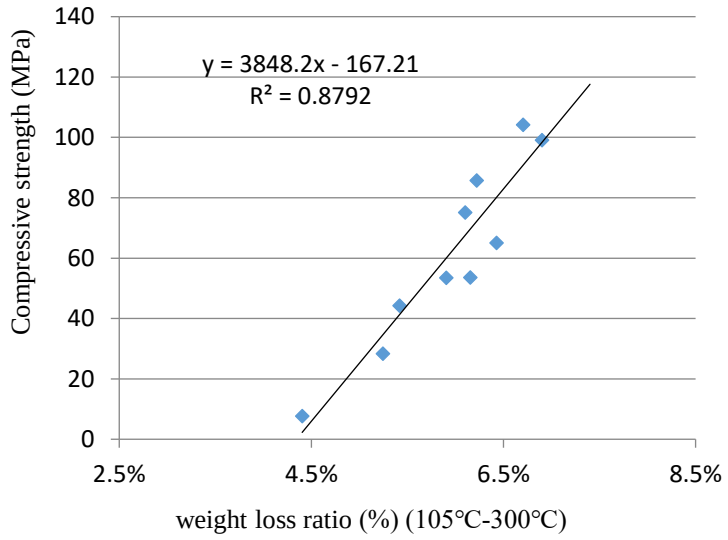

Fig.3.3.19 the relationship between weight loss ratio (105℃-300℃) and compressive strength

3.3.9 Evaluation of compressive strength: strength index

The compressive strength of cement concrete is mainly determined by the type and amount of reaction products and the pore structure of the hardened body [40]. As a hardened body, zero-cement will produce a hardened structure similar to cement. Therefore, the compressive strength of zero-cement mortar is also mainly determined by the type and amount of reaction products and pore structure of the hardened body. Therefore, in order to develop a single and comprehensive index to evaluate the compressive strength of zero-cement. A general format for such an index can be sketched as follows:

$$C = f(RP) \cdot f(P)$$

Here, C: compressive strength;

RP: types and amounts of reaction products;

P: pore structure

In this study, the strength index is proposed to evaluate the compressive strength of zero-cement. Produce more and stronger reaction products, the higher the compressive strength. The denser the pore structure, the higher the compressive strength. The amount of main reaction products can be evaluated by the amount of bound water of binding gels, and weight loss ratio (105℃-300℃) is related to the removal of physically bound water present within the pores of binding gels. The pore structure can be evaluated by the porosity. Therefore, a preliminary equation is proposed to simply link reaction products and pore structure as follow:

$$I = \frac{100 * W}{P}$$

Here, I: strength index

W: Weight loss ratio (105℃-300℃) (%)

P: Porosity (%)

For the porosity, it can be simply expressed as the percentage of water content of hardened body. Here, try to express its porosity with the percentage of water content. Fig.3.3.20 show the relationship between strength index (calculated by W and S (percentage of water content)) and compressive strength. It can be seen from the figure that the strength and strength index have a low correlation. Therefore, in the case of high alkaline activation, it is not appropriate to use percentage of water content to express porosity as an index. Because the unreacted highly alkaline activator present in the alkali-activated zero-cement will dissolve in the water, the quality of the sample is reduced, resulting in the inability to accurately measure the porosity.

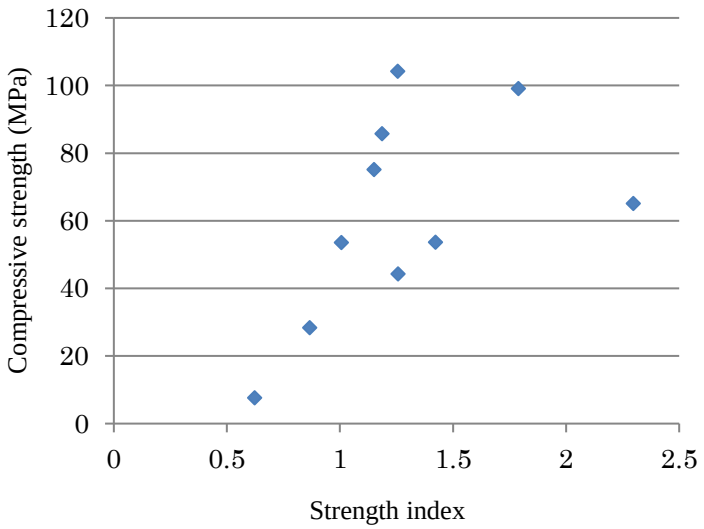

Fig.3.3.20 the relationship between strength index (calculated by W and S) and strength

In order to accurately represent the porosity of zero-cement, the porosity results obtained by MIP measurement are used here. The strength index is shown in Table.3.3.9. Fig.3.3.21 show the relationship between strength index (calculated by W and P) and compressive strength. It can be seen from the figure that the strength and strength index have a high correlation (R=0.9533), so it is effective to use the strength index to evaluate the compressive strength of the zero-cement mortar. Therefore, the compressive strength can be predicted by the dehydration amount at 105 to 300°C and the porosity.

Since measuring the porosity with MIP while destroying the pores, there is a possibility that produce error. Therefore, when trying to predict strength more accurately, it is best to use water vapor adsorption method other than MIP to measure the porosity, the results will be more accurate.

Table.3.3.9 Strength index (calculated by W and P)

Sample	Weight loss ratio (%) (105℃-300℃)	Porosity （%）	Strength index	Mortar strength (MPa)
FA100	4.40%	16.47%	26.7	7.6
FA75BF25	5.24%	18.18%	28.8	28.3
FA50BF50	5.90%	13.57%	43.5	53.5
FA25BF75	6.10%	11.40%	53.5	75.2
BF100	6.22%	11.06%	56.2	85.7
FA100	5.42%	16.35%	33.1	44.3
FA75BF25	6.15%	15.51%	39.7	53.6
FA50BF50	6.43%	12.54%	51.2	65.1
FA25BF75	6.70%	10.23%	65.5	104.2
BF100	6.90%	10.60%	65.1	99.0

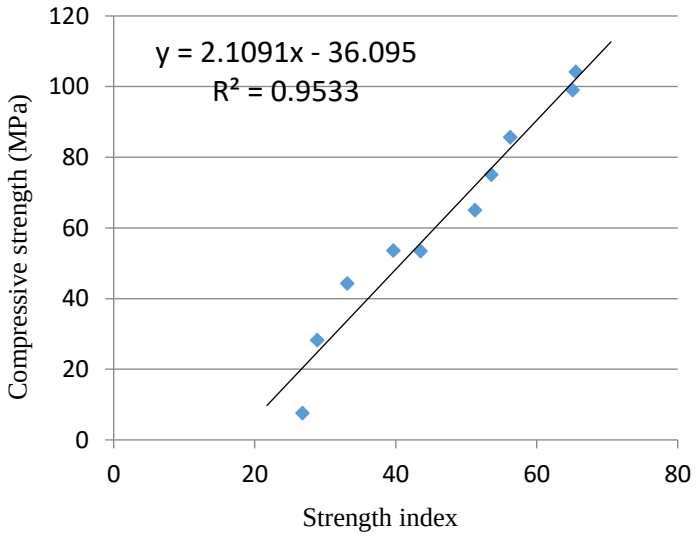

Fig.3.3.21 The relationship between strength index (calculated by W and P) and strength

3.4 Conclusions

Based on the results conducted in this chapter, the following conclusions can be inferred:

(1) The optimum combination is achieved by 50 wt% Slag8000, NaOH concentration of 10 M and silica modulus M=2, the compressive strength reach up to 113.3 MPa. NaOH concentration (M/L) have the highest contribution to compressive strength.

(2) Crystallization occurred in Solutions of modulus 0.4−1.0. Therefore, when preparing the alkali activator, the solutions of modulus should be avoided within the range of 0.4−1.0.

(3) As the substitution rate of blast furnace slag increases, the workability of mortar increases first and then decreases. Specimen FA50BF50 showed the best workability. Even if each mortar was given 15 falling movements, each specimen increased only about 20 mm, which showed high viscosity.

(4) At 7 days, the compressive strength tended to increase as the substitution rate of ground granulated blast furnace slag increased. The 7 days compressive strength of the specimen BF100 was 86 MPa. At 28 days, the specimen FA25BF75 showed the highest strength instead

of the specimen BF100, and its compressive strength reached up to 104 MPa.

(5) The total pore volume tended to decrease as the substitution rate of ground granulated blast furnace slag increased. Compared with 7 days, the total pore volume of all the specimens decrease at 28 days. The compressive strengths of the specimens FA100 and FA75BF25 increased by about 483% and 90% from 7 days, respectively. Consistent with that, the shift from the large pore diameter to the smaller pore diameter is considered to have led to a significant increase in the compressive strength.

(6) Unlike cement mortar, the compressive strength of high alkali activated zero-cement mortar showed a low correlation with the pore volume of more than 50 nm, and it was considered that it was related to the reaction products of high alkali activated zero-cement.

(7) Hardened paste of high alkali activated zero-cement is mainly composed of the amorphous phase indicated by a halo peak of 18 to 35°(2θ) and unreacted crystal phase.

(8) Specimen FA75BF25 and FA50BF50 had the highest gel content, but not the highest strength. The compressive strength of zero-cement is not simply determined by the gel content, the type of gel also has a huge effect on the strength.

(9) The strength and strength index have a high correlation (R^2=0.9533), so it is effective to use the strength index to evaluate the compressive strength of the zero-cement.

References

(1) Atis C, Gorur E, Karahan O, Bilim C, Ilkentapar S, Luga E: Very high strength (120 MPa) class F fly ash geopolymer mortar activated at different NaOH amount, heat curing temperature and heat curing duration. Constr Build Mater 2015;96:673-678.

(2) Phoo-ngernkham T, Maegawa A, Mishima N, Hatanaka S, Chindaprasirt P: Effects of sodium hydroxide and sodium silicate solutions on compressive and shear bond strengths of FA–GBFS geopolymer. Constr Build Mater 2015;91:1-8.

(3) Khan M, Shaikh F, Hao Y, Hao H: Synthesis of high strength ambient cured geopolymer composite by using low calcium fly ash. Constr Build Mater 2016;125:809-820.

(4) Chi M, Huang R: Binding mechanism and properties of alkali-activated fly ash/slag mortars. Constr Build

Mater 2013;40:291-298.
(5) Lloyd RR: The durability of inorganic polymer cements: The University of Melbourne; 2008.
(6) 一宮一夫,原田耕司,津郷俊二,池田攻:活性フィラーにフライアッシュと高炉スラグ微粉末を用いたジオポリマーの耐酸性と高温特性,コンクリート工学年次論文集,Vol. 35, No. 1, pp. 2005-2010, 2013. 7.
(7) I. Türkmen, R. Gül, C. Çelik, A Taguchi approach for investigation of some physical properties of concrete produced from mineral admixtures, Build. Environ. 43 (6) (2008) 1127–1137.
(8) Hadi MNS, Farhan NA, Sheikh MN. Design of geopolymer concrete with GGBFS at ambient curing condition using Taguchi method. Constr Build Mater 2017;140:424-431.
(9) G. Khalaj, S.E.S. Hassani, A. Khezrloo, Split tensile strength of OPC-based geopolymers: application of DOE method in evaluating the effect of production parameters and their optimum condition, Ceram. Int. 40 (7) (2014) 10945–10952.
(10) M. Olivia, H. Nikraz, Properties of fly ash geopolymer concrete designed by Taguchi method, Mater. Des. 36 (2012) 191–198.
(11) S. Riahi, A. Nazari, D. Zaarei, G. Khalaj, H. Bohlooli, M.M. Kaykha, Compressive strength of ash-based geopolymers at early ages designed by Taguchi method, Mater. Des. 37 (2012) 443–449.
(12) Nazari A, Bagheri A, Riahi S. Properties of geopolymer with seeded fly ash and rice husk bark ash. Mater Sci Eng A 2011;528(24):7395–401.
(13) Sata V, Sathonsaowaphak A, Chindaprasirt P. Resistance of lignite bottom ash geopolymer mortar to sulfate and sulfuric acid attack. Cem Concr Compos 2012;34(5):700–8.
(14) Sukmak P, Horpibulsuk S, Shen S-L. Strength development in clay-fly ash geopolymer. Constr Build Mater 2013;40:566–74.
(15) Ridtirud C, Chindaprasirt P, Pimraksa K. Factors affecting the shrinkage of fly ash geopolymers. Int J Miner Metall Mater 2011;18(1):100–4.
(16) Guo X, Shi H, Dick WA. Compressive strength and microstructural characteristics of class C fly ash geopolymer. Cem Concr Compos 2010;32(2):142–7.
(17) Law D, Adam A, Molyneaux T, Patnaikuni I, Wardhono A. Long term durability properties of class F fly ash geopolymer concrete. Mater Struct 2014:1–11.
(18) Gorhan G, Kurklu G. The Influence of the NaOH solution on the properties of the fly ash–based geopolymer mortar cured at different temperatures. Composites B Eng 2013.
(19) Somna K, Jaturapitakkul C, Kajitvichyanukul P, Chindaprasirt P. NaOHactivated ground fly ash geopolymer cured at ambient temperature. Fuel 2011;90(6):2118–24.
(20) Jaturapitakkul C, Somna K. NaOH-activated ground fly ash geopolymer cured at ambient temperature. Fuel 2011;90:2118–24.
(21) Rattanasak Ubolluk, Chindaprasirt Prinya. Influence of NaOH solution on the synthesis of fly ash geopolymer. Miner Eng 2009;22(12):1073–8.
(22) Provis J, Kilcullen A, Duxson P, Brice D, van Deventer J. Stabilization of Low-Modulus Sodium Silicate Solutions by Alkali Substitution. Ind Eng Chem Res 2012;51(5):2483-2486.
(23) S. Puligilla, P. Mondal, Co-existence of aluminosilicate and calcium silicate gel characterized through

selective dissolution and FTIR spectral subtraction, Cem.Concr. Res. 70 (2015) 39–49.

(24) 玲奈 石, 豊春 名, 孝広 佐. 加熱試料を用いたX線回折─リートベルト法による高炉セメント中のスラグ反応率測定法の検討. セメント・コンクリート論文集 2015;69(1):76-81.

(25) S. Songpiriyakij, T. Kubprasit, C. Jaturapitakkul, P. Chindaprasirt: Compressive strength and degree of reaction of biomass-and fly ash-based geopolymer, Constr. Build. Mater. 24 (3) (2010) 236–240.

(26) Samantasinghar S, Singh SP: Effect of synthesis parameters on compressive strength of fly ash-slag blended geopolymer. Constr Build Mater 2018;170:225-234.

(27) P.K. Mehta, P.J. Monteiro, M.-H: Education, Concrete: Microstructure, Properties, and Materials, McGraw-Hill, New York, 2006.

(28) 内川 浩, 羽原 俊祐, 沢木 大介: 混合セメントモルタル及びコンクリートの硬化体構造が強度発現性状に及ぼす影響, セメント・コンクリート論文集 No.44,1990.

(29) Provis JL, Bernal SA. Geopolymers and Related Alkali-Activated Materials. Annual Review of Materials Research 2014;44(1):299-327.

(30) Hunnicutt WA: Characterization of calcium-silicate- hydrate and calciumalumino-silicate-hydrate: University of Illinois at UrbanaChampaign; 2013.

(31) Chindaprasirt P, De Silva P, Sagoe-Crentsil K, et al: Effect of SiO_2 and Al_2O_3 on the setting and hardening of high calcium fly ash-based geopolymer systems [J]. Journal of Materials Science, 2012, 47(12): 4876-4883.

(32) Gao X, Yu Q L, Brouwers H J H. Apply 29Si, 27Al MAS NMR and selective dissolution in identifying the reaction degree of alkali activated slag-fly ash composites[J]. Ceramics International, 2017, 43(15): 12408-12419.

(33) Zhang J, Scherer GW. Comparison of methods for arresting hydration of cement. Cem Concr Res 2011;41(10):1024-1036.

(34) DeJong MJ, Ulm F. The nanogranular behavior of C-S-H at elevated temperatures (up to 700 °C). Cem Concr Res 2007;37(1):1-12.

(35) S.A. Bernal, E.D. Rodríguez, R. Mejía de Gutiérrez, M. Gordillo, J.L. Provis, Mechanical and thermal characterization of geopolymers based on silicate-activated metakaolin/slag blends, J. Mater. Sci. 46 (16) (2011) 5477–5486.

(36) Khan M Z N, Hao Y, Hao H. Synthesis of high strength ambient cured geopolymer composite by using low calcium fly ash[J]. Construction and Building Materials, 2016, 125: 809-820.

(37) Kapeluszna E, Kotwica Ł, Różycka A, et al. Incorporation of Al in CASH gels with various Ca/Si and Al/Si ratio: Microstructural and structural characteristics with DTA/TG, XRD, FTIR and TEM analysis[J]. Construction and Building Materials, 2017, 155: 643-653.

(38) K Scrivener, R Snellings, B Lothenbach. A Practical Guide to Microstructural Analysis of Cementitious Materials.2016.

(39) De Weerdt K, Haha MB, Le Saout G, Kjellsen KO, Justnes H, Lothenbach B. Hydration mechanisms of ternary Portland cements containing limestone powder and fly ash. Cem Concr Res 2011;41(3):279-291.

(40) 反応モデル解析研究委員会報告書, 1996, 日本コンクリート工学協会.

4. Development of low alkali activated zero-cement mortar

4.1 Introduction

The chemical activator has a significant effect on strength development of the alkali activated zero-cement. Therefore, the choice of alkali activator is crucial. Current typical alkali activators are high alkali such as NaOH and Na_2SiO_3. Although the use of these highly alkaline activators can achieve high strength development, there are also many practical problems, such as high cost, dangerous chemical corrosion and quick setting time [(1)]. Besides, in highly alkaline environments, the water reducer does not work.

$Ca(OH)_2$ and CaO are much less expensive than NaOH or Na_2SiO_3. Also, it is not strongly corrosive and the water reducer will work. So there are potential alternatives as low alkali activators. There are some studies [(1-8)] that use CaO or $Ca(OH)_2$ as a low alkali activator to activate waste by-products, but none of these studies systematically clarify the relationship between compressive strength and various influencing factors.

This chapter are devoted to study the development of low alkali activated zero-cement mortar. Elucidate the relationship between influencing factors and compressive strength. Considering factors such as the amount of alkaline activator used and curing conditions, ratio of chemical components, W/B ratio, particle size distribution, type of material, etc. Besides, the strength index is proposed to evaluate the strength of zero-cement mortar.

4.2 Preliminary experiment for comparison of low alkali and high alkali activated zero-cement mortar

4.2.1 Materials and Experimental Methods

As a preliminary experiment, the purpose of the study in this section is to confirm the feasibility of using low-alkaline activator to develop high-strength zero-cement, and to compare the

compressive strength of high-alkali and low-alkali activated zero-cement.

The materials used in this study to make zero-cement mortar were comprised of fly ash, granulated blast furnace slag, silica fume, sodium hydroxide (NaOH). Table.4.2.1 presents the materials used. Table.4.2.2 show the proportion and workability.

Table.4.2.1 Materials used

	Material	Material characters	Symbol
Binder（B）	Fly ash Type I	Density:2.4g/cm^3, Specific surface area:5680cm^2/g	FA
	Silica fume		SF
	Slag	Density:2.89g/cm^3, Specific surface area:4370cm^2/g	BF
	Alkali avtivator	CaO-expansion material	EX
Chemical admixture	High performance water reducing agent		SP
	Defoamer		AF
Fine aggregate	Ferro-nickel slag	Absolute dry density: 2.9g/cm^3, water absorption:2.15%	S

Table.4.2.2 Proportion and workability

Sample	W/B[%]	B mass ratio (SF:FA:BF)	FNS/B	Concentration of NaOH (mol/L)	EX[B×%]	AF[B×%]	SP[B×%]	Workability [mm]
1-1	12	1.5 : 2 : 6.5	1.6 : 1	/	3.5	0.003	1.3	220
1-2	12	1.5 : 2.5 : 6	1.6 : 1	/	3.5	0.003	1.3	244
1-3	12	1.5 : 3 : 5.5	1.6 : 1	/	3.5	0.003	1.3	246
1-4	12	1.5 : 3.5 : 5	1.6 : 1	/	3.5	0.003	1.3	227
2-2	20	1.5 : 2.5 : 6	1.6 : 1	12M	0	0	0	122
2-3	20	1.5 : 3 : 5.5	1.6 : 1	12M	0	0	0	128
2-4	20	1.5 : 3.5 : 5	1.6 : 1	12M	0	0	0	126

4.2.2 Compressive strength

The Fig.4.2.1 shows that the longer the curing age, the higher the compressive strength. The

specimens 1-2 (SF: FA: BF = 1.5: 2.5: 6) are optimal. The compressive strength at 3 days increased to 35 MPa and the compressive strength at 28 days increased to 95 MPa.

The series 2 (NaOH-activated) specimens are small overall as compared with the series1 (CaO-activated) specimens. At 3 days, the higher the amount of BFS used, the higher the compressive strength. However, at 28 days, the compressive strength of the specimen with relatively little amount of BFS used is higher. It shows that it is possible to develop a high strength zero-cement mortar by using low alkaline activator.

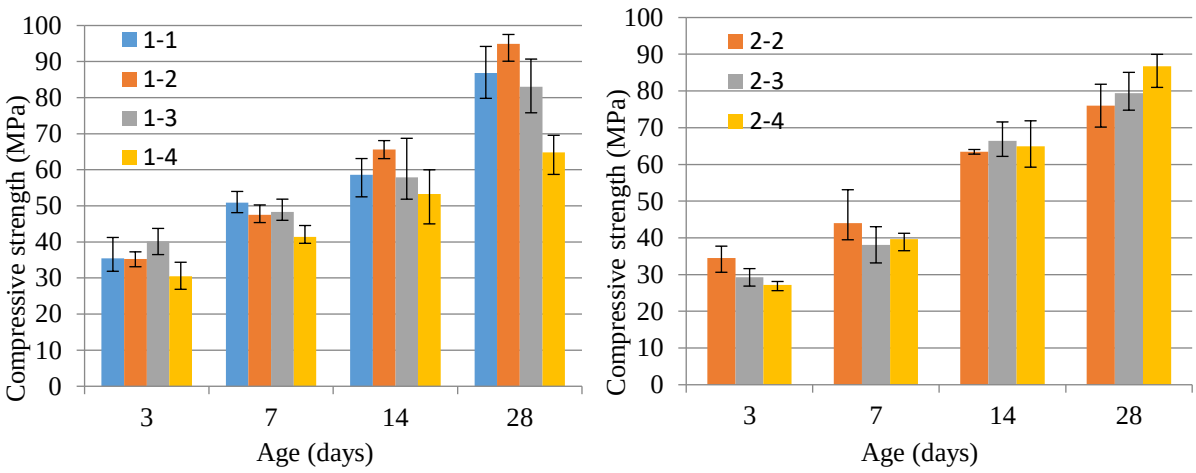

Fig.4.2.1 Compressive strength

For the compressive strength of low alkali activated zero-cement mortar, compressive strength is mainly affected by various factors such as alkali activator content, curing regime, zero-cement's RCaO, RAl_2O_3 and $RSiO_2$ content, water/binder ratio, particle size distribution and type of raw materials. In order to study the influence of various factors on the strength of zero-cement, the following series of experiments were conducted.

4.3 Effects of alkali activators content and curing condition

4.3.1 Materials and Experimental Methods

If there is not enough CaO alkali activator, it will not be able to produce strength; while excessive CaO alkali activator will cause expansion cracking. Therefore, it is very important to study the appropriate amount of CaO. In addition, the curing conditions should not be ignored for strength development. The purpose of this section is to study the effects of the amount of alkali-activator and curing conditions on compressive strength.

The materials used in this study to make zero-cement mortar were comprised of granulated blast furnace slag, silica fume and low alkali activator. Table.4.3.1 presents the materials used. Table.4.3.2 and Table.4.3.3 show the SF and BF chemical composition. Table.4.3.4 shows the factors and level of experiment. The water/binder ratio is 14% and the fine aggregate/binder weight ratio is 1.4: 1. The mix proportion of the raw materials used are fixed at binder mass ratio (SF: BF=2: 8). The amount of alkali activator used are 20, 40, 60, 80 and 100kg/m^3, respectively. Two types of curing regime are adopted, sealing curing (20℃) and heating curing (48 hours storage at 20℃Cenvironment⇒120 hours storage at 90℃Cenvironment).Table.4.3.5 show the mortar proportion.

Table.4.3.1 Materials used

	Material	Material characters	Symbol
Binder（B）	Silica fume		SF
	Slag4000	Density:2.91g/cm^3, Specific surface area:4040cm^2/g	BF
	Alkali avtivator	CaO-expansion material	EX
Chemical admixture	Water reducer		SP
	Defoamer		AF
Fine aggregate	Land sand	Absolute dry density: 2.55g/cm^3, water absorption:2%	S

Table.4.3.2 SF chemical composition

SiO2	Fe2O3	Al2O3	CaO	Na2O	MgO	SO3	Cl	K2O	TiO2	MnO	P2O5
93.60%	3.45%	0.80%	0.30%	0.38%	0.39%	0.14%	0.10%	0.63%	0.01%	0.13%	0.03%

Table.4.3.3 BF chemical composition

CaO	SiO2	Al2O3	MgO	SO3	Fe2O3	Cl	K2O	Na2O	TiO2	MnO	SrO	ZrO2	BaO
45.45%	32.23%	12.87%	5.69%	1.92%	0.33%	0.02%	0.35%	0.26%	0.52%	0.18%	0.05%	0.03%	0.07%

Table.4.3.4 Factors and Levels of Experiment

Sample	W/B[%]	B mass ratio (SF:BF)	S/B	EX[kg/m^3]	SP[B×%]	AF[B×%]
1-1	14.0%	2 : 8	1.4 : 1	20	2.4	0.005
1-2				40		
1-3				60		
1-4				80		
1-5				100		

Table.4.3.5 mortar proportion

Sample	Water [kg/m^3]	SF[kg/m^3]	BF[kg/m^3]	AE [kg/m^3]	Sand [kg/m^3]	EX[kg/m^3]	AF[kg/m^3] （Diluted 100 times）	Air volume [%]	0-hit flow[mm]
1-1	110.0	189.8	757.9	22.7	1327.4	20	4.74	4.2	144
1-2						40		3.9	130.7
1-3						60		3.3	129
1-4						80		6.9	116
1-5						100		7.9	111

4.3.2 Compressive strength

Fig.4.3.1 show the result of flexural Strength, as the amount of alkali activator increases, the flexural strength increases first and then decreases. At 20℃ curing, the more the low alkali activator content, the greater the flexural strength at 7 days and 28 days. As the age increases

and the reaction progresses, the 28 days flexural strength increases. At 90℃ heat curing, the flexural strength is greatly improved. When the amount of low-alkali activator is 60 kg/m^3, the maximum flexural strength reaching up to 22.4 MPa.

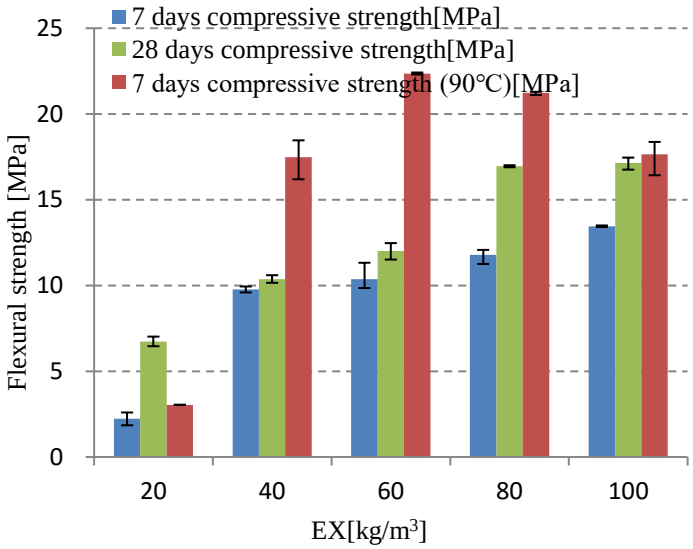

Fig.4.3.1 Flexural Strength

Fig.4.3.2 show the result of compressive strength. It shows that at 20℃ curing, the more the low alkali activator content, the greater the compressive strength at 7 days and 28 days. The maximum strength at 7 days is 70.2 MPa, and the maximum strength at 28 days is 79.8 MPa. At 90℃ heat curing, as the amount of low-alkali activator increases, the compressive strength increases first and then decreases. When the amount of low-alkali activator is 80 kg/m^3, the maximum compressive strength at 7 days reaching up to 136 MPa.

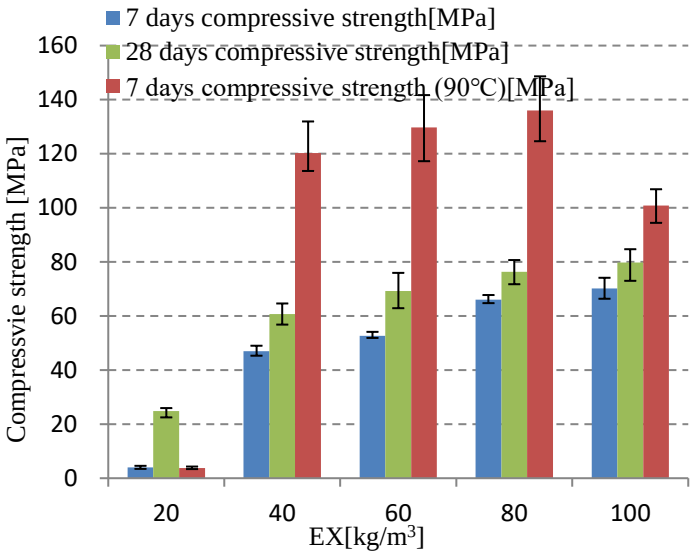

Fig.4.3.2 Compressive strength

4.3.3 XRD analysis

As previously reported by Shi and Day [9], the main reaction products of CaO-activated materials are ettringite (AFt) and C-A-S-H/C-S-H gels. Fig.4.3.3 show the result of XRD, It shows that the main products of zero-cement is C-A-S-H/C-S-H gels. Only when the amount of alkali activator is 40 kg/m^3 at 20℃ curing, a small amount of ettringite (AFt) was generated. At 20℃ curing, a small amount of calcium hydroxide is generated, and at 90℃ heat curing, the peak of calcium hydroxide disappears, indicating that under high-temperature curing conditions, calcium hydroxide is completely consumed, and the degree of pozzolanic reaction is high, forming a denser hardened matrix. The chemical reaction equation is as follows:

$$CaO + H_2O \rightarrow Ca(OH)_2$$

$$CaSO_4 + 2H_2O \rightarrow CaSO_4 \cdot 2H_2O$$

$$2[Al(OH)_4]^- + 3SO_4^{2+} + 16Ca^{2+} + 4OH^- + 26H_2O \rightarrow C_3A \cdot 3CaSO_4 \cdot 32H_2O \quad (\text{or ettringite})$$

$$Y[SiO(OH)_3]^- + XCa^{2+} + (Z - X - Y)H_2O + (2X - Y)OH^- \rightarrow C_X - S_Y - H_Z \quad (\text{or } C - S - H)$$

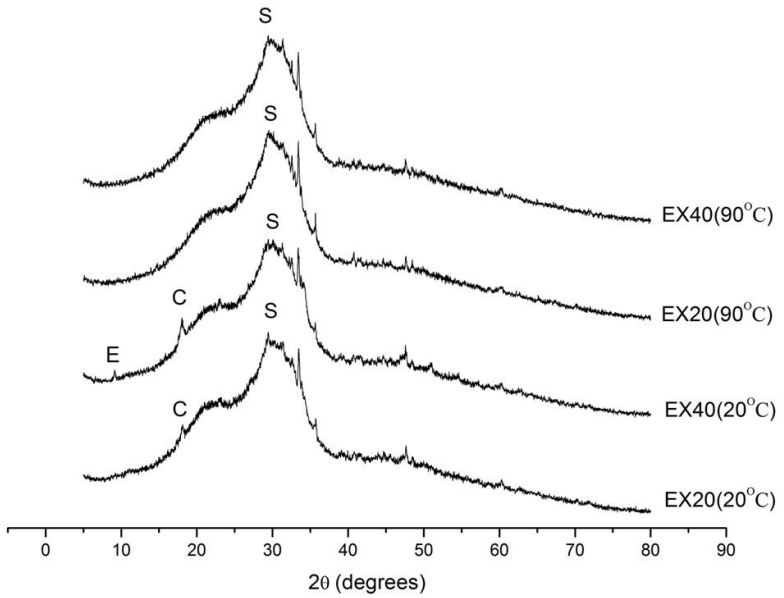

C = Calcium Hydroxide ($Ca(OH)_2$) , S=Calcium Silicate Hydrate(C-S-H) , E = Ettringite (AFt)

Fig.4.3.3 XRD

4.3.4 MIP analysis

Fig.4.3.4 shows the results of MIP, as the amount of low alkali activator content or curing temperature increasing, the total pore volume is greatly decreased. It shows that at 20℃ curing, when the amount of alkali activator is 20 and 40 kg/m^3, the total pore volume is 0.1014 mL/g and 0.0805 mL/g, respectively. At 90℃ heat curing, the total pore volume is greatly reduced, the total pore volume is 0.0523 mL/g and 0.0315 mL/g, respectively. The incremental pore volume has the same trend. The pore size is mainly concentrated between 3-10 nm.

Fig.4.3.5 show the results of porosity. It shows that at 20℃ curing, when the amount of alkali activator is 20 and 40 kg/m^3, the porosity is 20.84% and 16.79%, respectively. At 90℃ heat curing, the porosity is greatly reduced, the porosity is 11.20% and 6.82%, respectively.

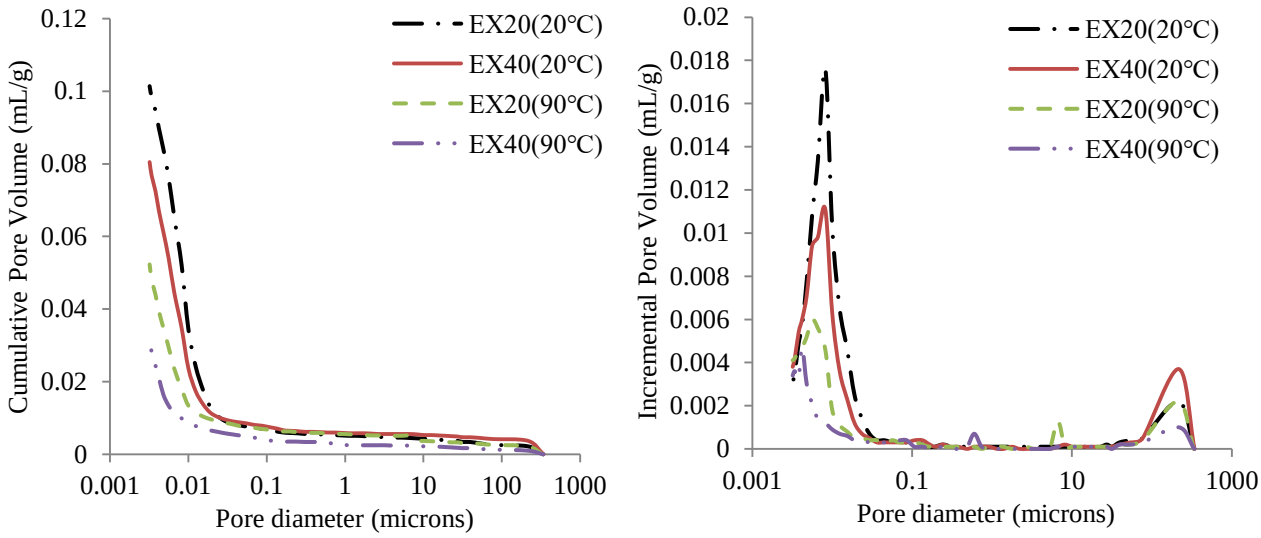

Fig.4.3.4 MIP results

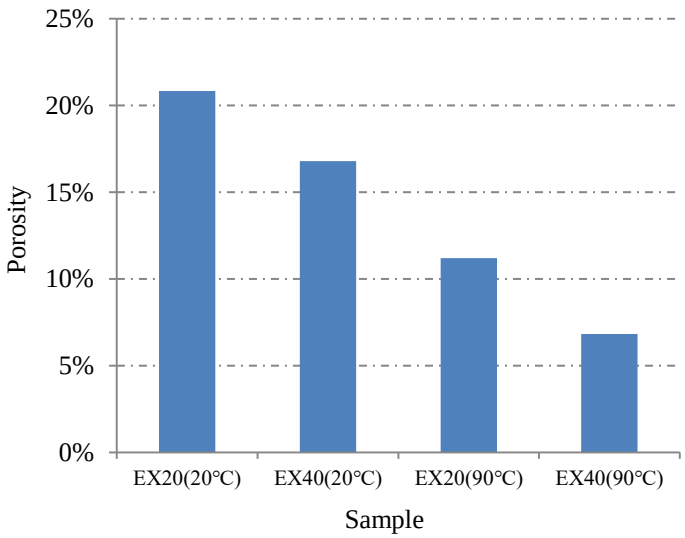

Fig.4.3.5 Porosity

Compared to the reaction products, the difference in strength is more likely due to the porosity. Increase in the content of the low alkali activator and the increase in the curing temperature both greatly reduce the porosity of the specimen and make the compressive strength greatly improved.

4.4 Effects of active CaO-Al_2O_3-SiO_2 content

4.4.1 Introduction

At present, there is no uniform design method for alkali activated zero-cement materials. Unlike cement, the chemical composition of cement is relatively stable, and a standardized and unified design method has been formed. However, alkali activated zero-cement mortar use industrial waste as raw materials, the different types and properties of the raw materials used will produce different compressive strengths, making it difficult to form a unified design method. At present, the most scientific and reasonable design method is based on the ratio of the three components of RAl_2O_3, $RSiO_2$ and $RCaO$ contained in the raw materials. By adopting this method, even if raw materials of different origins and different properties are used, it can be designed by the active constituent in the raw materials that can participate in the reaction, making it possible to propose a design method for alkali activated zero-cement mortar.

This chapter study the relationship between the $RSiO_2$, $RCaO$, and RAl_2O_3 and compressive strength. Clarifies the relationship between compressive strength, reaction products, Young's modulus and pore structure, elucidate mechanism of strength development of low alkali activated zero-cement mortar and proposes a method of strength evaluation for zero-cement mortar.

4.4.2 Materials and Experimental Methods

4.4.2.1 Factors and level of experiment

Table.4.4.1 shows the materials used. Fig.4.4.1 shows Crystalline and amorphous contents of each raw material. As can be seen from the figure, BF is basically amorphous phase, and MK is mainly composed of amorphous phase, quartz, feldspar and muscovite. SR is mainly composed of amorphous phase, quartz and albite. Fig.4.4.2 shows particle size distribution of

raw material. Table.4.4.2, Table.4.4.3 and Table.4.4.4 show BF, SR and MK chemical composition respectively.

Table.4.4.1 Materials used

	Material	Material characters
Binder	Metakaolin	Density:2.59 g/cm^3, mean particle size:3.96um
	Shirasu	Density:2.36g/cm^3, mean particle size:5.28um
	Slag8000	Density:2.91 g/cm^3, Specific surface area:8020cm^2/g mean particle size:5.46um
Low alkali activator	CaO	Density:3.35g/cm^3

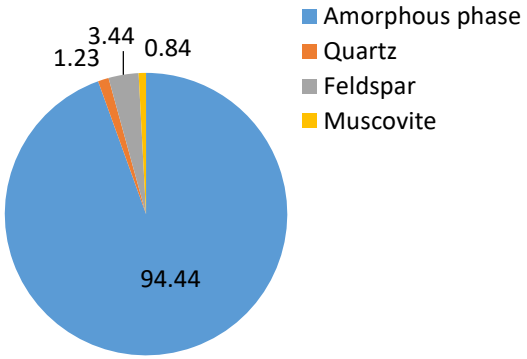

(a)Metakaolin

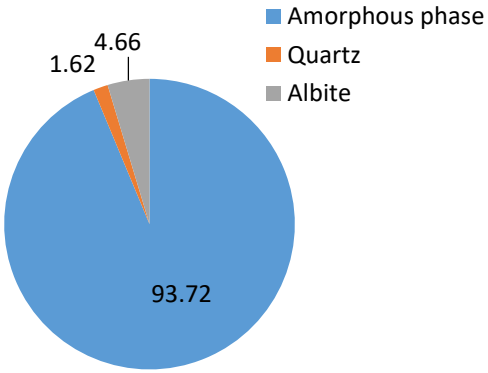

(b) Shirasu

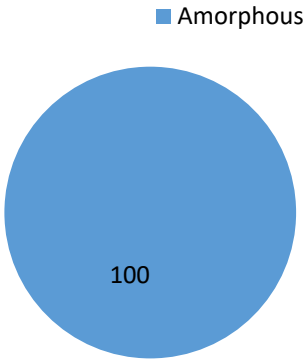

(c) Slag

Fig.4.4.1 Crystalline and amorphous contents of each raw material

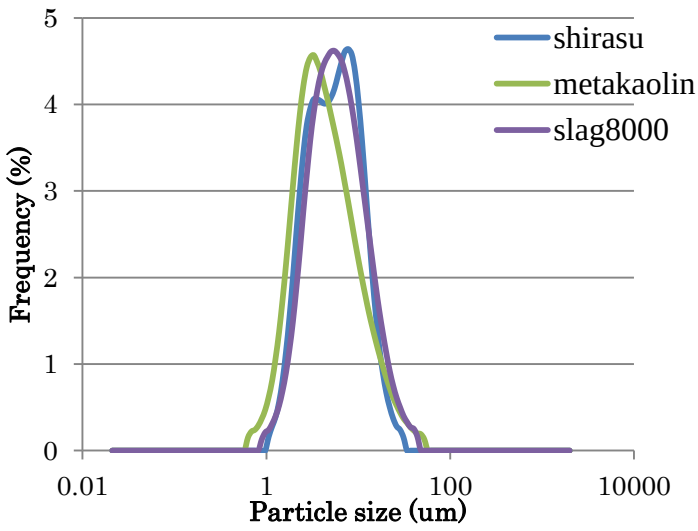

Fig.4.4.2 Particle size distribution of raw material

Table.4.4.2 BF chemical composition

CaO	SiO2	Al2O3	MgO	SO3	Fe2O3	Cl	K2O	Na2O	TiO2	MnO	SrO	ZrO2	BaO
45.45%	32.23%	12.87%	5.69%	1.92%	0.33%	0.02%	0.35%	0.26%	0.52%	0.18%	0.05%	0.03%	0.07%

Table.4.4.3 SR chemical composition

SiO2	Al2O3	CaO	Fe2O3	Na2O	MgO	K2O	SO3
73.60%	12.30%	1.35%	1.49%	3.73%	0.25%	4.37%	0.00%

Table.4.4.4 MK chemical composition

SiO2	Al2O3	CaO	Fe2O3	Na2O	MgO	K2O	SO3	TiO2	Cr2O3	P2O5
50.81%	46.63%	0.08%	0.64%	0.24%	0.03%	0.17%	0.04%	1.16%	0.02%	0.12%

Before designing the mix proportion, the contents of $RSiO_2$, RAl_2O_3 and RCaO in the raw materials must be calculated. The calculation method is show in Section.3.3.2, Table.4.4.5 shows $RSiO_2$, RAl_2O_3 and RCaO content of each raw material.

Table.4.4.5 $RSiO_2$, RAl_2O_3 and RCaO content of each raw material

	BF	SR	MK
RSiO2	0.322	0.688	0.473
RAl2O3	0.129	0.114	0.460
RCaO	0.455	0.014	0.000
Sum	0.906	0.815	0.933

Fig.4.4.3 shows the RCaO-RAl_2O_3-$RSiO_2$ ternary diagram. There are 13 samples, the amounts of RCaO were 17%, 27%, 37% and 47%, respectively. The molar ratios of $RSiO_2/RAl_2O_3$ are 2.5, 4 and 6.

4.4.2.2 Mixture proportions

Table.4.4.6 shows factors and levels of experiment. Table.4.4.7 shows the mortar mixture proportion. The type II shirasu, metakaolin and the blast furnace slag fine powder 8000 were used. The mass ratio of low alkali activator CaO to binder was 6%. The mass ratio of water to binder in mortar was 45%.The mass ratio of fine aggregate sand to binder in mortar was 1.4: 1. Table.4.4.8 show the samples molar ratio of $RSiO_2$-RAl_2O_3-RCaO.

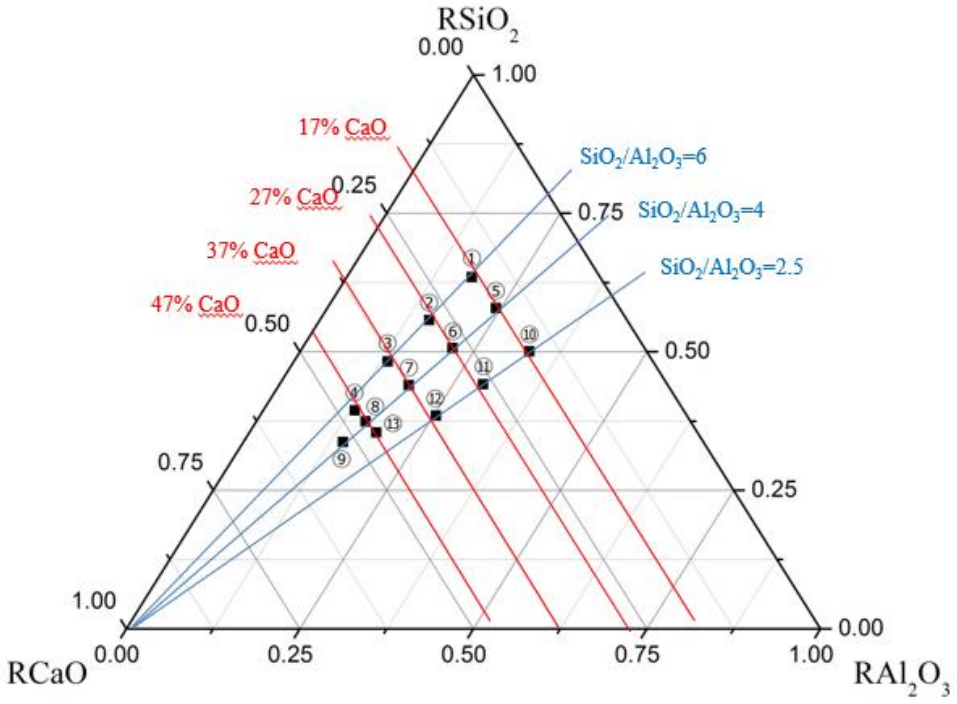

Fig.4.4.3 the $RCaO$-RAl_2O_3-$RSiO_2$ ternary diagram.

Table.4.4.6 Factors and Levels of Experiment

Sample	Slag(g)	Metakaolin(g)	Shirasu(g)	CaO(g)	W/B	S/B
1	20	13	61	6	45	1.4
2	40	7	47			
3	60	1	33			
4	80	0	14			
5	20	30	44			
6	40	23	31			
7	60	15	19			
8	80	7	7			
9	91	3	0			
10	20	55	19			
11	40	45	9			
12	60	34	0			
13	80	14	0			

Table.4.4.7 Mortar mixture proportion

Name	Water (kg/m^3)	Metakaolin (kg/m^3)	Shirasu (kg/m^3)	BF(kg/m^3)	CaO (kg/m^3)	Sand (kg/m^3)
1-1	322.7	93.6	438.9	142.0	42.9	1003.6
1-2	325.9	52.2	339.0	290.1	43.4	1013.8
1-3	329.3	7.3	241.5	439.1	43.8	1024.1
1-4	333.1	0.0	103.6	592.2	44.3	1036.0
1-5	324.3	216.2	317.1	144.1	43.1	1008.5
1-6	327.4	167.4	225.6	291.1	43.5	1018.3
1-7	330.5	110.2	139.6	440.8	44.0	1028.1
1-8	333.8	51.9	51.9	593.3	44.4	1038.0
1-9	335.6	22.4	0.0	678.6	44.6	1043.6
1-10	348.1	399.0	137.9	145.1	43.4	1015.4
1-11	333.8	329.4	65.9	292.8	43.8	1024.5
1-12	332.3	251.1	0.0	443.1	44.2	1033.5
1-13	334.4	104.0	0.0	594.5	44.5	1040.0

Table.4.4.8 The samples molar ratio of $RSiO_2$-RAl_2O_3-RCaO.

Sample	$RSiO_2$	RAl_2O_3	RCaO	Glass content	SiO_2/Al_2O_3	CaO/SiO_2	CaO/Al_2O_3
①	54.57	15.50	15.91	95.45	5.98	0.31	1.87
②	48.54	13.72	24.81	96.66	6.01	0.55	3.29
③	42.52	11.94	33.72	97.87	6.05	0.85	5.14
④	35.42	11.89	42.55	99.12	5.06	1.29	6.52
⑤	50.91	21.38	15.68	95.57	4.05	0.33	1.34
⑥	45.10	19.26	24.60	96.77	3.98	0.58	2.33
⑦	39.51	16.78	33.53	97.97	4.00	0.91	3.64
⑧	33.91	14.31	42.45	99.17	4.03	1.34	5.40
⑨	30.75	13.09	47.36	99.83	3.99	1.65	6.59
⑩	45.54	30.03	15.35	95.75	2.58	0.36	0.93
⑪	40.38	26.87	24.30	96.93	2.55	0.64	1.65
⑫	35.43	23.36	33.27	98.11	2.58	1.01	2.59
⑬	32.41	16.73	42.36	99.22	3.29	1.40	4.61

4.4.2.3 Mixing method

Using a mortar mixer, in order to make the powder and the fine aggregate uniform, the powder was mixed for 3 minutes, then water was added, and the mixture was mixed again for 3 minutes. In this experiment, the mixing amount of one batch was 2 L.

4.4.2.4 Experimental method

(1) Compressive strength experiment

As for curing, zero-cement mortar was mixed and then poured into a Φ50mm×100mm sample mold, sealed the top of the mold with a vinyl sheet, The curing was performed at a temperature of 20°C, 60%RH. The compressive strength experiments were conducted at 7days, 28days and 140 days using a universal testing machine. The reported compressive strengths are an average of three samples.

(2) Percentage of saturated water content

Select 3 pieces of dried samples with a weight of 1～2g, weigh them separately, and then immerse them in water, and weigh them again after 2h, 6h, 24h, 72h, 168h. Note that the initial sample mass is m_0, the mass after soaking is m_i, and the calculation equation of percentage of mass change is: $P= 100\%*(m_i -m_0)/m_0$。 The percentage of mas change(%) is the average of three samples.

(3) Thermogravimetric (TG) analysis

Thermogravimetric (TG) analysis, in a TG differential thermal analysis instruments (MTC1000SA). Samples were crushed, approximately 20mg of ground sample powders was heated at 10°C/min from normal temperature to 1000°C in a nitrogen environment at 150 mL/min purge rate. In this experiment, thermogravimetric (TG) analysis was adopted to quantify the weight loss ratio(105℃-300℃) and CH contents.

(4) X-ray diffraction analysis (XRD)

X-ray diffraction (hereinafter referred to as XRD) was performed using an X-ray diffractometer. After grinding the hardened paste of each specimen, XRD analysis was performed. The X-ray diffraction measurement conditions were: tube voltage: 40 kV, tube current: 15 mA, measurement range: 2θ = 5 to 70 °, step angle: 0.02°, bead: 2deg/min.

4.4.3 Compressive strength

Fig.4.4.4 shows the compressive strength results. It shows that as the age increases, the compressive strength of the zero-cement mortar also increased. At 7 days, the more RCaO content in the sample, the higher the compressive strength. In the case of $RSiO_2/RAl_2O_3$=2.5, $RSiO_2/RAl_2O_3$=4 and $RSiO_2/RAl_2O_3$=6 all show the same strength change tendency. In addition, when the RCaO content is the same, the more the RAl_2O_3 content in the sample, the higher the compressive strength. At 28 days and 140 days, the change of compressive strength have the same trend like 7 days. The more RCaO content in the sample, the higher the compressive strength.

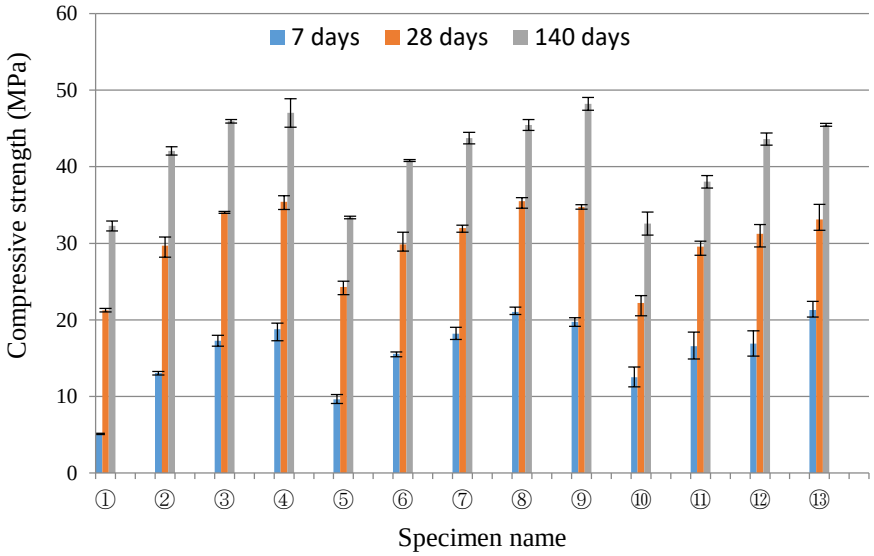

Fig.4.4.4 compressive strength

In order to more easily understand the relationship between compressive strength and molar ratio of $RSiO_2$-RAl_2O_3-RCaO, the triangle diagram is shown below. Fig.4.4.5, Fig.4.4.6 and Fig4.4.7 shows 7days, 28days and 140days triangle diagram of mortar Compressive strength. The triangle diagram of compressive strength can intuitively reflect the relationship between active constituent and compressive strength. It shows that the higher the content of RCaO and RAl_2O_3, the greater the 7days compressive strength. The higher the RCaO content, the greater the 28days compressive strength. The content of RAl_2O_3 has a positive effect on the 7days strength. But it has little effect on 28days and 140days compressive strength. The 140 days compressive strength of zero-cement mortar is consistent with the development law of 28 days compressive strength. Therefore, it can be concluded that the compressive strength of 7 days is mainly determined by the content of RCaO and RAl_2O_3, and the compressive strength of 28 days and 140 days is mainly determined by the content of RCaO.

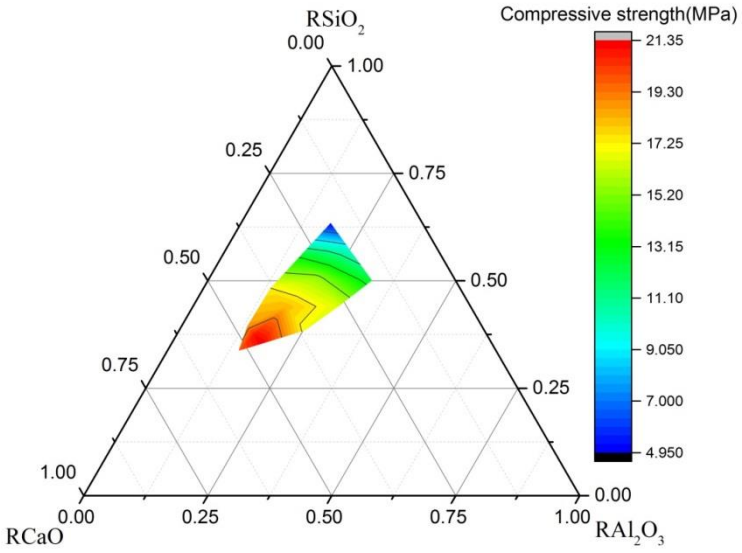

Fig.4.4.5 Triangle diagram of 7days mortar Compressive strength

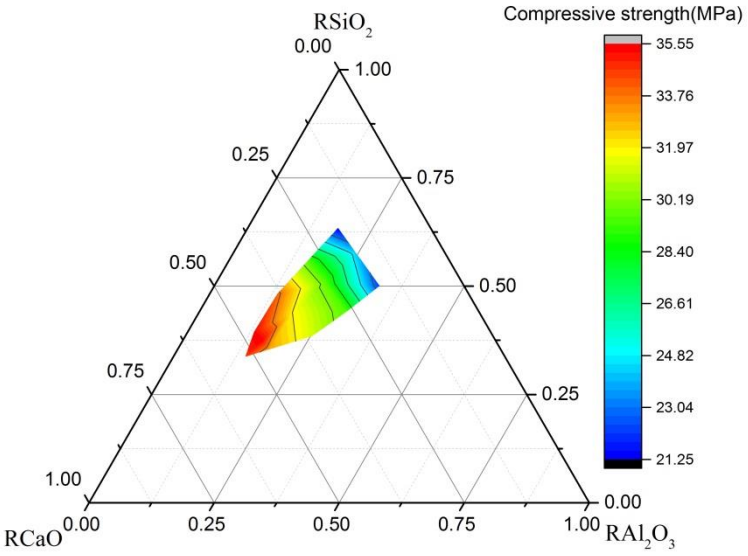

Fig.4.4.6 Triangle diagram of 28days mortar Compressive strength

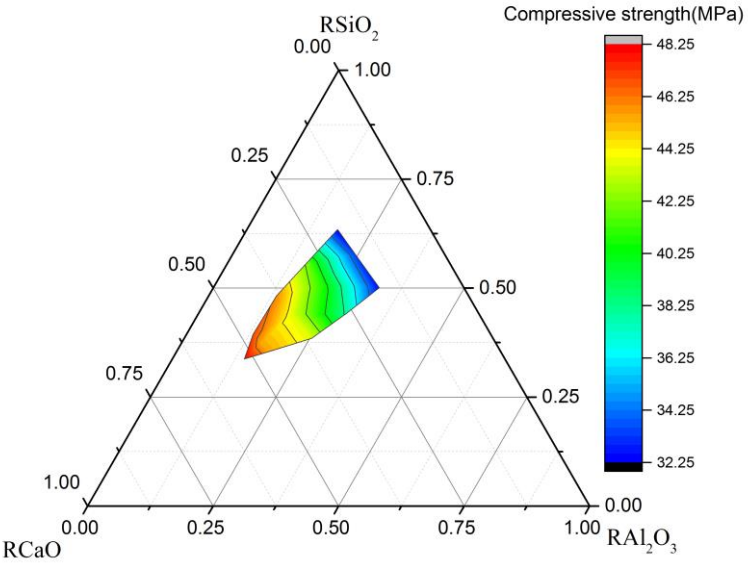

Fig.4.4.7 Triangle diagram of 140days mortar Compressive strength

4.4.4 Young's modulus

Fig.4.4.8 and Fig.4.4.9 shows 7days and 28days Young's modulus. In general, the Young's

modulus of concrete is determined by a secant of a stress-strain curve connecting a point at which a strain of 50×10^{-6} is measured and a point at which stress is 1/3 of the fracture stress (JIS A 1149). The equation for Young's modulus is as follows:

$$E_c = \frac{(S_1 - S_2)}{(\varepsilon_1 - \varepsilon_2)} * 10^{-3}$$

Here, Ec: Young's modulus;

S_1: Stress equivalent to 1/3 of the maximum load;

S_2: Stress at longitudinal strain of 50×10^{-6} for the specimen;

ε_1: Longitudinal strain of the specimen caused by S_1 stress;

ε_2: 50×10^{-6};

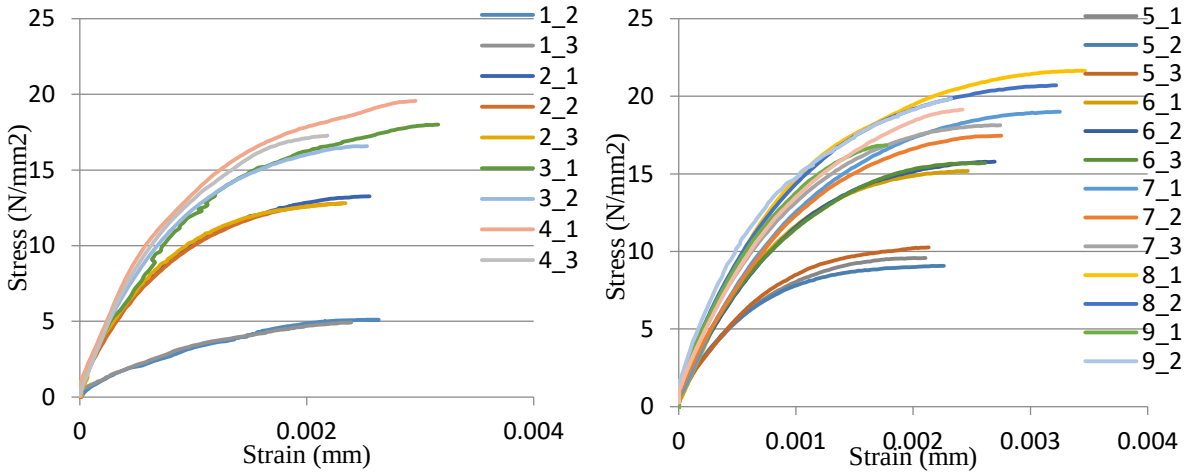

(a) (b)

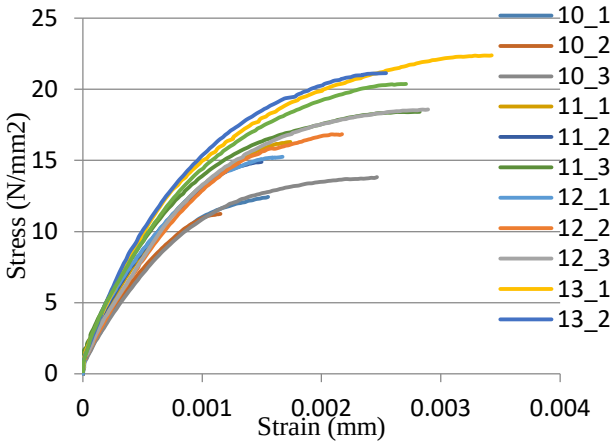

(c)

Fig.4.4.8 7days Young's modulus (a) SiO_2/Al_2O_3=6 (b) SiO_2/Al_2O_3=4 (c) SiO_2/Al_2O_3=2.5

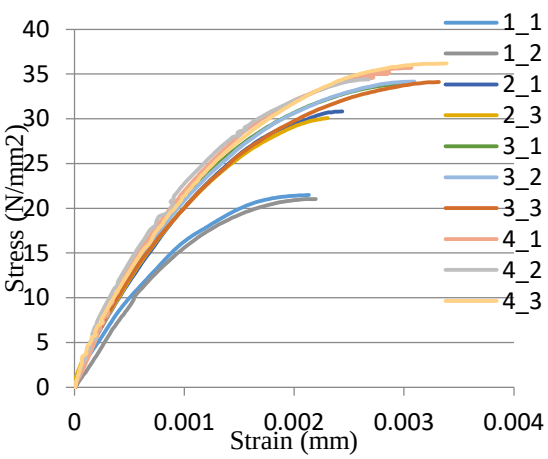

(a)

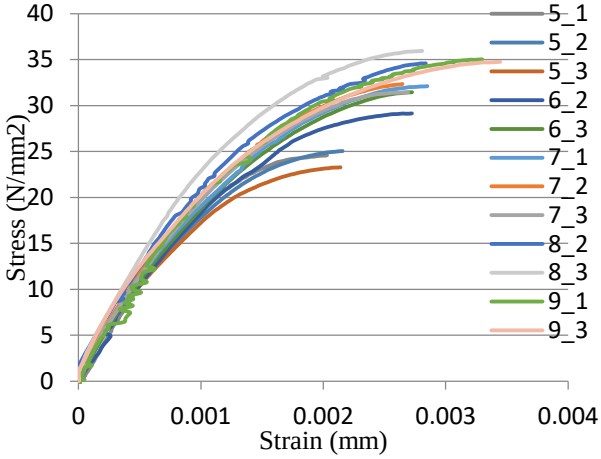

(b)

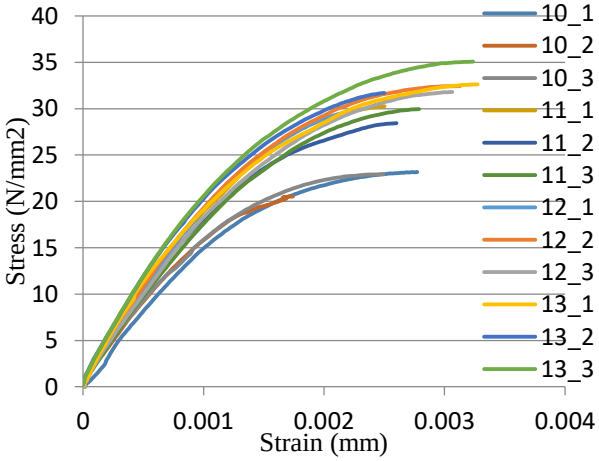

(c)

Fig.4.4.9 28days Young's modulus (a) SiO_2/Al_2O_3=6 (b) SiO_2/Al_2O_3=4 (c) SiO_2/Al_2O_3=2.5

Fig.4.4.10 shows 7days and 28days Young's modulus of each specimen. Fig.4.4.11 shows the relationship between Young's modulus and compressive strength. Compressive strength has a linear relationship with Young's modulus. The larger the Young's coefficient, the higher the compressive strength, it shows that the strength is controlled by the interatomic bond.

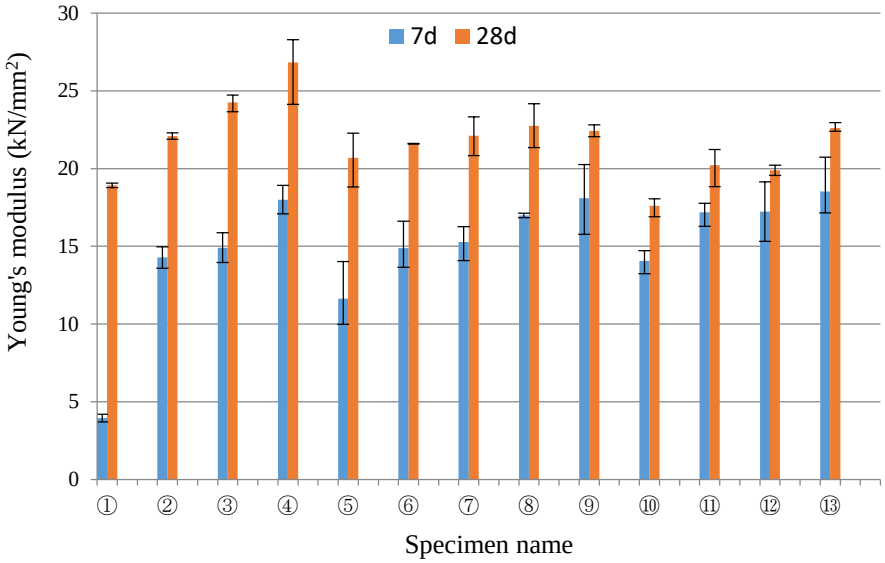

Fig.4.4.10 Young's modulus of each specimen

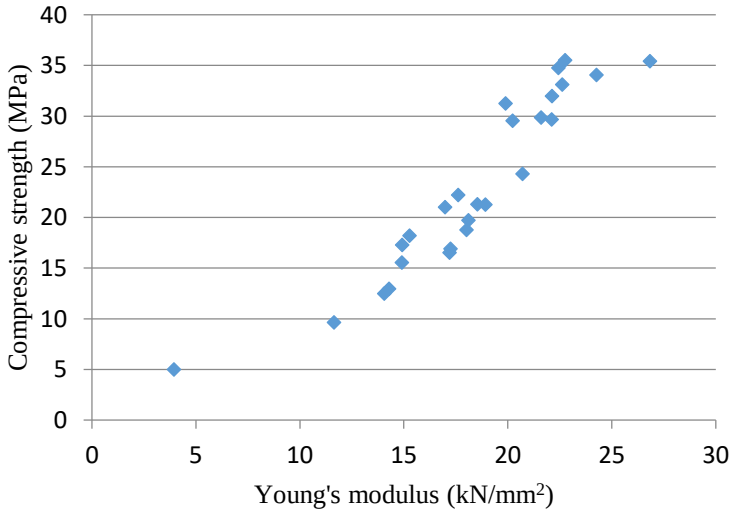

Fig.4.4.11 the relationship between mortar strength and Young's modulus

4.4.5 Percentage of saturated water content

Fig.4.4.12 and Fig.4.4.13 shows 7days and 28days percentage of mass change (%). At 7 days, when $RSiO_2/RAl_2O_3 = 6$ (samples 1-4), the more RCaO, the lower the saturated water content; when $RSiO_2/RAl_2O_3 = 4$ (samples 5-9), the more RCaO, The lower the saturated water content; when $RSiO_2/RAl_2O_3 = 2.5$ (samples 10-13) also has the same change law, the more RCaO, the lower the saturated water content.

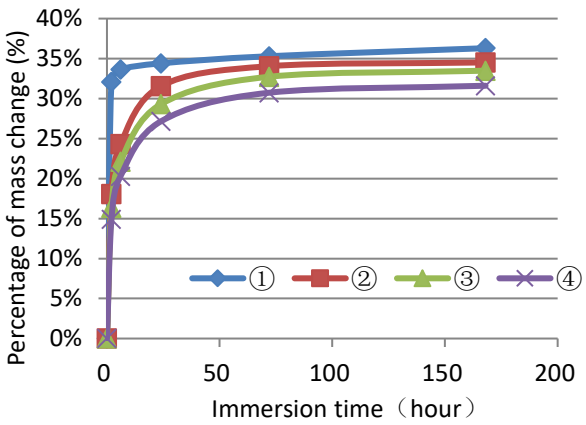

(a) $SiO_2/Al_2O_3=6$

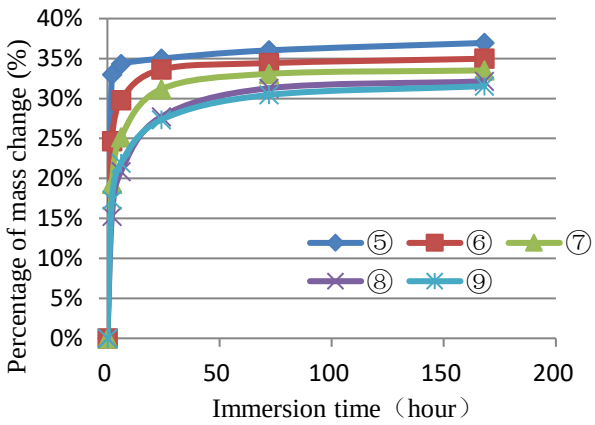

(b) $SiO_2/Al_2O_3=4$

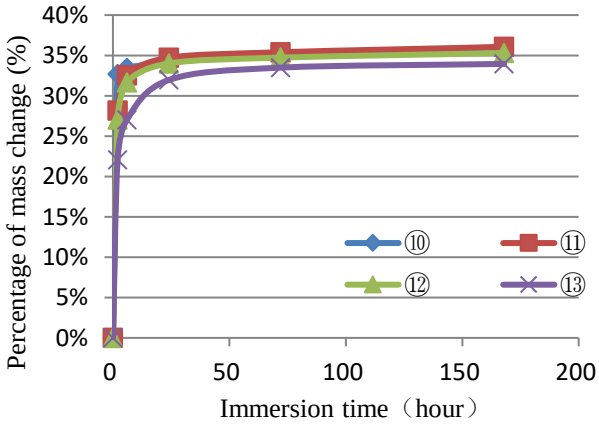

(c) $SiO_2/Al_2O_3=2.5$

Fig.4.4.12 7days percentage of mass change (%)

(a) $SiO_2/Al_2O_3=6$ (b) $SiO_2/Al_2O_3=4$ (c) $SiO_2/Al_2O_3=2.5$

At 28 days, the change pattern was consistent with 7 days. It shows that the content of RCaO has a great influence on the pore structure of the hardened zero-cement paste. The more RCaO, the denser the hardened zero-cement paste, and the greater the compressive strength. Fig.4.4.14 shows the relationship between compressive strength and saturated water content. Overall, compressive strength has a correlation with saturated water content. The lower the saturated water content, the greater the compressive strength.

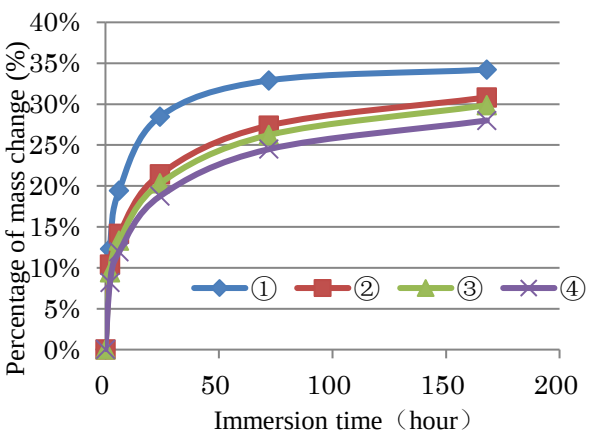

(a) SiO_2/Al_2O_3=6

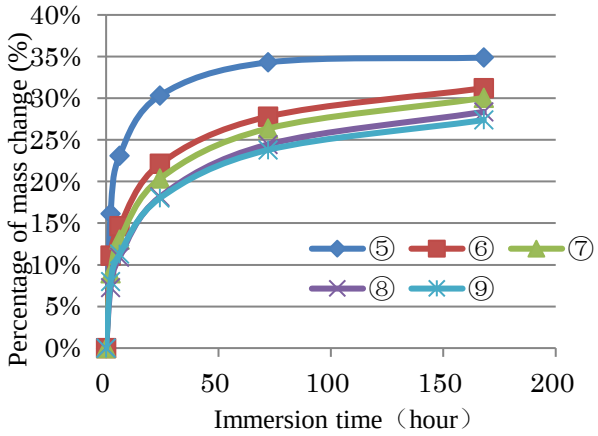

(b) SiO_2/Al_2O_3=4

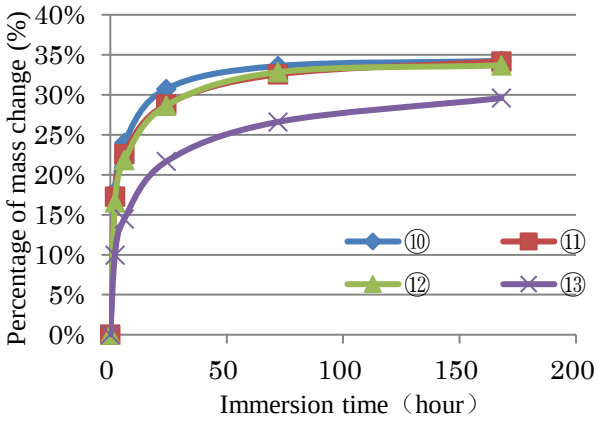

(c) SiO_2/Al_2O_3=2.5

Fig.4.4.13 28days Percentage of mass change (%)

(a) SiO_2/Al_2O_3=6 (b) SiO_2/Al_2O_3=4 (c) SiO_2/Al_2O_3=2.5

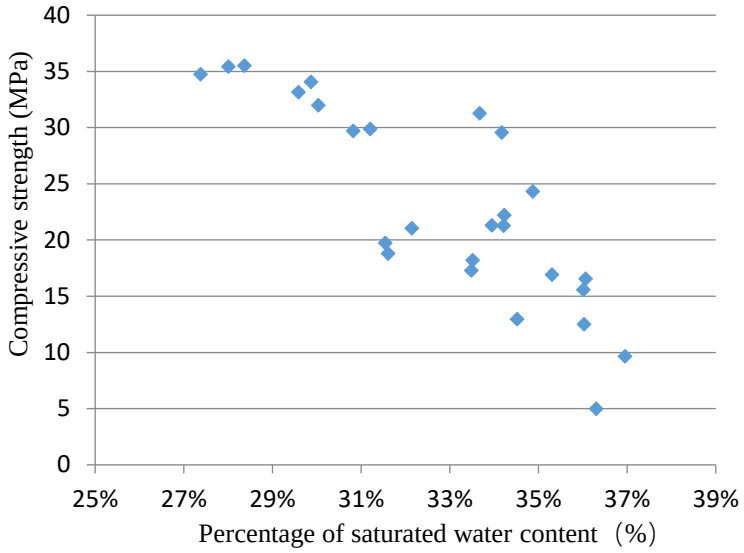

Fig.4.4.14 the relationship between strength and percentage of saturated water content

4.4.6 XRD analysis

Fig.4.4.15 and Fig.4.4.16 shows 7days and 28days XRD results. As can be seen from the figure, in addition to the crystal phase in raw materials that is not involved in the reaction: quartz and albite, the main reaction product is composed of a glass phase (gel) indicated by a halo peak of 18 to 35°(2θ) and a crystal phase of Hemicarbonate ($C_4Ac_{0.5}H_{12}$), Straetlingite (C_2ASH_8) and Portlandite ($Ca(OH)_2$).

From the XRD results, the hydration products consisting of C_2ASH_8, $C_4Ac_{0.5}H_{12}$ and C-A-S-H/ C-S-H gels were precipitated. The main chemical reaction equation is as follows:

$$CaO + H_2O \rightarrow Ca(OH)_2$$

$$CaSO_4 + 2H_2O \rightarrow CaSO_4 \cdot 2H_2O$$

$$2Ca^{2+} + 2Al(OH)^{4-} + SiO(OH)^{3-} + OH^{-} + 2H_2O \rightarrow \quad C_2ASH_8$$

$$4Ca^{2+} + 2Al(OH)^{4-} + 0.5CO_3^{2-} + 5OH^{-} + 7H_2O \quad \rightarrow C_4Ac_{0.5}H_{12}$$

$$Y[\mathrm{SiO(OH)_3}]^- + X\mathrm{Ca}^{2+} + (Z - X - Y)\mathrm{H_2O} + (2X - Y)\mathrm{OH}^-$$
$$\rightarrow C_X - S_Y - H_Z \quad (\text{or } C - S - H)$$

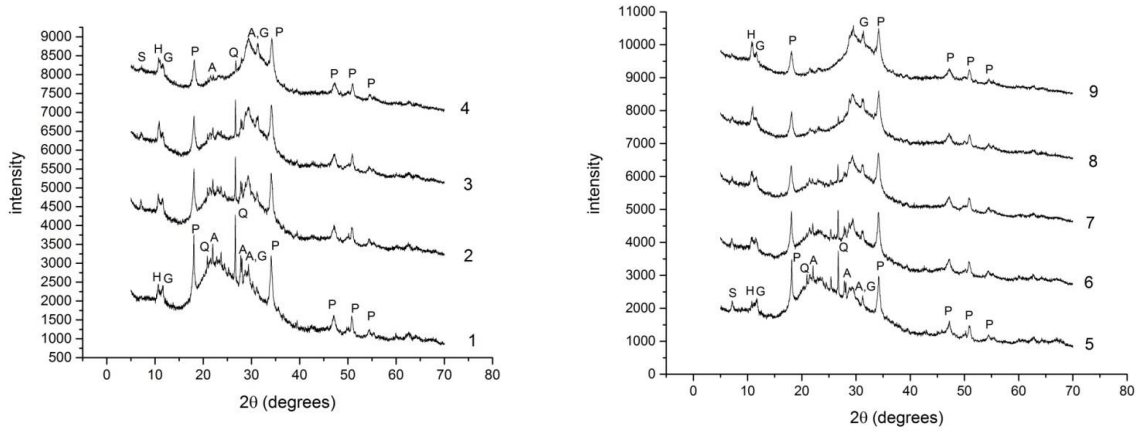

(a) SiO_2/Al_2O_3=6 (b) SiO_2/Al_2O_3=4

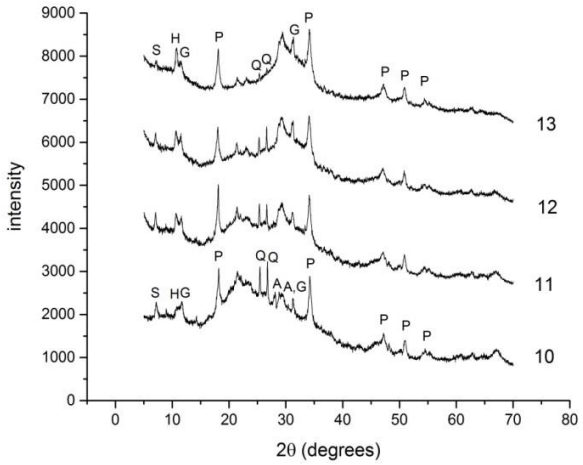

(c) SiO_2/Al_2O_3=2.5

P- Portlandite A- Albite G- Gypsum Q- Quartz

H- Hemicarbonate ($C_4Ac_{0.5}H_{12}$) S- Straetlingite (C_2ASH_8)

Fig.4.4.15 7days XRD (a) SiO_2/Al_2O_3=6; (b) SiO_2/Al_2O_3=4; (c) SiO_2/Al_2O_3=2.5.

The main reaction products at 7 days and 28 days is same. Compared with 7 days at 28 days, the amount of Straetlingite is increased. Especially at 28days, sample 1 ($RSiO_2$ / RAl_2O_3=6),

sample 5 ($RSiO_2$ / RAl_2O_3=4) and sample 10 ($RSiO_2$ / RAl_2O_3=2.5) with low RCaO content, which are particularly obvious. As the content of RCaO increases, the amount of Straetlingite produced gradually decreases. Therefore, it can be concluded that irrespective of the $RSiO_2/RAl_2O_3$ molar ratio, when the RCaO content is low, low-alkali activated zero-cement tends to form Straetlingite.

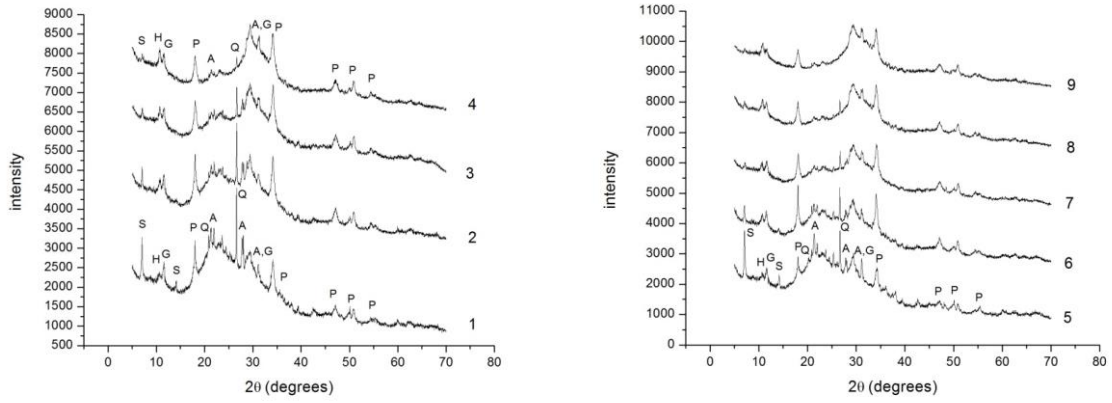

(a) SiO_2/Al_2O_3=6 (b) SiO_2/Al_2O_3=4

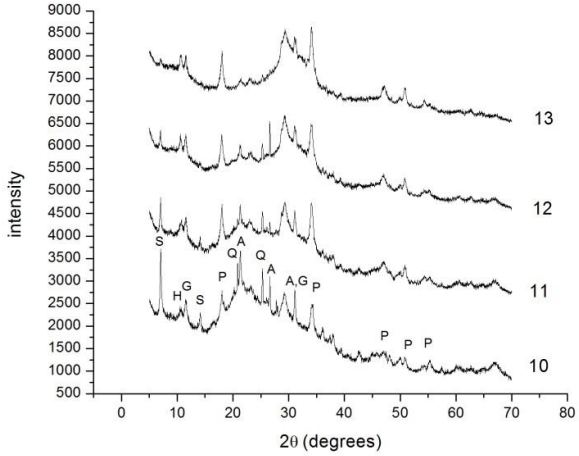

(c) SiO_2/Al_2O_3=2.5

P- Portlandite A- Albite G- Gypsum Q- Quartz

H- Hemicarbonate ($C_4Ac_{0.5}H_{12}$) S- Straetlingite (C_2ASH_8)

Fig.4.4.16 28days XRD (a) SiO_2/Al_2O_3=6; (b) SiO_2/Al_2O_3=4; (c) SiO_2/Al_2O_3=2.5.

4.4.7 TG analysis

Fig.4.4.17 and Fig.4.4.18 show the TGA and DTA curves of the hardened pastes for 7days curing. Fig.4.4.19 and Fig.4.4.20 show the TGA and DTA curves of the hardened pastes for 28days curing.

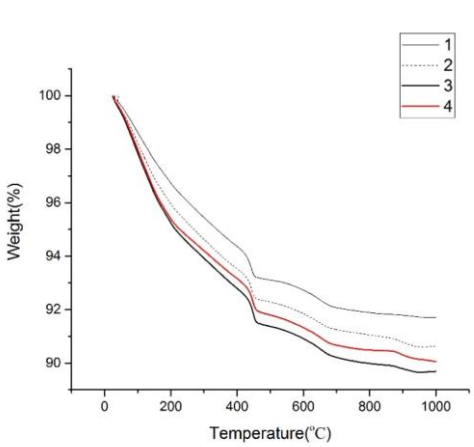

(a) SiO_2/Al_2O_3=6

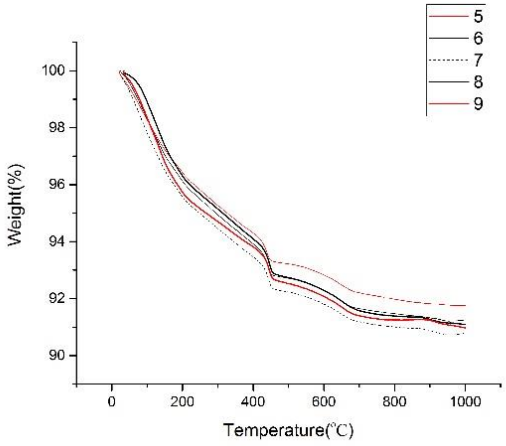

(b) SiO_2/Al_2O_3=4

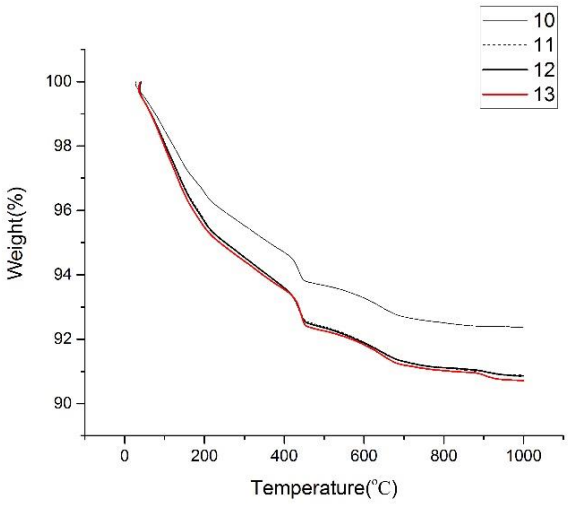

(c) SiO_2/Al_2O_3=2.5

Fig.4.4.17 7days TGA (a) SiO_2/Al_2O_3=6; (b) SiO_2/Al_2O_3=4; (c) SiO_2/Al_2O_3=2.5.

Considering that the weight loss accumulated before 300 °C in TGA data is an indicator of the

interlayer water weight of C–S–H or C–A–S–H for zero-cement, compared with the 7days zero-cement, 28days zero-cement have greater mass loss rate, which indicates more C–S–H/ C–A–S–H gel formation, possibly leading to higher compressive strength. The weight loss peak around 450°C is the dehydration peak of $Ca(OH)_2$, the mass loss peak around 650°C is the dehydration peak of $CaCO_3$, and the mass loss peak around 900°C is likely the recrystallization peak of C–S–H or C–A–S–H.

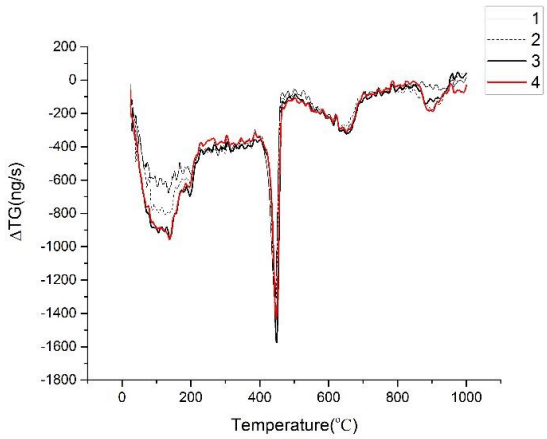

(a) SiO_2/Al_2O_3=6

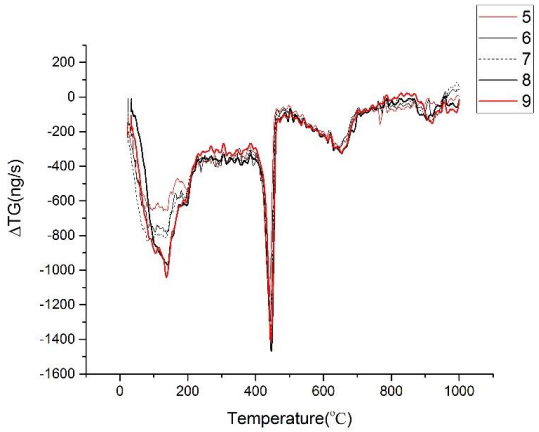

(b) SiO_2/Al_2O_3=4

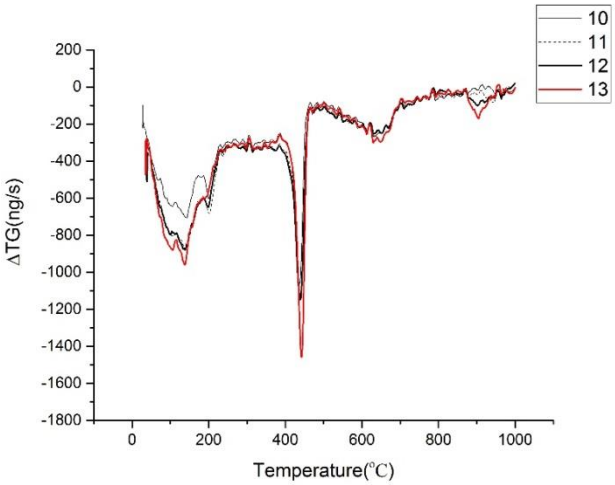

(c) SiO_2/Al_2O_3=2.5

Fig.4.4.18 7days DTA (a) SiO_2/Al_2O_3=6; (b) SiO_2/Al_2O_3=4; (c) SiO_2/Al_2O_3=2.5.

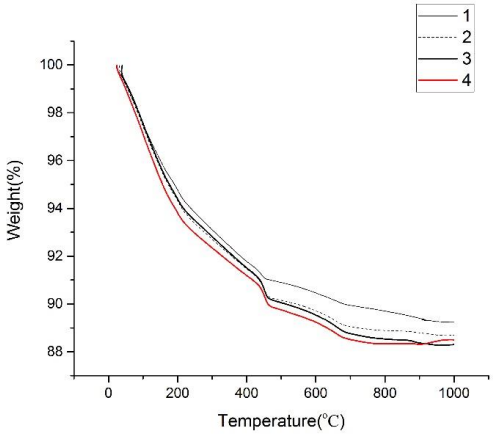

(a) SiO_2/Al_2O_3=6

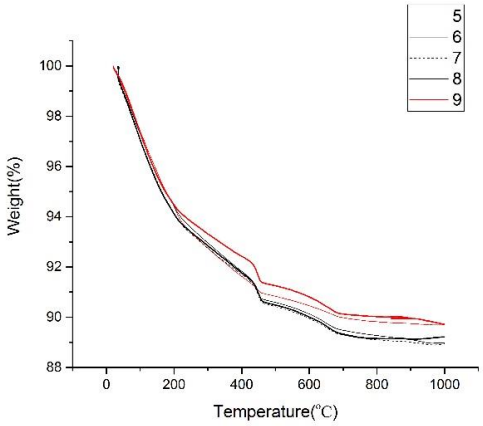

(b) SiO_2/Al_2O_3=4

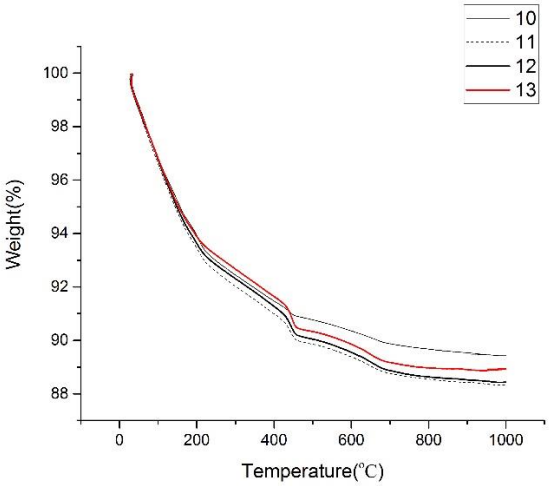

(c) SiO_2/Al_2O_3=2.5

Fig.4.4.19 28days TGA (a) SiO_2/Al_2O_3=6; (b) SiO_2/Al_2O_3=4; (c) SiO_2/Al_2O_3=2.5.

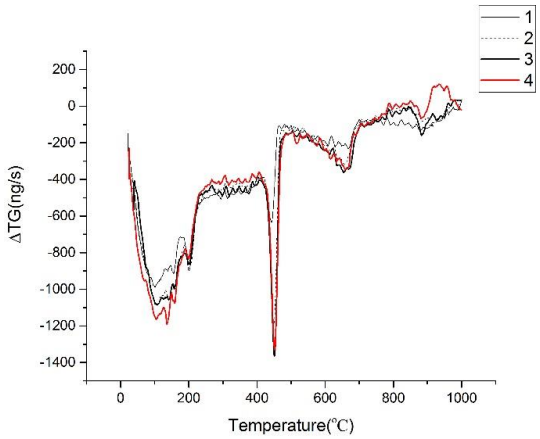

(a) SiO_2/Al_2O_3=6

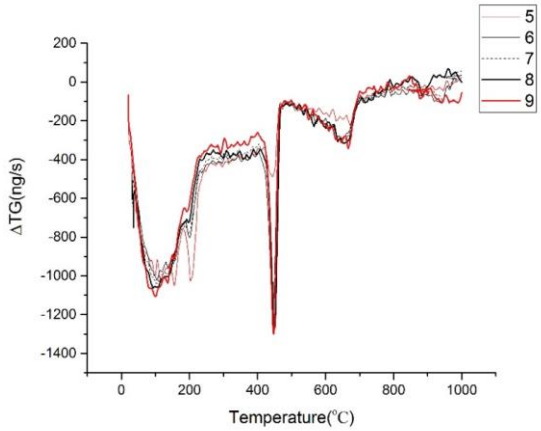

(b) SiO_2/Al_2O_3=4

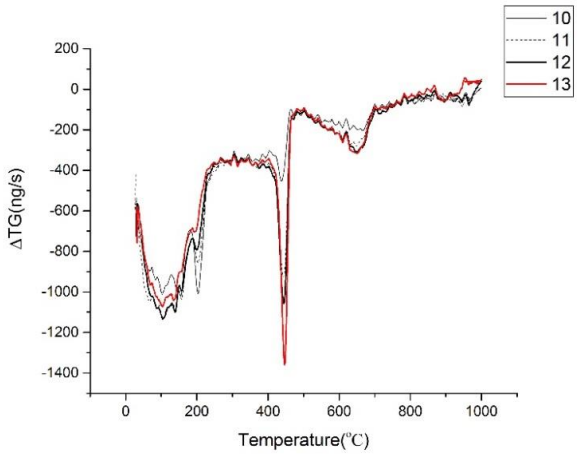

(c) SiO_2/Al_2O_3=2.5

Fig.4.4.20 28days DTA (a) SiO_2/Al_2O_3=6; (b) SiO_2/Al_2O_3=4; (c) SiO_2/Al_2O_3=2.5.

The amount of weight loss ratio (W) (105℃-300℃) are expressed as% of the dry sample weight at 300 ℃ (W_{300}):

$$W = \frac{W_{105} - W_{300}}{W_{300}}$$

The amount of hydrate water (H) are expressed as% of the dry sample weight at 550 ℃ (W_{550}) [10]:

$$H = \frac{W_{40} - W_{550}}{W_{550}}$$

The amount of Portlandite (CH) are expressed as% of the dry sample weight at 500 ℃ (W_{500}):

$$CH = \frac{W_{500} - W_{400}}{W_{500}}$$

Fig..4.4.21 show the relationship between bound water and compressive strength. From the overall trend, the greater the bound water, the greater the compressive strength. Fig.4.4.22 show the relationship between $Ca(OH)_2$ and compressive strength. Fig.4.4.23 shows the relationship

between weight loss ratio(105℃-300℃) and compressive strength. From the overall trend, the greater the weight loss ratio(105℃-300℃), the greater the compressive strength. However, some points deviate from the linear relationship. In order to evaluate the compressive strength more accurately, a new index needs to be proposed.

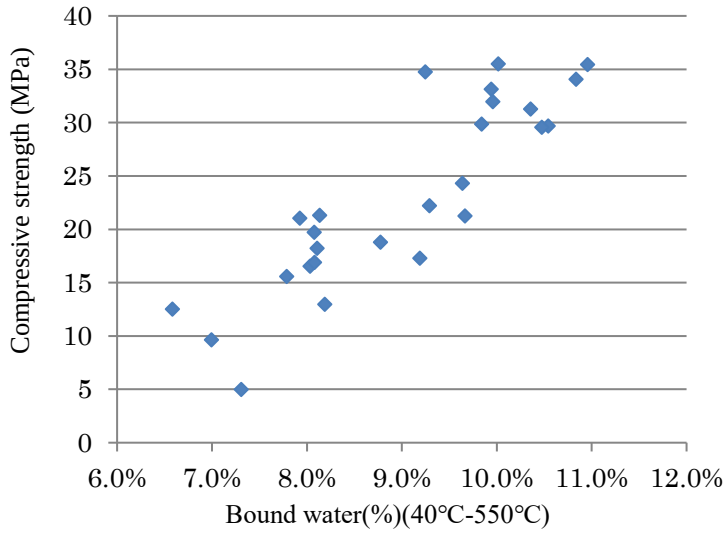

Fig.4.4.21 the relationship between bound water and compressive strength

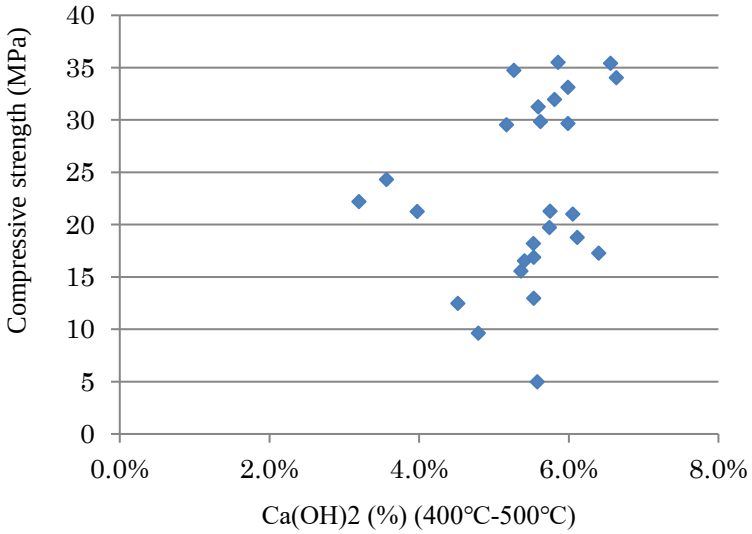

Fig.4.4.22 The relationship between $Ca(OH)_2$ and compressive strength

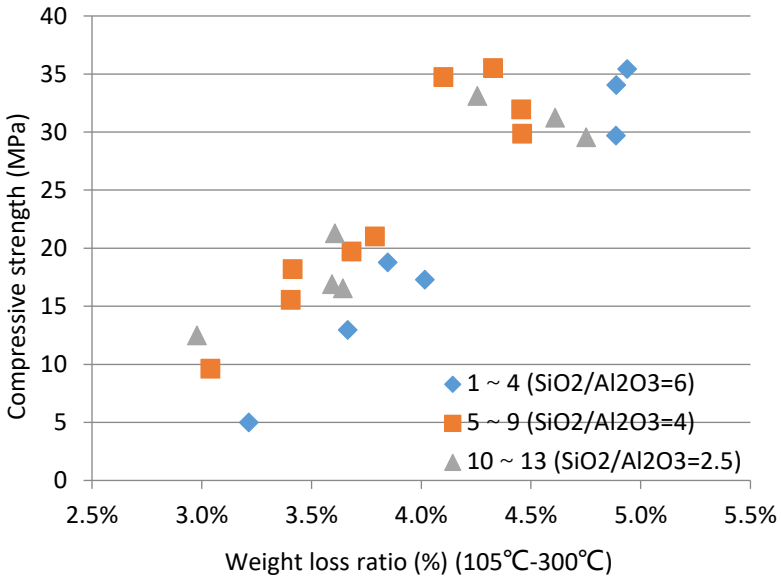

Fig.4.4.23 the relationship between weight loss ratio (105℃-300℃) and compressive strength

4.4.8 Evaluation of compressive strength: strength index

Same as the strength index in Chapter 3, it can be used to evaluate the compressive strength of zero-cement mortar. The porosity measured using MIP can only measure a part of the porosity, in order to evaluate the total porosity of hardened body more accurately, the saturated water content is used here to express the total porosity. A preliminary equation is proposed to simply link reaction products and pore structure in this study:

$$I = \frac{100 * W}{S}$$

Here, I: strength index

W: Weight loss ratio (105℃-300℃) (%)

S: Percentage of saturated water content (%)

The strength index is shown in Table.4.4.9.

Table.4.4.9 Strength index

Sample	Weight loss ratio (%) (105℃-300℃)	Percentage of saturated water content（%）	strength index	mortar strength (MPa)
①_7d	3.22%	36.30%	8.86	4.99
②_7d	3.66%	34.52%	10.62	12.96
③_7d	4.02%	33.48%	12.00	17.29
④_7d	3.85%	31.60%	12.18	18.79
⑤_7d	3.04%	36.95%	8.23	9.64
⑥_7d	3.41%	34.98%	9.74	15.56
⑦_7d	3.41%	33.51%	10.19	18.20
⑧_7d	3.79%	32.14%	11.79	21.03
⑨_7d	3.68%	31.54%	11.67	19.72
⑩_7d	2.98%	36.02%	8.27	12.50
⑪_7d	3.64%	36.06%	10.10	16.54
⑫_7d	3.59%	35.30%	10.18	16.90
⑬_7d	3.61%	33.95%	10.62	21.31
①_28d	4.58%	34.22%	13.40*	21.26
②_28d	4.89%	30.82%	15.85	29.69
③_28d	4.89%	29.86%	16.37	34.06
④_28d	4.94%	28.01%	17.63	35.43
⑤_28d	4.82%	34.87%	13.83*	24.32
⑥_28d	4.46%	31.21%	14.29	29.87
⑦_28d	4.46%	30.03%	14.84	31.97
⑧_28d	4.33%	28.36%	15.26	35.51
⑨_28d	4.10%	27.37%	14.98	34.75
⑩_28d	4.56%	34.23%	13.31*	22.21
⑪_28d	4.75%	34.17%	13.91	29.55
⑫_28d	4.61%	33.67%	13.69	31.25
⑬_28d	4.26%	29.59%	14.38	33.13

*Note: certain Straetlingite (C_2ASH_8) is generated and affects the Strength index.

Fig.4.4.24 shows very interesting experimental results: when $RSiO_2/RAl_2O_3$ is consistent, the compressive strength and strength index have a very high liner correlation (R^2 is 0.9749, 0.9799 and 0.9894). The fitting line of the relationship of samples 1-4 ($RSiO_2/RAl_2O_3$=6), samples 5-9 ($RSiO_2/RAl_2O_3$=4) and samples 10-13 ($RSiO_2/RAl_2O_3$=2.5) between the compressive

strength and the strength index is close to parallel. Therefore, when $RSiO_2/RAl_2O_3$ is consistent, the strength index can evaluate the compressive strength accurately. At the same strength index, as the $RSiO_2/RAl_2O_3$ ratio is different, the compressive strength is also different. The smaller the $RSiO_2/RAl_2O_3$ ratio, the greater the compressive strength, indicating that the generated CASH gel of lower $RSiO_2/RAl_2O_3$ ratio contributes more to the strength. This conclusion is consistent with the results of Kapeluszna E et al. [11]: increase of Ca/Si ratio as well as Al/Si ratio results in more compacted, foil–like morphology of C-(A)-S-H gels.

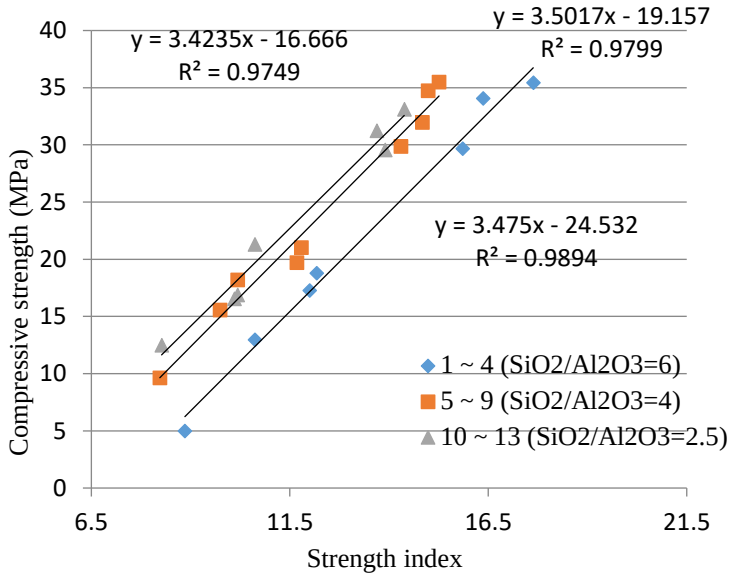

Fig.4.4.24 the relationship between strength index and compressive strength

When the strength is 0, the strength index of SiO_2/Al_2O_3 =6, 4, 2.5 are: I_0=7.1, 5.5, 4.9, respectively. I_0 varies depending on the mix proportion, which means it don not have strength. The smaller the SiO_2/Al_2O_3 molar ratio, the higher the compressive strength, that is, the faster the strength developments. When the pore structures are the same, the larger the $RSiO_2/RAl_2O_3$ molar ratio, I_0 becomes higher, more produced gel is required until strength

development appears. In other words, it is considered that the generated CASH gel, which is a reaction product with a low $RSiO_2/RAl_2O_3$ molar ratio, has a higher contribution to strength development than the CASH gel with a high $RSiO_2/RAl_2O_3$ molar ratio.

Strength index and compressive strength of zero-cement mortar can be approximated by the following linear functions:

$$f_c = \mathrm{a} \cdot \frac{100 * W}{S} + \mathrm{b}$$

f_c: Compressive strength;

W: Weight loss ratio (105℃-300℃) (%)

S: Percentage of saturated water content (%)

a and b: constant.

The strength index and compressive strength of zero cement mortar can be approximated by a linear function. Table.4.4.10 shows a value and b value. a value is basically the same, approximately equal to 3.5. The $RSiO_2/RAl_2O_3$ molar ratio has a high correlation with the b value. Fig.4.4.25 the relationship between SiO_2/Al_2O_3 molar ratio and b value. The smaller the $RSiO_2/RAl_2O_3$ ratio, the higher the b value and the higher the strength index. In other words, it is considered that the generated CASH gel with a low $RSiO_2/RAl_2O_3$ molar ratio contributes significantly to the compressive strength.

According to this equation, the compressive strength can be predicted by the dehydration amount at 105 to 300°C and the percentage of saturated water content.

Table.4.4.10 a value and b value

SiO_2/Al_2O_3 molar ratio	a	b
2.5	3.4235	-16.666
4	3.5017	-19.157
6	3.475	-24.532

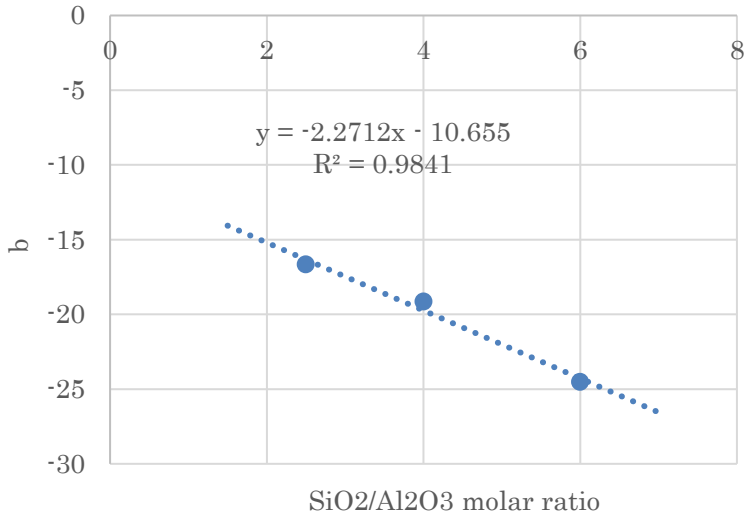

Fig.4.4.25 the relationship between SiO_2/Al_2O_3 molar ratio and b value

4.5 Effects of water/binder ratio

4.5.1 Materials and Experimental Methods

The purpose of this section is to study the effect of water/binder ratio on compressive strength. Table.4.5.1 shows the materials used. The type II shirasu, metakaolin and the blast furnace slag fine powder 8000 were used. BF mainly provides RCaO, SR mainly provides $RSiO_2$, MK mainly provides RAl_2O_3 and $RSiO_2$. Table.4.5.2 shows factors and levels of experiment. The mass ratio of low alkali activator CaO to binder was 6%. The mass ratio of water to binder in mortar were 35%,45% and 55%.The mass ratio of fine aggregate sand to binder in mortar was 1.4: 1. Table.4.5.3 shows the mortar mixture proportion.

Table.4.5.1 Materials used

	Material	Material characters
Binder	Metakaolin	Density:2.59 g/cm^3, mean particle size:3.96um
	Shirasu	Density:2.36g/cm^3, mean particle size:5.28um
	Slag8000	Density:2.91 g/cm^3, Specific surface area:8020cm^2/g mean particle size:5.28um
Low alkali activator	CaO	Density:3.35g/cm^3

Table.4.5.2 Factors and Levels of Experiment

Sample	Metakaolin (%)	Shirasu (%)	Slag (%)	CaO (%)	W/B
⑥	23	31	40	6	35% 45% 55%
⑦	15	19	60		
⑧	7	7	80		
⑨	3	0	91		

Table.4.5.3 Mortar mixture proportion

Name	Water (kg/m^3)	Metakaolin (kg/m^3)	Shirasu (kg/m^3)	BF (kg/m^3)	CaO (kg/m^3)	Sand (kg/m^3)
⑥_35%	274.6	180.5	243.2	313.8	47.1	1098.4
⑦_35%	277.5	118.9	150.6	475.6	47.6	1109.8
⑧_35%	280.3	56.1	56.1	640.8	48.1	1121.3
⑨_35%	281.9	24.2	0.0	733.1	48.3	1127.9
⑥_45%	327.5	167.4	225.6	291.0	43.7	1018.3
⑦_45%	330.6	110.2	139.6	440.7	44.1	1028.0
⑧_45%	333.9	51.9	51.9	593.3	44.5	1037.9
⑨_45%	335.6	22.4	0.0	678.6	44.7	1043.6
⑥_55%	372.8	155.9	210.1	271.1	40.7	950.5
⑦_55%	376.1	102.6	129.9	410.3	41.0	959.0
⑧_55%	379.4	48.3	48.3	551.9	41.4	967.6
⑨_55%	381.4	20.8	0.0	631.0	41.6	972.5

Using a mortar mixer, in order to make the powder and the fine aggregate uniform, the mixture mixed for 3 minutes, then water was added, and the mixture was mixed again for 3 minutes. In this experiment, the mixing amount of one batch was 2 L. As for curing, zero-cement mortar was mixed and then poured into a Φ50mm×100mm sample mold, sealed the top of the mold with a vinyl sheet, The curing was performed at a temperature of 20°C, 60%RH. The compressive strength experiment were conducted at the ages of 7 days, 28days and 90 days using a universal testing machine. The results of compressive strengths are an average of three samples.

4.5.2 Compressive strength

Fig.4.5.1, Fig.4.5.2 and Fig.4.5.3 shows 7days, 28days and 90days compressive strength results respectively. The strength of sample 7 of water/binder ratio=35% is comparatively higher than that of the other samples at 7days, 28 days and 90 days , the strength are 24.60MPa, 43.36MPa and 54.31MPa respectively. At 7 days, when the water/binder ratio=45% and 55%, the compressive strength increases with the increase of CaO content, while when the water/binder ratio =35%, there are different trends of compressive strength. At 28 days and 90 days, the relationship between B/W ratio and compressive strength was similar. Sample 6 have optimal strength at water/binder ratio=45%, although the sample 7 have optimal strength at water/binder ratio =35%. The higher the SiO_2 content, the greater the growth rate of compressive strength at 28 days and 90 days, which is attributed to the continuing pozzolanic reaction.

It can be seen from the figure that the higher the binder/water ratio, the greater the compressive strength of each sample, and it showed an approximate linear function correlation. As the mass ratio of binder to water increase, however, each sample exhibits a different compressive strength growth rate. Regardless of curing age, the Sample 7 show the best compressive strength growth

rate as mass ratio of binder to water increasing. V. Sata et al. [12] demonstrates that the degree of compressive strength due to pozzolanic reaction increases with an increase in W/B ratio. The higher is the W/B ratio, the higher is the degree of pozzolanic reaction. The higher the $Ca(OH)_2$ concentration, the higher the rate of pozzolanic reaction [13]. When W/B = 55%, Sample 8 and Sample 9 have more calcium content, the compressive strength is best due to higher degree of pozzolanic reaction. When the water content decreases, the degree of pozzolanic reaction decreases, and the strength is also effected by the distance between the particles. The size of metakaolin is relatively small. Sample 6 used metakaolin most, followed by sample 7. Therefore, the filling rate of samples with more metakaolin content is higher and have higher filling rate. It can be considered that the relationship between strength and B/W mass ratio is determined by the combined effect of the degree of pozzolanic reaction and the distance between the particles.

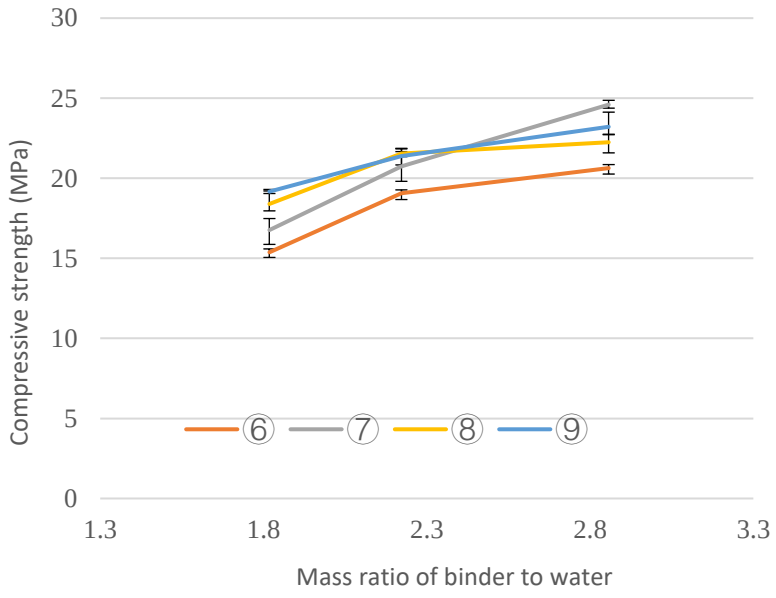

Fig.4.5.1 Relationship between 7days compressive strength and mass ratio of binder to water

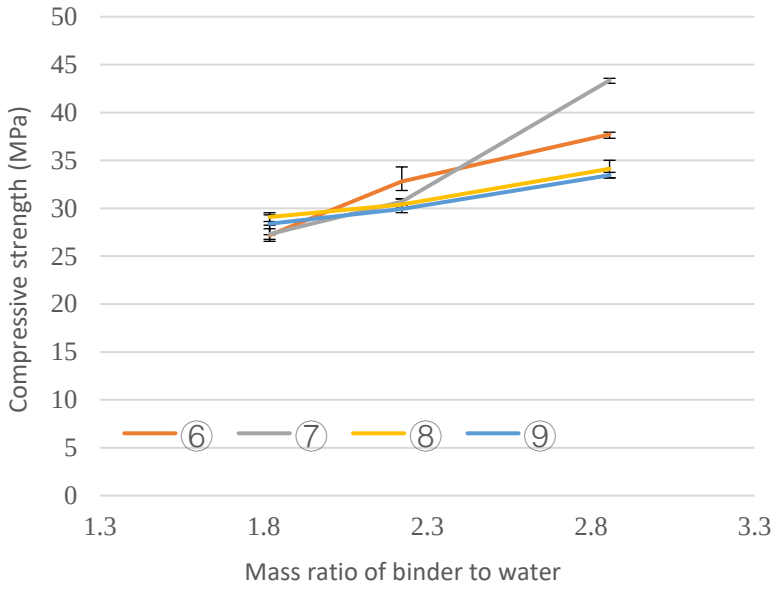

Fig.4.5.2 Relationship between 28days compressive strength and mass ratio of binder to water

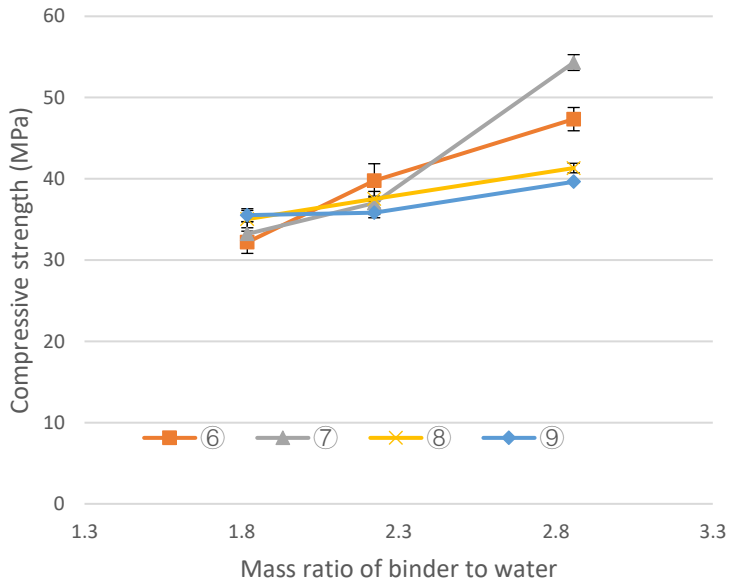

Fig.4.5.3 Relationship between 90days compressive strength and mass ratio of binder to water

4.6 Effects of particle size

4.6.1 Materials and Experimental Methods

The purpose of this section is to study the effect of particle size distribution on compressive

strength. Table.4.6.1 shows the materials used. The metakaolin, type I shirasu, type II shirasu, type III shirasu, and the blast furnace slag fine powder 4000, the blast furnace slag fine powder 8000 were used. BF mainly provides RCaO, SR mainly provides $RSiO_2$, MK mainly provides RAl_2O_3 and $RSiO_2$. Fig.4.6.1 shows the raw material particle size.

Table.4.6.1 Materials used

	Material	Material characters
Binder	Metakaolin	Density:2.59 g/cm^3, mean particle size:3.956um
	Shirasu（type I）	Density:2.36 g/cm^3, mean particle size:2.350um
	Shirasu（type II）	Density:2.36 g/cm^3, mean particle size:5.466um
	Shirasu（type III）	Density:2.36 g/cm^3, mean particle size:6.989um
	Slag 4000	Density:2.91 g/cm^3, Specific surface area:4040cm^2/g mean particle size:15.82um
	Slag 8000	Density:2.91 g/cm^3, Specific surface area:8020cm^2/g mean particle size:5.46um
Low alkali activator	CaO	Density:3.35 g/cm^3

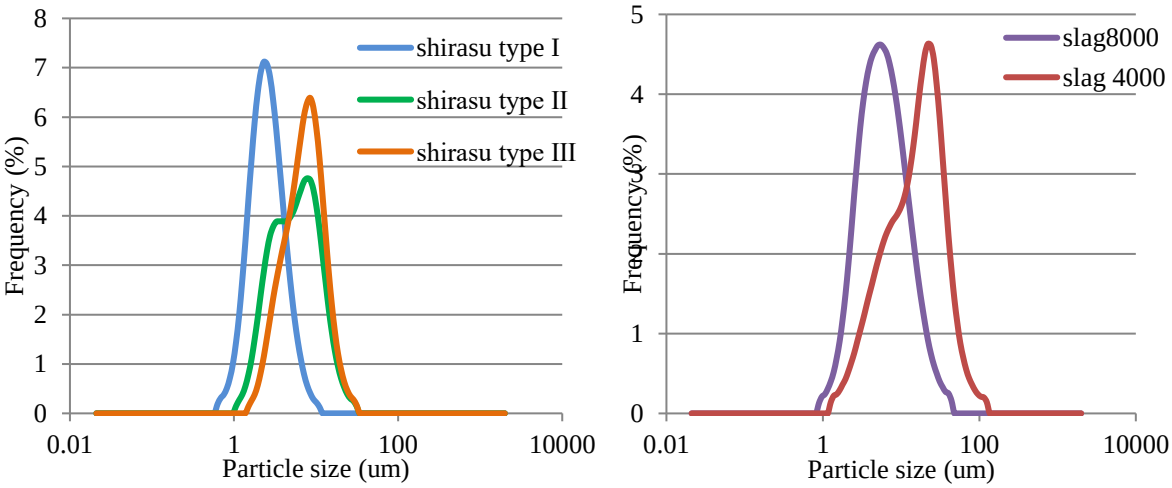

Fig.4.6.1 Raw material particle size

Table.4.6.2 shows the mortar mixture proportion (series 1), mainly study the effect of three different SR particle sizes on strength. Table.4.6.3 shows the mortar mixture proportion (series 2), mainly study the effect of two different BF particle sizes on strength. The mass ratio of low alkali activator CaO to binder was 6%. The mass ratio of water to binder in mortar were 45%.The mass ratio of fine aggregate sand to binder in mortar was 1.4: 1.

Using a mortar mixer, in order to make the powder and the fine aggregate uniform, the powder and fine aggregate were mixed for 3 minutes, then water was added, and the mixture was mixed again for 3 minutes. In this experiment, the mixing amount of one batch was 2 L. As for curing, zero-cement mortar was mixed and then poured into a Φ50mm×100mm sample mold, sealed the top of the mold with a vinyl sheet, The curing was performed at a temperature of 20°C, 60%RH. The compressive strength tests were conducted at the ages of 7days, 28 days and 90days using a universal testing machine. The compressive strengths are an average of three samples.

Table.4.6.2 Mortar mix proportion (series 1)

Mix	Type of Shirasu	Water (kg/m^3)	Metakaolin(kg/m^3)	Shirasu (kg/m^3)	BF (kg/m^3)	CaO (kg/m^3)	Sand (kg/m^3)
SR I ⑥	Type I SR	327.5	167.4	225.6	291	43.7	1018.3
SR I ⑦		330.6	110.2	139.6	440.7	44.1	1028
SR I ⑧		333.9	51.9	51.9	593.3	44.5	1037.9
SR II ⑥	Type II SR	327.5	167.4	225.6	291	43.7	1018.3
SR II ⑦		330.6	110.2	139.6	440.7	44.1	1028
SR II ⑧		333.9	51.9	51.9	593.3	44.5	1037.9
SR III ⑥	Type III SR	327.5	167.4	225.6	291	43.7	1018.3
SR III ⑦		330.6	110.2	139.6	440.7	44.1	1028
SR III ⑧		333.9	51.9	51.9	593.3	44.5	1037.9

Table.4.6.3 Mortar mix proportion (series 2)

Mix	Type of slag	Water (kg/m^3)	Metakaolin(kg/m^3)	Shirasu (kg/m^3)	BF (kg/m^3)	CaO (kg/m^3)	Sand (kg/m^3)
BF8000 ⑥	BF8000	327.5	167.4	225.6	291	43.7	1018.3
BF8000 ⑦		330.6	110.2	139.6	440.7	44.1	1028
BF8000 ⑧		333.9	51.9	51.9	593.3	44.5	1037.9
BF8000 ⑨		335.6	22.4	0	678.6	44.7	1043.6
BF4000⑥	BF4000	327.5	167.4	225.6	291	43.7	1018.3
BF4000⑦		330.6	110.2	139.6	440.7	44.1	1028
BF4000⑧		333.9	51.9	51.9	593.3	44.5	1037.9
BF4000⑨		335.6	22.4	0	678.6	44.7	1043.6

4.6.2 Compressive strength

Fig.4.6.2 shows the compressive strength results. The results show that the finer the particle size of BF, the higher the compressive strength of the mortar at 7days. Higher fineness BF and higher specific surface area can increase the speed of pozzolanic reaction. However, at 28 days and 90 days, the compressive strength of most of BF4000 samples even exceed BF8000 samples. The main reason is that the amount of slag participating in the reaction is the same. Although the specific surface area of BF4000 is small, it will slowly dissolve Ca in the later age and participate in the pozzolanic reaction, resulting in the compressive strength gradually increasing. The BF8000 group has a large specific surface area, and the gel is generated too quickly in the early age, which hinders the further dissolution of Ca, resulting in a slow increase in strength in the later age.

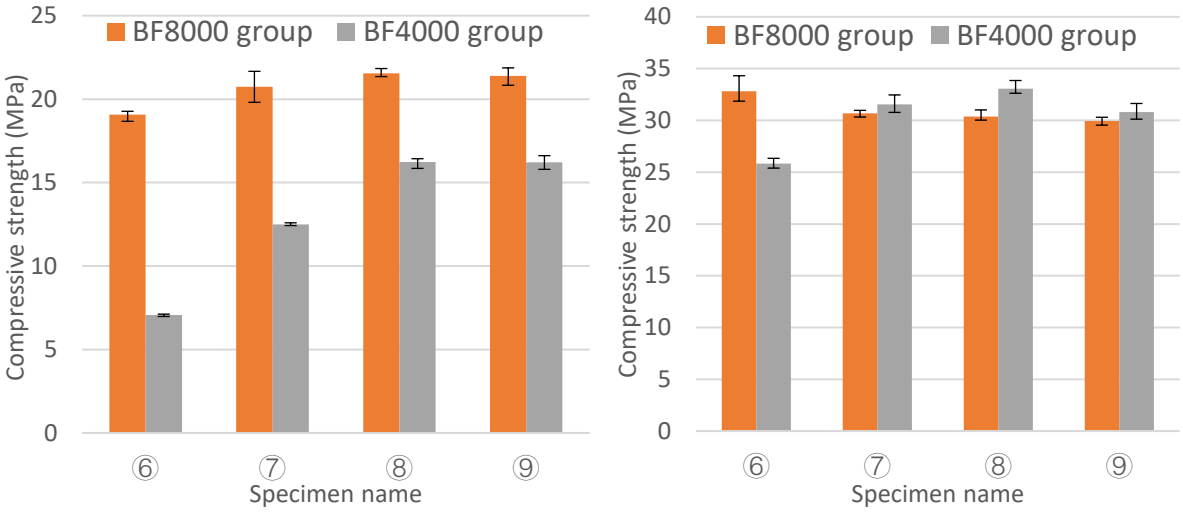

(a) 7days

(b) 28days

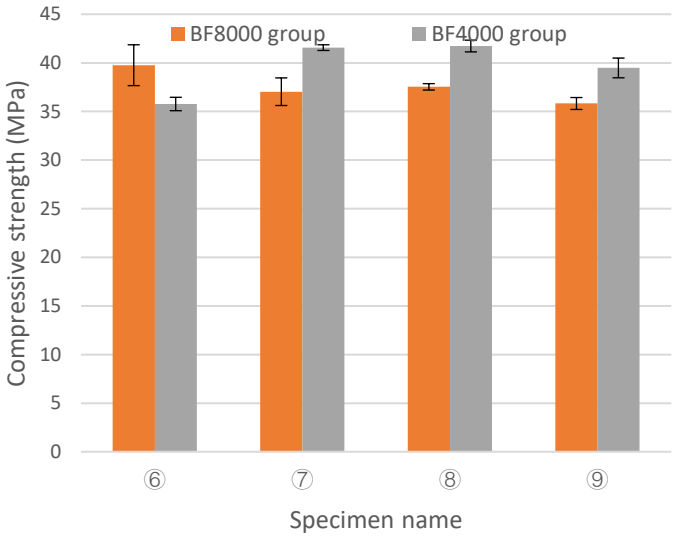

(c) 90days

Fig.4.6.2 compressive strength (a) 7days (b) 28days (c) 90days

Fig.4.6.3 shows effects of using different particle sizes of SR on compressive strength. The results show that the difference in compressive strength between the type Ⅱ SR group and the typeⅢ SR group is very small, while the type Ⅰ SR group with the largest specific surface area have higher compressive strength. The change in compressive strength is different from the BF group, the reason may be that the dissolution speed of Si is much lower than that of Ca. The use

of finer SR has a higher specific surface area, the dissolution speed of Si increases, and more Si participates in the pozzolanic reaction, which increases the compressive strength.

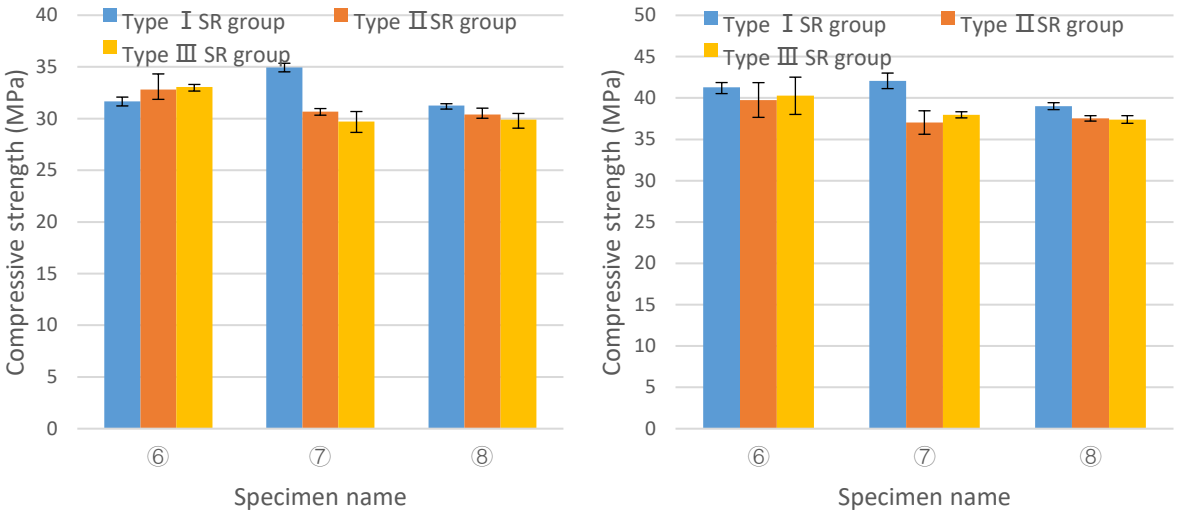

(a) 28days (b) 90days

Fig.4.6.3 compressive strength (a) 28days (b) 90days

4.7 Effects of type of raw materials

4.7.1 Materials and Experimental Methods

The purpose of this section is to study the effect of raw material type on compressive strength. Table.4.7.1 shows the materials used. The fly ash, type II shirasu, metakaolin and the blast furnace slag fine powder 8000 were used. BF mainly provides RCaO, SR and FA mainly provides $RSiO_2$, MK mainly provides RAl_2O_3 and $RSiO_2$. Fig.4.7.1 shows the particle size distribution of raw materials.

Table.4.7.1 Materials used

	Material	Material characters
Binder	Fly ash	Density:2.45g/cm^3, mean particle size:5.318um Specific surface area:5680 cm^2/g
	Metakaolin	Density:2.59 g/cm^3, mean particle size:3.956um
	Shirasu（type II）	Density:2.36 g/cm^3, mean particle size:5.466um
	Slag 8000	Density:2.91 g/cm^3, mean particle size:5.46um Specific surface area:8020cm^2/g
Low alkali activator	CaO	Density:3.35 g/cm^3

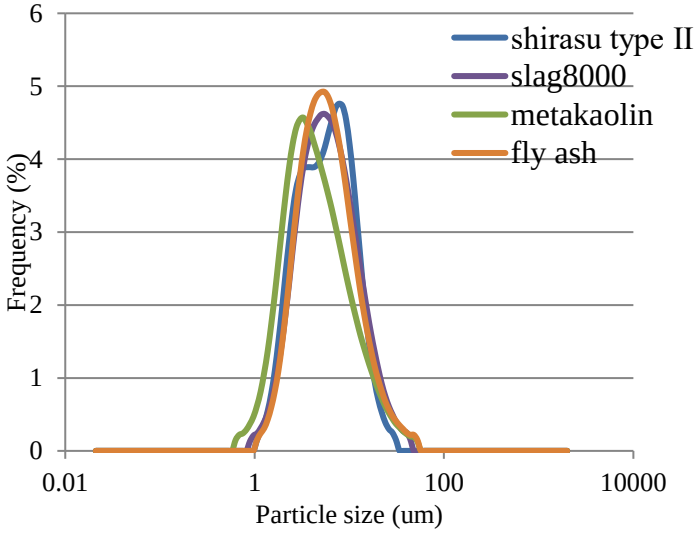

Fig.4.7.1 Particle size distribution of raw material.

Table.4.7.2 and Table.4.7.3 show the mortar mixture proportion. For series 1 group, study the effect of different types of raw material on strength at same W/B ratio. For series 2 group, study the effect of different types of raw material on strength at same W/G ratio. The mass ratio of low alkali activator CaO to binder was 6%. The mass ratio of fine aggregate sand to binder was 1.4: 1.

Table.4.7.2 Mortar mixture proportion (series 1)

Group name	Specimen	Water (kg/m^3)	Metakaolin (kg/m^3)	SR or FA (kg/m^3)	BF (kg/m^3)	CaO (kg/m^3)	Sand (kg/m^3)
SR group （W/B=45%）	SR⑥	327.5	167.4	225.6	291.0	43.7	1018.3
	SR⑦	330.6	110.2	139.6	440.7	44.1	1028.0
	SR⑧	333.9	51.9	51.9	593.3	44.5	1037.9
FA group (W/B=45%)	FA⑥	326.1	87.0	347.9	246.4	43.5	1014.2
	FA⑦	329.6	65.9	219.7	402.8	43.9	1024.9
	FA⑧	333.3	37.0	88.8	570.1	44.4	1036.2

Table.4.7.3 Mortar mixture proportion (series 2)

Group name	Specimen	Water (kg/m^3)	Metakaolin (kg/m^3)	SR or FA (kg/m^3)	BF (kg/m^3)	CaO (kg/m^3)	Sand (kg/m^3)
SRG group (W/G=45%)	SRG⑥	327.5	176.8	241.6	291.0	43.7	992.8
	SRG⑦	330.6	117.5	148.4	440.7	44.1	1011.9
	SRG⑧	333.9	56.4	54.1	593.3	44.5	1031.3
FAG group (W/G=45%)	FAG⑥	326.1	101.5	384.1	282.6	43.5	927.2
	FAG⑦	329.6	69.6	241.7	432.1	43.9	970.0
	FAG⑧	333.3	37.0	88.8	592.3	44.4	1014.0

Using a mortar mixer, in order to make the powder and the fine aggregate uniform, the powder and fine aggregate were mixed for 3 minutes, then water was added, and the mixture was mixed again for 3 minutes. In this experiment, the mixing amount of one batch was 2 L. As for curing, zero-cement mortar was mixed and then poured into a Φ50mm×100mm sample mold, sealed the top of the mold with a vinyl sheet, The curing was performed at a temperature of 20°C, 60%RH. The compressive strength tests were conducted at the ages of 7days, 28 days and 90days using a universal testing machine. The reported compressive strengths are an average

of three samples.

4.7.2 Compressive strength

Fig.4.7.2 shows the compressive strength (series 1) results. The results show that as the age increases, the compressive strength of SR group and FA group gradually increases. When the amount of SR or FA used is small, the compressive strength of the SR group and the FA group is very close. However, when the content of SR or FA increase, the compressive strength of the FA group is smaller than that of the SR group, especially in the early age. In the later age, the difference between the compressive strength of the FA group and the SR group gradually decreased. The main reason may be that the dissolution speed of SR is faster than that of FA, resulting in a difference in initial compressive strength. As FA gradually dissolves and the pozzolanic reaction proceeds, the gap in compressive strength gradually decreases in the later age.

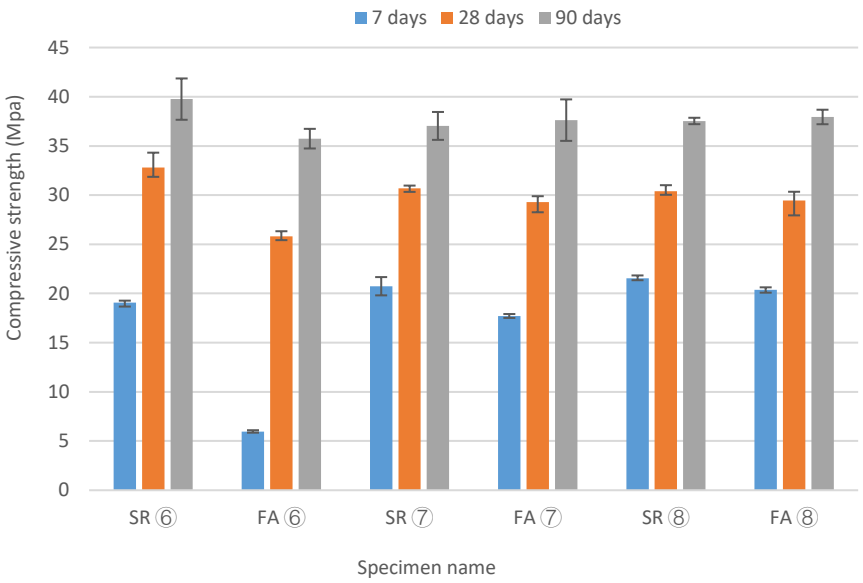

Fig.4.7.2 compressive strength (series 1)

Fig.4.7.3 shows the compressive strength (series 2) results. The results show that as the age

increases, the compressive strength of SR group and FA group gradually increases. The development of the compressive strength of Series 2 and Series 1 is basically the same. Compared with the W/B=45% group, the W/G=45% group contained higher amorphous content. At 7 days, there was no significant difference in compressive strength between the two groups, and at 28 days, the compressive strength of the W/G=45% group was greater than the W/B=45% group, mainly because in the W/G=45% group, More amorphous components participate in the pozzolanic reaction, resulting in higher compressive strength.

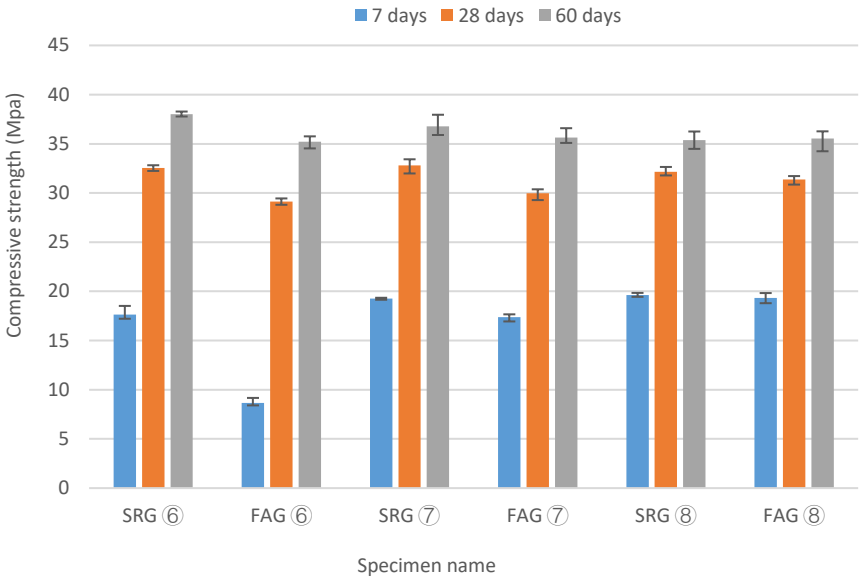

Fig.4.7.3 compressive strength (series 2)

4.8 Conclusions

Based on the results conducted in this chapter, the following conclusions can be inferred:

(1) The longer the curing age, the higher the compressive strength. The specimens 1-2 (SF: FA: BF = 1.5: 2.5: 6) are optimal. The compressive strength at 3 days increased to 35 MPa and the compressive strength at 28 days increased to 95 MPa.

(2) At 20℃ curing, the more low alkali activator content, the greater the compressive strength.

The maximum strength at 7 days is 70.2 MPa, and the maximum strength at 28 days is 79.8 MPa. At 90℃ heat curing, as the amount of low-alkali activator increases, the compressive strength increases first and then decreases. When the amount of low-alkali activator is 80kg/m^3, the maximum compressive strength in 7 days reaching up to 136 MPa.

(3) The higher the content of RCaO and RAl_2O_3, the greater the 7days compressive strength. The higher the RCaO content, the greater the 28days and 140days compressive strength.

(4) The change of Young's modulus is consistent with the change of compressive strength. The larger the Young's coefficient, the higher the compressive strength.

(5) Compressive strength has a correlation with saturated water content. The lower the saturated water content, the greater the compressive strength.

(6) The XRD analysis shows that the main reaction product of low alkali zero-cement is composed of a glass phase (gel) indicated by a halo peak of 18 to 35°(2θ) and a crystal phase of Hemicarbonate ($C_4Ac_{0.5}H_{12}$), Straetlingite (C_2ASH_8) and Portlandite ($Ca(OH)_2$). As the content of RCaO increases, the amount of Straetlingite produced gradually decreases. Regardless of the $RSiO_2/RAl_2O_3$ molar ratio, when the RCaO content is low, low-alkali activated zero-cement tends to form Straetlingite.

(7) When $RSiO_2/RAl_2O_3$ is consistent, the compressive strength and strength index have a very high liner correlation (R^2 is 0.9749, 0.9799 and 0.9894). It is possible to use the strength index to evaluate the compressive strength. At the same strength index, The smaller the $RSiO_2/RAl_2O_3$ ratio, the greater the compressive strength, indicating that the generated CASH gel with lower $RSiO_2/RAl_2O_3$ ratio contributes more to the strength. The compressive strength can be predicted by the dehydration amount at 105 to 300℃ and the percentage of saturated water content.

(8) The bigger the binder/water ratio, the greater the compressive strength, and it showed an

approximate linear function correlation. The strength is determined by the combined effect of the degree of pozzolanic reaction and the distance between the particles.

(9) The finer the particle size of BF, the higher the compressive strength of the mortar at early age. Higher fineness BF and higher specific surface area can increase the speed of pozzolanic reaction. However, the compressive strength of some BF4000 samples even exceed BF8000 samples at later age. The difference in compressive strength between the type Ⅱ SR group and the typeⅢ SR group is very small, while the type Ⅰ SR group with the largest specific surface area has the highest compressive strength.

(10) Regardless of W/B=45% or W/G=45%, when the amount of SR or FA used is small, the compressive strength of the SR group and the FA group is very close. However, when the content of SR or FA increase, the compressive strength of the FA group is smaller than that of the SR group, especially in the early age. In the later age, the gap between the compressive strength of the FA group and the SR group gradually decreased.

References

(1) Kim MS, Jun Y, Lee C, Oh JE. Use of CaO as an activator for producing a price-competitive non-cement structural binder using ground granulated blast furnace slag. Cem Concr Res 2013;54:208-214.

(2) Yum WS, Jeong Y, Yoon S, Jeon D, Jun Y, Oh JE. Effects of CaCl 2 on hydration and properties of lime(CaO)-activated slag/fly ash binder. Cement and Concrete Composites 2017;84:111-123.

(3) Jeong Y, Park H, Jun Y, Jeong JH, Oh JE. Influence of slag characteristics on strength development and reaction products in a CaO-activated slag system. Cement and Concrete Composites 2016;72:155-167.

(4) 松田拓ほか：ポルトランドセメントを使用しない超低収縮・高強度コンクリート，日本建築学会大会学術講演梗概集，pp.1185-1186，2017

(5) Zhao F, Ni W, Wang H, Liu H. Activated fly ash/slag blended cement. Resources, Conservation & Recycling 2007;52(2):303-313.

(6) Morsy MS, Alsayed SH, Salloum YA. Development of eco-friendly binder using metakaolin-fly ash–lime-anhydrous gypsum. Constr Build Mater 2012;35:772-777.

(7) Şahin M, Mahyar M, Erdoğan ST. Mutual activation of blast furnace slag and a high-calcium fly ash rich in free lime and sulfates. Constr Build Mater 2016;126:466-475.

(8) Sharma AK, Sivapullaiah PV. Strength development in fly ash and slag mixtures with lime. Proceedings of

the Institution of Civil Engineers - Ground Improvement 2016;169(3):194-205.

(9) Shi, C., and Day, R. L. (2000). “Pozzolanic reaction in the presence of chemical activators. II: Reaction products and mechanism.” Cem.Concr. Res., 30(4), 607–613.

(10) De Weerdt K, Haha MB, Le Saout G, Kjellsen KO, Justnes H, Lothenbach B. Hydration mechanisms of ternary Portland cements containing limestone powder and fly ash. Cem Concr Res 2011;41(3):279-291.

(11) Kapeluszna E, Kotwica Ł, Różycka A, et al. Incorporation of Al in CASH gels with various Ca/Si and Al/Si ratio: Microstructural and structural characteristics with DTA/TG, XRD, FTIR and TEM analysis[J]. Construction and Building Materials, 2017, 155: 643-653.

(12) Sata V, Tangpagasit J, Jaturapitakkul C, et al. Effect of W/B ratios on pozzolanic reaction of biomass ashes in Portland cement matrix[J]. Cement and Concrete Composites, 2012, 34(1): 94-100.

(13) H. Uchikawa, Effect of blending compressive strength on the hydration structure formation of blended cement, Cement Science and Concrete Technology, vol. 484, Japan Cement Association, 1987.

5. Proposal of design method for ultra-high strength zero-cement mortar

5.1 Introduction

So far, researchers have proposed many prediction models and equation for the compressive strength development of cement concrete. However, there is little research on the prediction model of zero-cement mortar. Based on the results of Chapters 3 and Chapters 4, predict the strength of zero-cement mortar with a similar design concept and design method, whether low alkali or high alkali. That is, if there is a need to achieve a certain design strength, it can derive the zero-cement mixing ratio according to the design method.

In this chapter, the author first used the ACI model that often used in cement to test its applicability in zero-cement, and re-proposed a new zero-cement model. The strength prediction results of these two models are compared. This new zero-cement model can expresses a value and b value: which are dependent on the zero-cement's RCaO, RAl_2O_3 and $RSiO_2$ content, in the form of a function of age, glass content/water ratio. This model is capable of explaining the strength change due to the change in the proportion of RCaO, RAl_2O_3 and $RSiO_2$ content, the relationship between the glass content/water ratio and strength of zero-cement mortar. Besides, verified the applicability of zero-cement model in the case of different ratios, different type of raw materials and different particle sizes. Finally, relationship between compressive strength of zero cement and each active constituents are discussed.

5.2 Prediction model of compressive strength development of zero-cement mortar

5.2.1 ACI model

Fig.5.2.1 shows the relationship between compressive strength and age. As the age increases, the early compressive strength increases rapidly, and the later compressive strength increases slowly. It shows that zero-cement mortar has similar strength development law as cement

concrete. Therefore, it is believed that zero-cement may also be applicable to the ACI model.

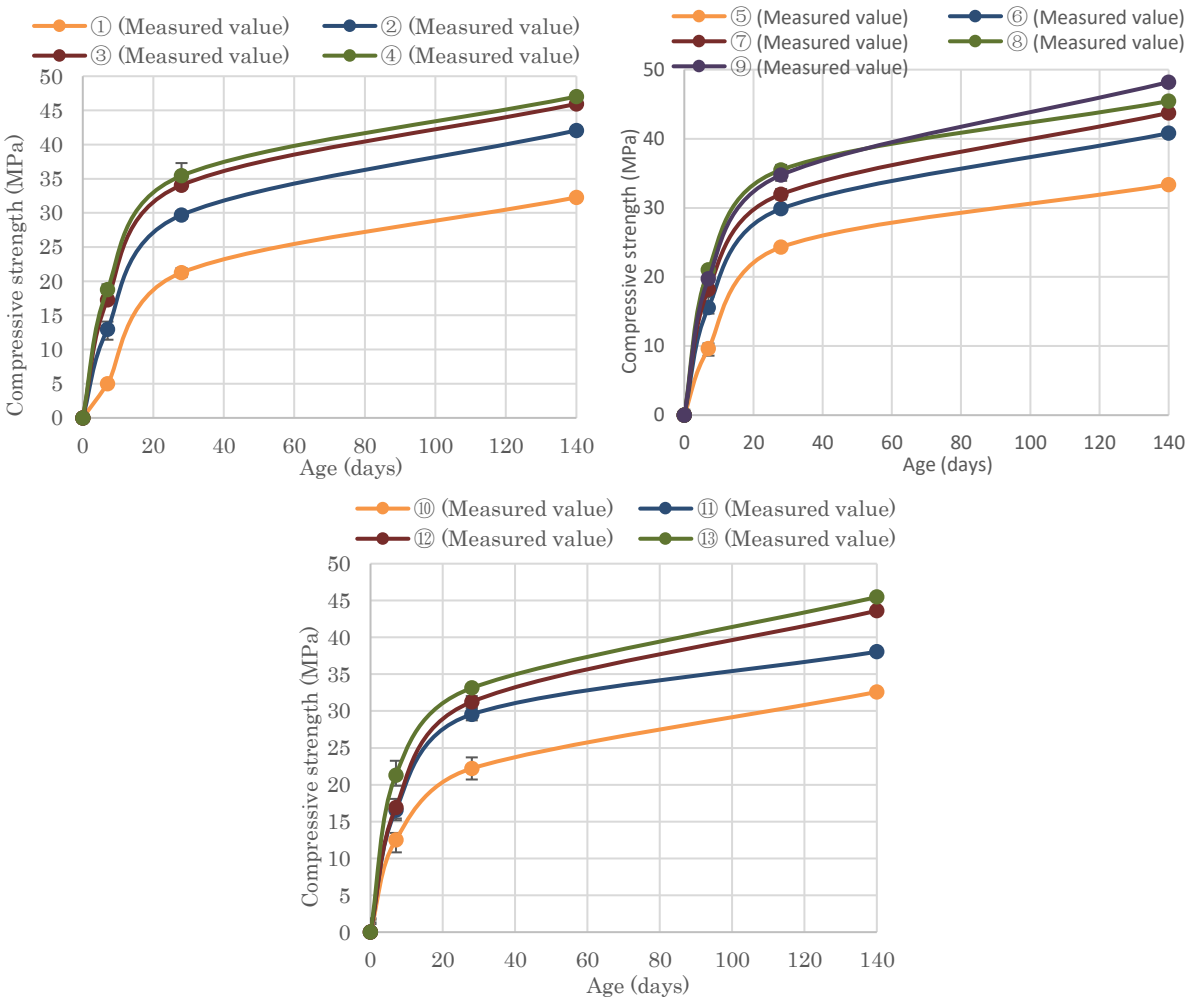

Fig.5.2.1 Relationship between compressive strength and age.

ACI model suggested the following model to evaluate the compressive strength evolution of cement concrete as curing time:

$$f_{cm}(t) = [\frac{t}{a + bt}] \cdot f_{cm} \qquad (1)$$

Where, f_{cm} : Mean tested compressive strength of concrete at the age of 28days; a and b: are dependent on the type of cement and the curing condition of concrete, which were suggested ranging from 0.05 to 9.25 and 0.67 to 0.98 in ACI code, respectively. For OPC concrete, they were taken as 4.0 and 0.85 [1], respectively.

By transforming the Eq. (1), we can get the following equation.

$$\frac{fcm}{fcm(t)} = \mathrm{a} \cdot \frac{1}{t} + b \qquad (2)$$

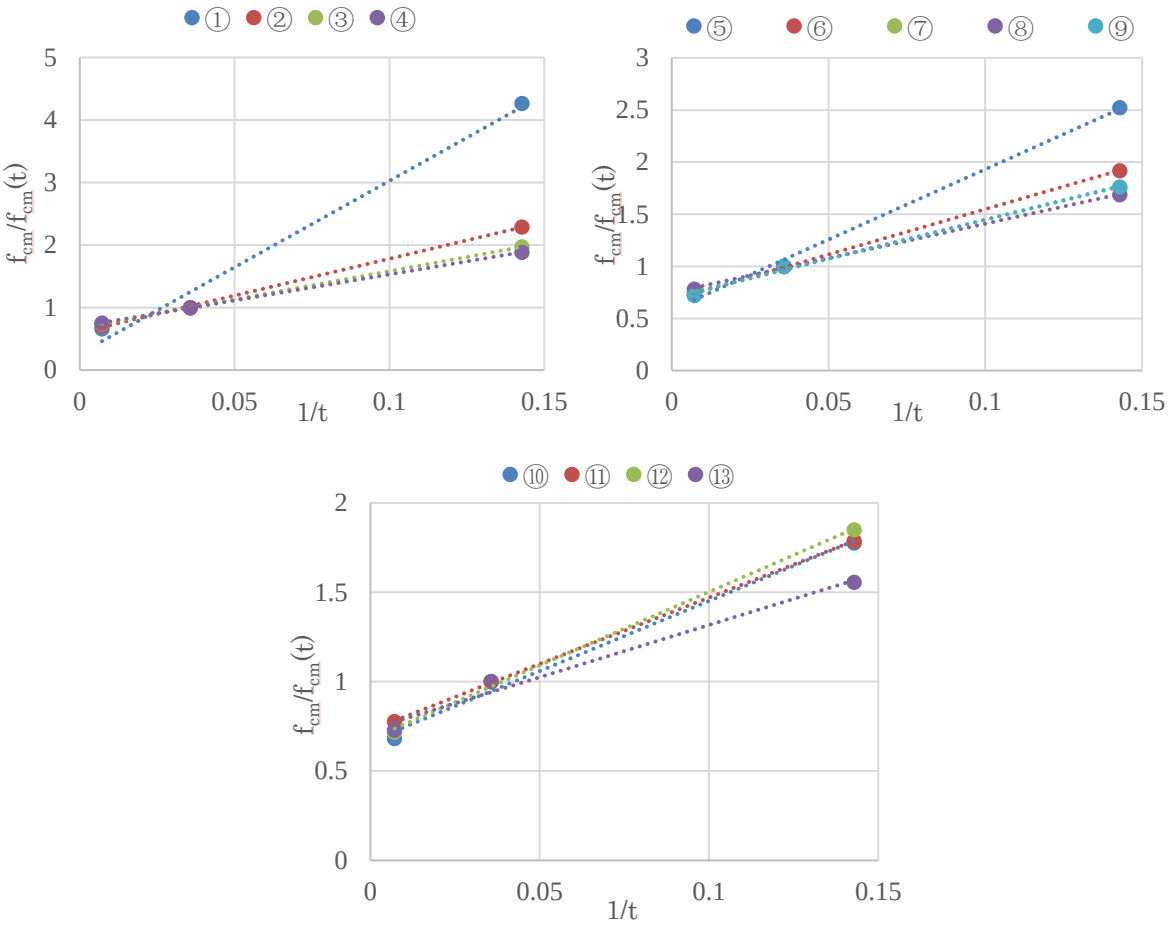

Fig.5.2.1 Relationship between $f_{cm}/f_{cm}(t)$ and 1/t.

The relationship between $f_{cm}/f_{cm}(t)$ and 1/t can be used to confirm whether this model is suitable for zero-cement mortar. The Fig.5.2.1 shows that in regard to the relationship between $f_{cm}/f_{cm}(t)$ and 1/t, most of the proportion have a linear approximation relationship, but mixture 1 does not match. a and b are Constants, which are dependent on the zero-cement's RCaO, RAl_2O_3 and $RSiO_2$ content. Table.5.2.1 shows a value and b value of each specimen. In this study, a value were taken as from 5 to 28, b value were taken as from 0.2 to 0.8. For OPC concrete, a value and b value were taken as 4.0 and 0.85, Compared with OPC, a value of zero-cement is larger and the b value of zero-cement is smaller. Fig.5.2.2 shows the relationship between a value and b value. It shows that a value and b value have a high linear correlation (R^2=0.9869). It can be concluded that: b=-0.0219a+0.8693.

Table.5.2.1 Values of a and b

Sample	①	②	③	④	⑤	⑥	⑦	⑧	⑨	⑩	⑪	⑫	⑬
a	27.63	11.78	9.05	8.32	13.49	8.70	7.42	6.62	7.52	7.85	7.41	8.23	5.84
b	0.26	0.60	0.68	0.70	0.58	0.68	0.70	0.75	0.70	0.67	0.73	0.68	0.73

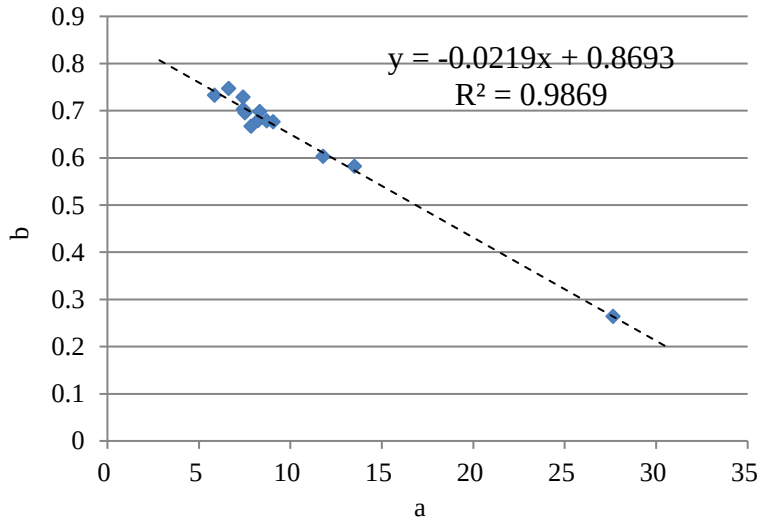

Fig.5.2.2 Relationship between a value and b value.

Therefore, the Eq. (1) can be further transformed, compressive strength of zero-cement mortar at various ages could be estimated from:

$$f_{cm}(t) = [\frac{t}{a + (0.8693 - 0.0219 \cdot a) \cdot t}] \cdot f_{cm} \qquad (3)$$

f_{cm}: Mean tested compressive strength of zero-cement mortar at the age of 28days;

a: is dependent on the zero-cement's RCaO, RAl_2O_3 and $RSiO_2$ content;

Note: This equation is suitable for t≥7, curing temperature at 20℃.

a value can approximately represent the reaction rate of zero-cement. The larger a value, the slower the reaction rate and the greater the strength increase in the later age; the smaller a value, the faster the reaction rate and the smaller the strength increase in the later age.

Fig.5.2.3 shows the relationship between a value and $RSiO_2$, RAl_2O_3 and RCaO content and glass content. a value has the high correlation with the $RSiO_2$ content. The more $RSiO_2$, the larger a value and the slower the reaction rate.

Fig.5.2.4 shows the relationship between a value and (C+S), (C+A), (S+A) and (C+S+A). The content of (C+A) is relative to the content of $RSiO_2$, the more content of (C+A), the smaller a value, the faster the reaction rate. a value also has the high correlation with the (C+S+A) content, The more active constituent that can participate in the reaction, the faster the reaction rate.

Fig.5.2.5 shows the relationship between a value and CaO-SiO_2-Al_2O_3 molar ratio.

Fig.5.2.6 shows the relationship between a value and C/(A+S), (C+A)/S molar ratio.

Fig.5.2.7 shows the relationship between a value and S/(C+A).The value of a have the highest correlation with S/(C+A) molar ratio. With the increase of S/(C+A) molar ratio, the value of a also increases.

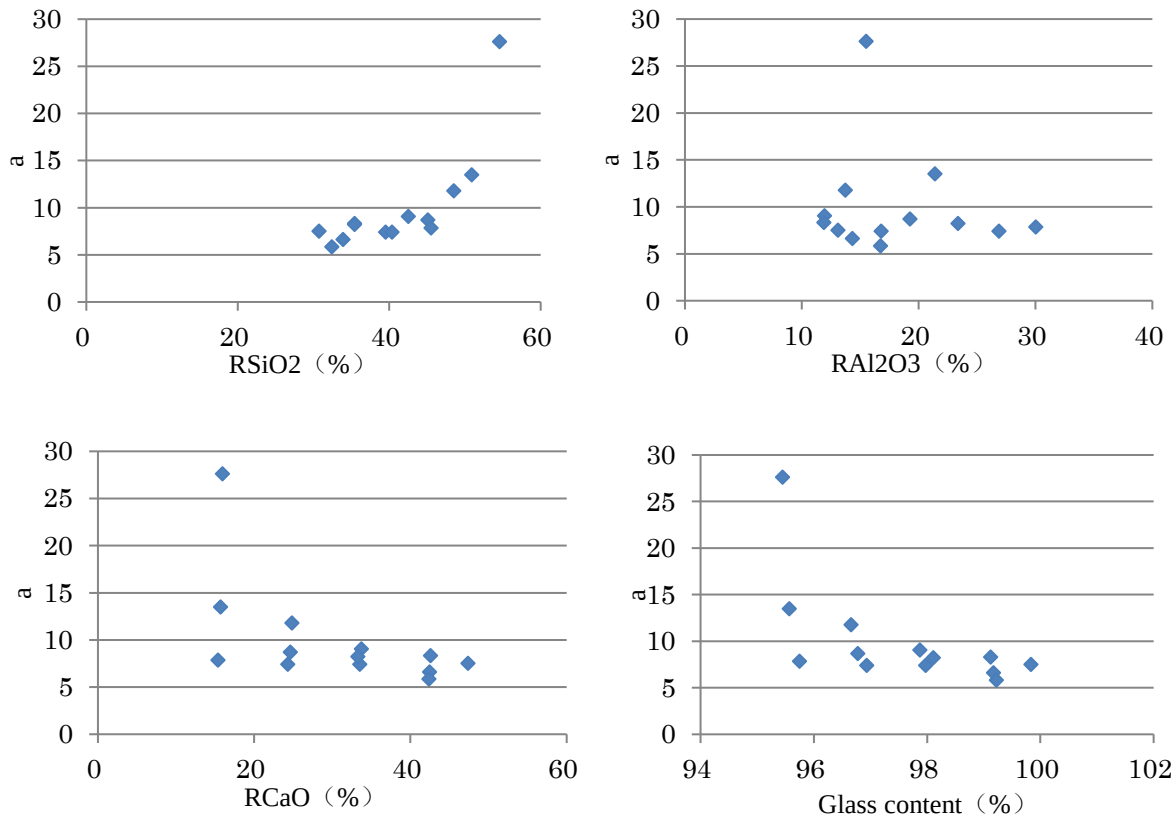

Fig.5.2.3 Relationship between a value and $RSiO_2$, RAl_2O_3, RCaO content and glass content.

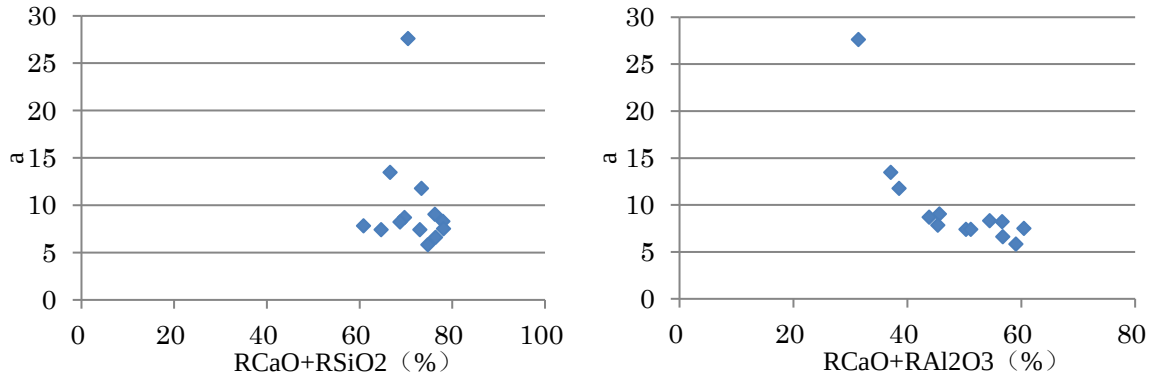

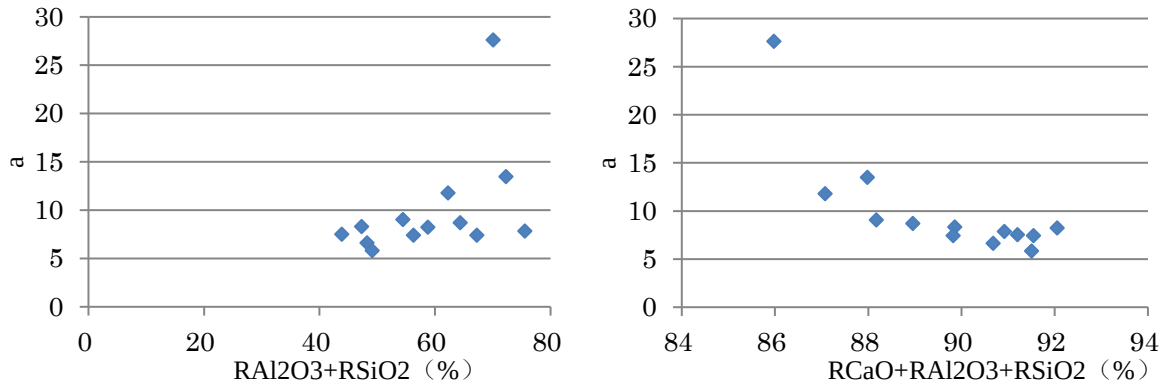

Fig.5.2.4 The relationship between a value and (C+S), (C+A), (S+A) and (C+S+A)

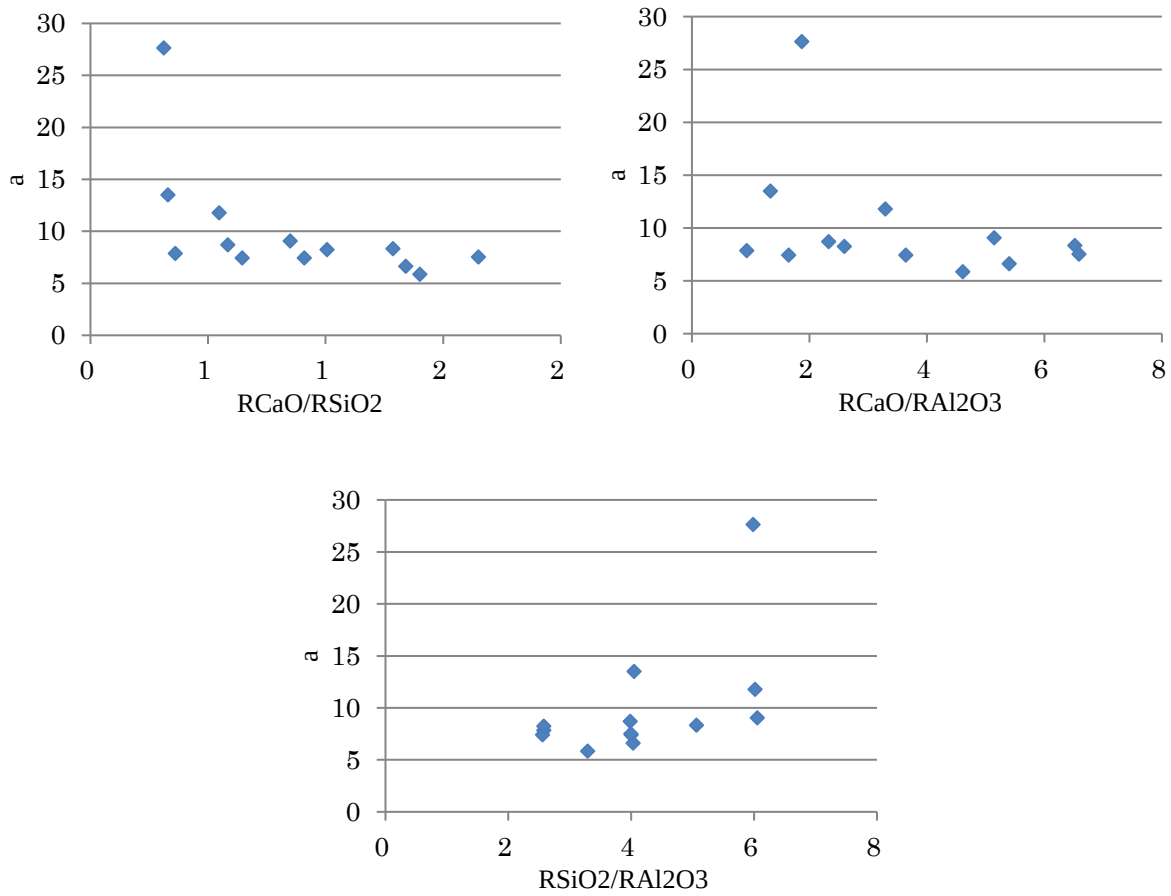

Fig.5.2.5 The relationship between a value and $CaO\text{-}SiO_2\text{-}Al_2O_3$ molar ratio

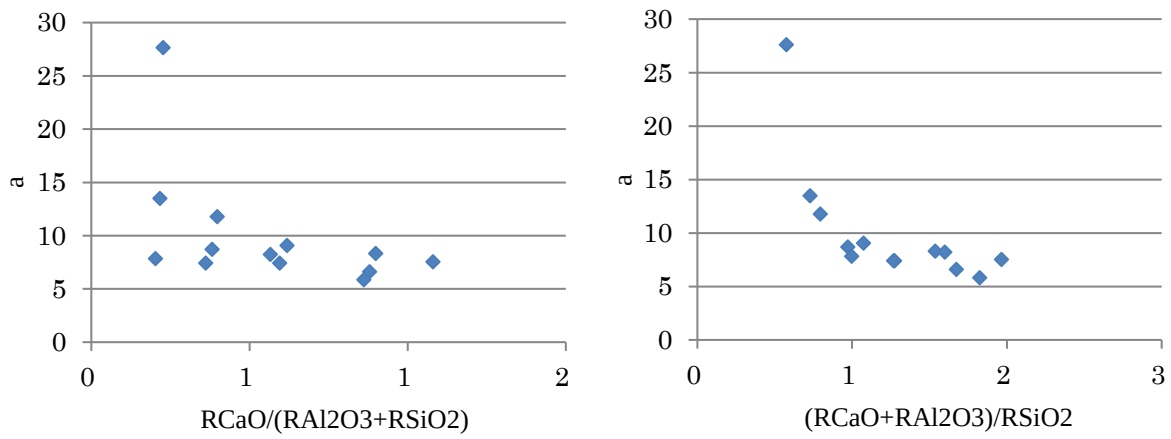

Fig.5.2.6 The relationship between a value and C/(A+S), (C+A)/S molar ratio

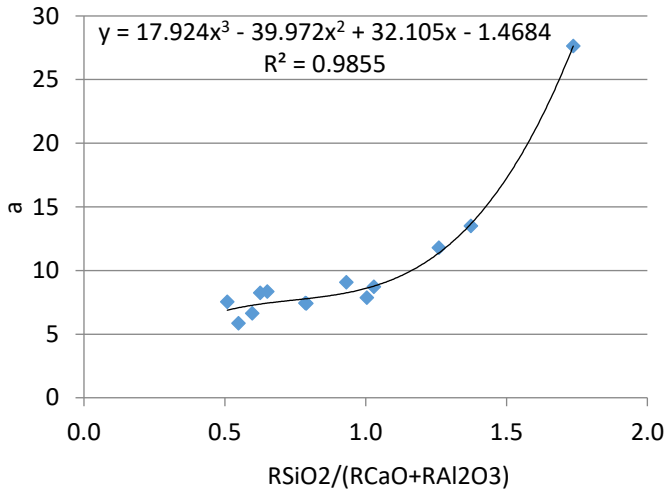

Fig.5.2.7 The relationship between a value and S/(C+A)

It can be seen from the above results that a value has the highest correlation (R^2=0.9855) with $RSiO_2/(RCaO+RAl_2O_3)$, which can be approximated by a cubic function as follows.

$$a = 17.924x^3 - 39.972x^2 + 32.105x - 1.4684 \quad (0.5 < x < 1.8)$$

x: S/(C+A) (%)

The greater the S/(C+A) molar ratio, the greater the value of a. Compared with CaO and Al_2O_3, the dissolution speed of SiO_2 is slower. Therefore, the higher the SiO_2 content, the slower the reaction rate and the larger the value of a. Therefore, as long as the percentage of $RSiO_2$, RCaO and RAl_2O_3 contained in zero-cement is determined, the strength development of zero-cement mortar can be predicted.

Fig.5.2.8 shows the relationships between the measured value and the prediction values calculated by the ACI model (Eq. (3) and Eq. (1)). (a) is when a and b are regarded as linear correlation. (b) is to consider a and b uncorrelated. (a) compared with (b), there is no significant change in the relationship between the predicted value and the measured value, Therefore, considering a and b as a linear relationship can also predict the development of compressive strength of zero-cement mortar.

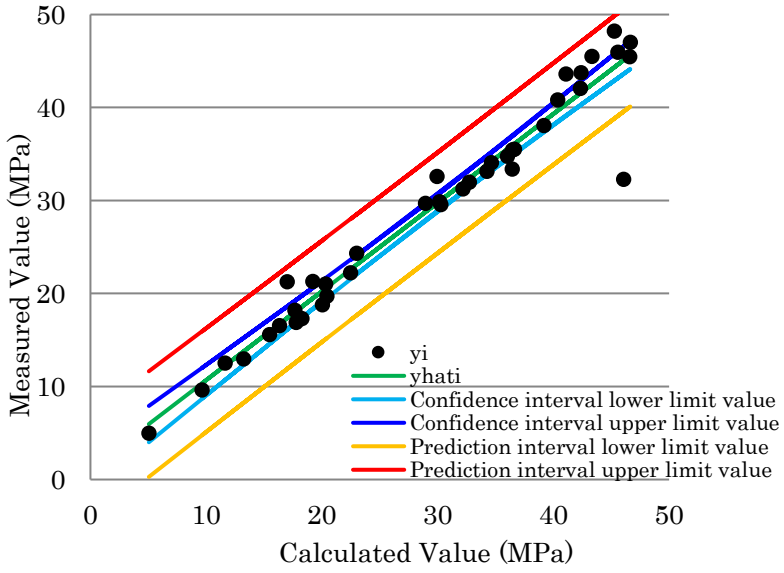

(a) Linear relationship between a and b.

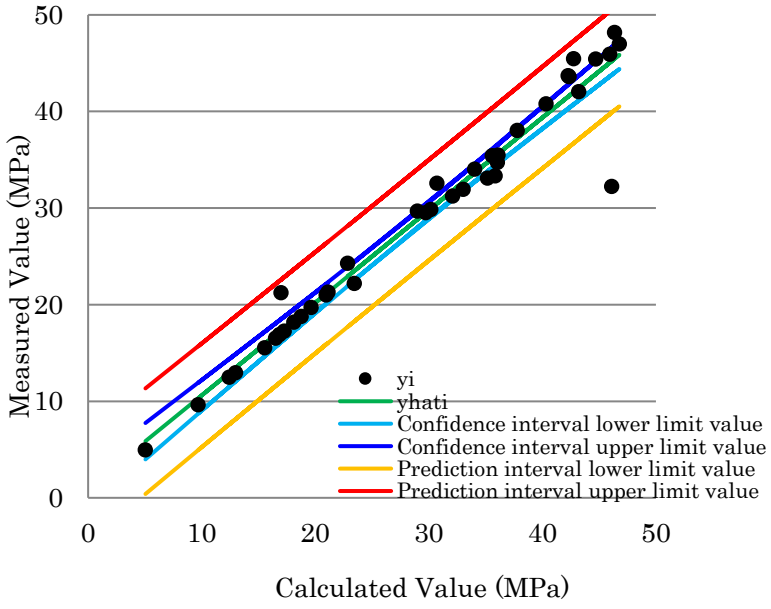

(b) No relationship between a and b.

Fig.5.2.8 Relationship between calculation value (by ACI model) and experimental value.

Fig.5.2.9 shows prediction curve (by ACI model) of compressive strength with increasing age. Since prediction curve of mixture1 do not match the measured value, it is necessary to propose a new prediction model in order to predict the compressive strength of zero-cement mortar more accurately.

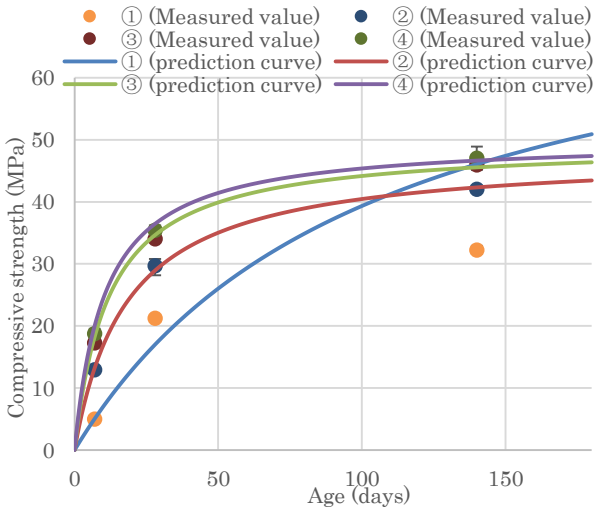

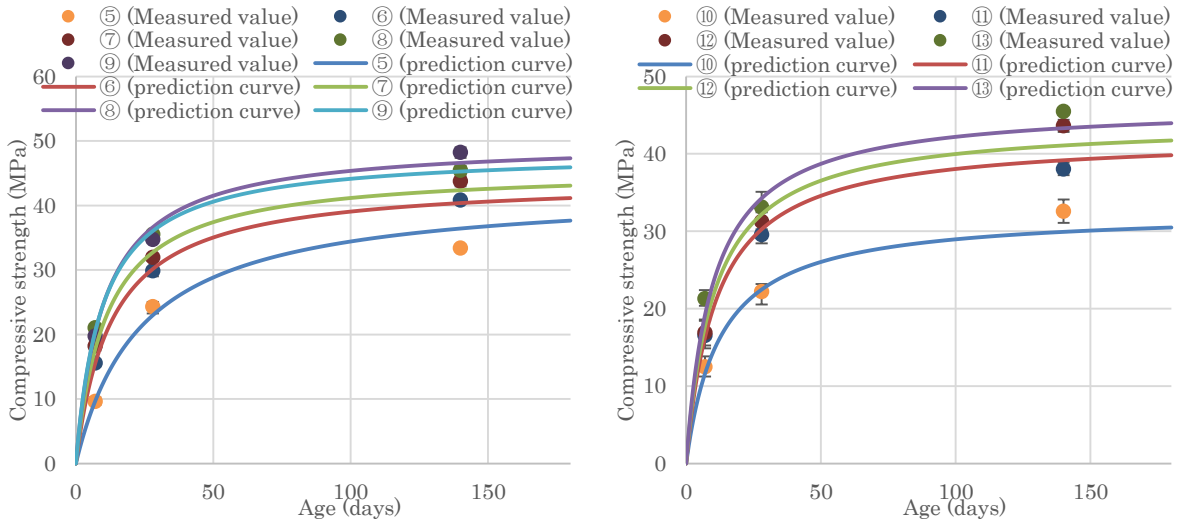

Fig.5.2.9 Prediction curve (by ACI model) of compressive strength with increasing age

5.2.2 Zero-cement model

The ACI model is a model suitable for the strength development of cement. The reaction rate of cement is fast, but the reaction rate of zero-cement is slow at early age. Mixture 1 contains a large amount of $RSiO_2$ and a small amount of RCaO and RAl_2O_3, the reaction rate and the early compressive strength is low. Fig.5.2.1 shows that the mixture 1 does not satisfy the linear relationship between fcm/fcm(t) and 1/t, it seems to satisfy the exponential function relationship.

The relationship between $\ln(f_{cm}/f_{cm}(t))$ and 1/t can be used to confirm whether this model is suitable for zero-cement mortar. The Fig.5.2.10 shows that $\ln(f_{cm}/f_{cm}(t))$ is a linear function of 1/t. it shows that the zero-cement model is suitable for predicting the strength development of zero-cement mortar. a and b are Constants, which are dependent on the zero-cement's RCaO, RAl_2O_3 and $RSiO_2$ content.

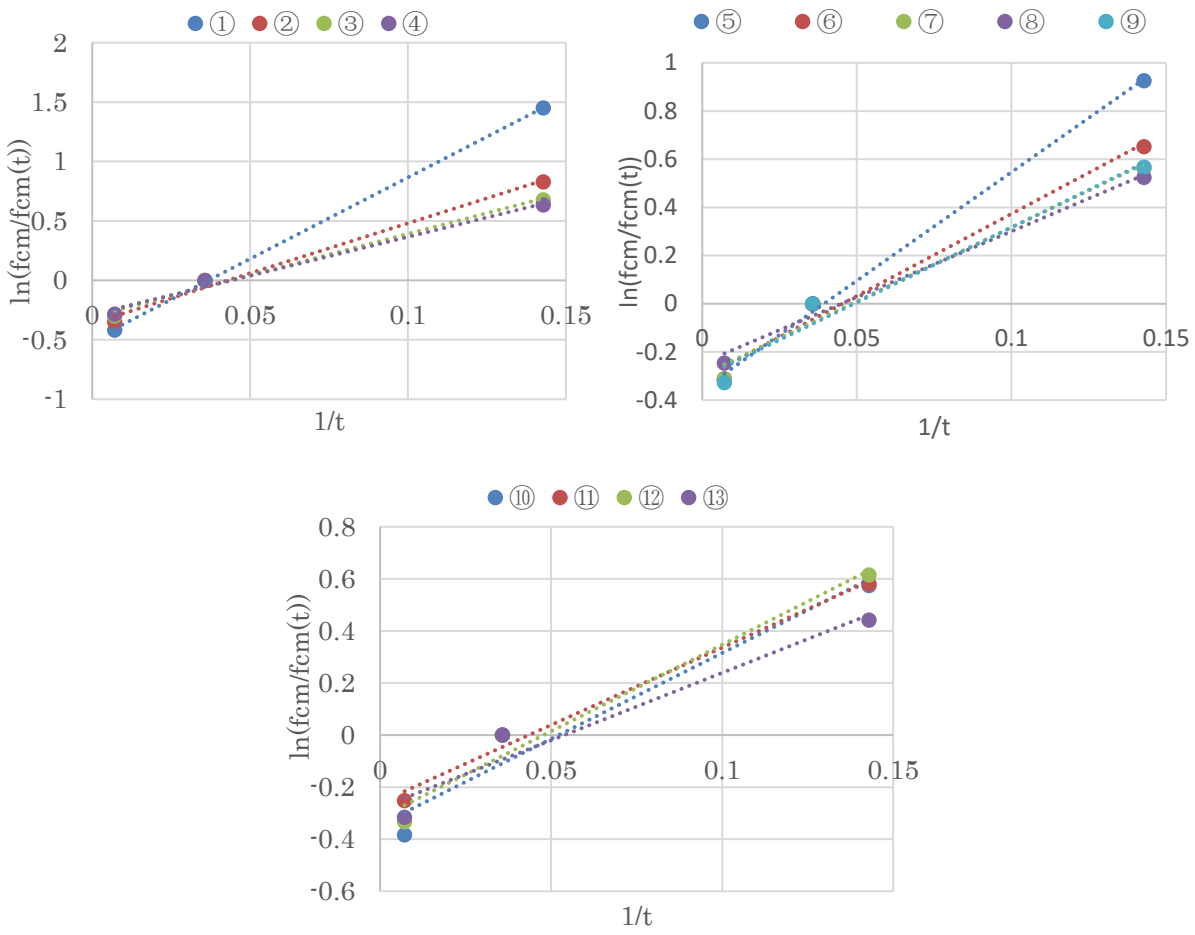

Fig.5.2.10 Relationship between ln($f_{cm}/f_{cm}(t)$) and 1/t.

$ln\ (fcm\ /fcm(t))$ and $1/t$ are linear relationships, therefore, Eq. (4) can be obtained as follow:

$$ln\frac{fcm}{fcm(t)} = a \cdot \frac{1}{t} + b \qquad (4)$$

When t tends to positive infinity, b=$ln\frac{fcm}{fcm(+\infty)}$. The larger b, the larger $\frac{fcm}{fcm(+\infty)}$. This means that when b is larger, the relative ratio of the 28 days compressive strength to the final compressive strength is larger. Meanwhile, when b is a fixed value, the larger a is, the larger

$ln\frac{fcm}{fcm(t)}$ is. This means that the bigger a, the slower the reaction rate, the lower the compressive strength increase at early age, and the greater the strength increase at later age. Then, Transform Eq. (4) to get Eq. (5), the proposed new prediction model is Eq. (5). The following model to evaluate the compressive strength evolution of zero-cement as curing time:

$$f_{cm}(t) = \frac{f_{cm}}{e^{\frac{a}{t}+b}} \quad (5)$$

f_{cm}: Mean tested compressive strength of mortar at the age of 28days;

a and b: are dependent on the zero cement's RCaO, RAl_2O_3 and $RSiO_2$ content;

a value and b value of each specimen are as given in Table.5.2.2. In this study, a value were taken as from 5 to 14, b value were taken as from -0.6 to -0.2.

Table.5.2.2 Values of a and b

Sample	①	②	③	④	⑤	⑥	⑦	⑧	⑨	⑩	⑪	⑫	⑬
a	13.698	8.417	6.963	6.530	9.010	6.823	6.130	5.463	6.230	6.595	5.940	6.644	5.185
b	-0.504	-0.361	-0.305	-0.287	-0.355	-0.309	-0.296	-0.246	-0.306	-0.344	-0.258	-0.317	-0.279

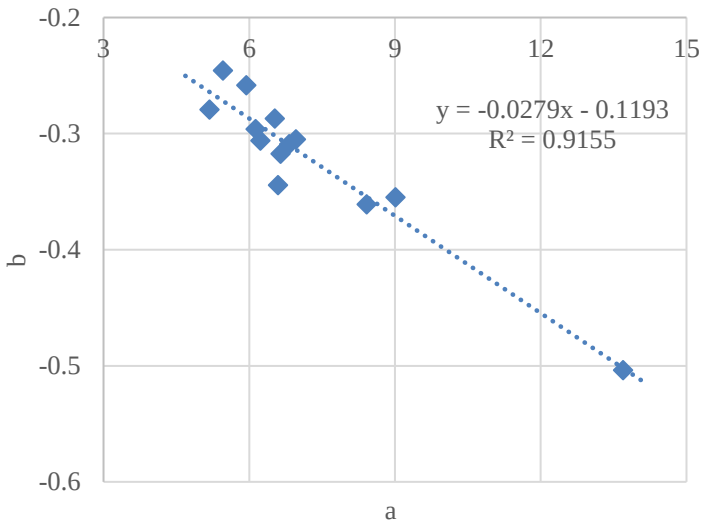

Fig.5.2.11 Relationship between a value and b value.

Fig.5.2.11 shows the relationship between a value and b value. It shows that a value and b value have a linear correlation (R^2=0.9155). It can be concluded that: b=-0.0279a-0.1193. Therefore, the Eq. (5) can be further transformed, compressive strength of zero-cement mortar at various ages could be estimated from:

$$f_{cm}(t) = \frac{fcm}{exp(\frac{a}{t} - 0.0279 \cdot a - 0.1193)} \qquad (6)$$

f_{cm}: Mean tested compressive strength of zero-cement mortar at the age of 28days;

a: is dependent on the zero-cement's RCaO, RAl_2O_3 and $RSiO_2$ content;

Fig.5.2.12 shows the relationship between a value and $RSiO_2$, RAl_2O_3 and RCaO content and glass content. a value has correlation with the $RSiO_2$ content. The more $RSiO_2$ content, the larger a value, which means the slower the reaction rate.

Fig.5.2.13 shows the relationship between a value and (C+S), (C+A), (S+A) and (C+S+A). The content of (C+A) is relative to the content of $RSiO_2$, the more (C+A) content, the smaller a value, the faster the reaction rate. a value also has correlation with the (C+S+A) content, The more active constituent that can participate in the reaction, the faster the reaction rate.

Fig.5.2.14 shows the relationship between a value and CaO-SiO_2-Al_2O_3 molar ratio.

Fig.5.2.15 shows the relationship between a value and C/(A+S), (C+A)/S molar ratio.

Fig.5.2.16 shows the relationship between a value and S/(C+A).The value of a have the highest correlation with S/(C+A) molar ratio. With the increase of S/(C+A) molar ratio, the value of a increases.

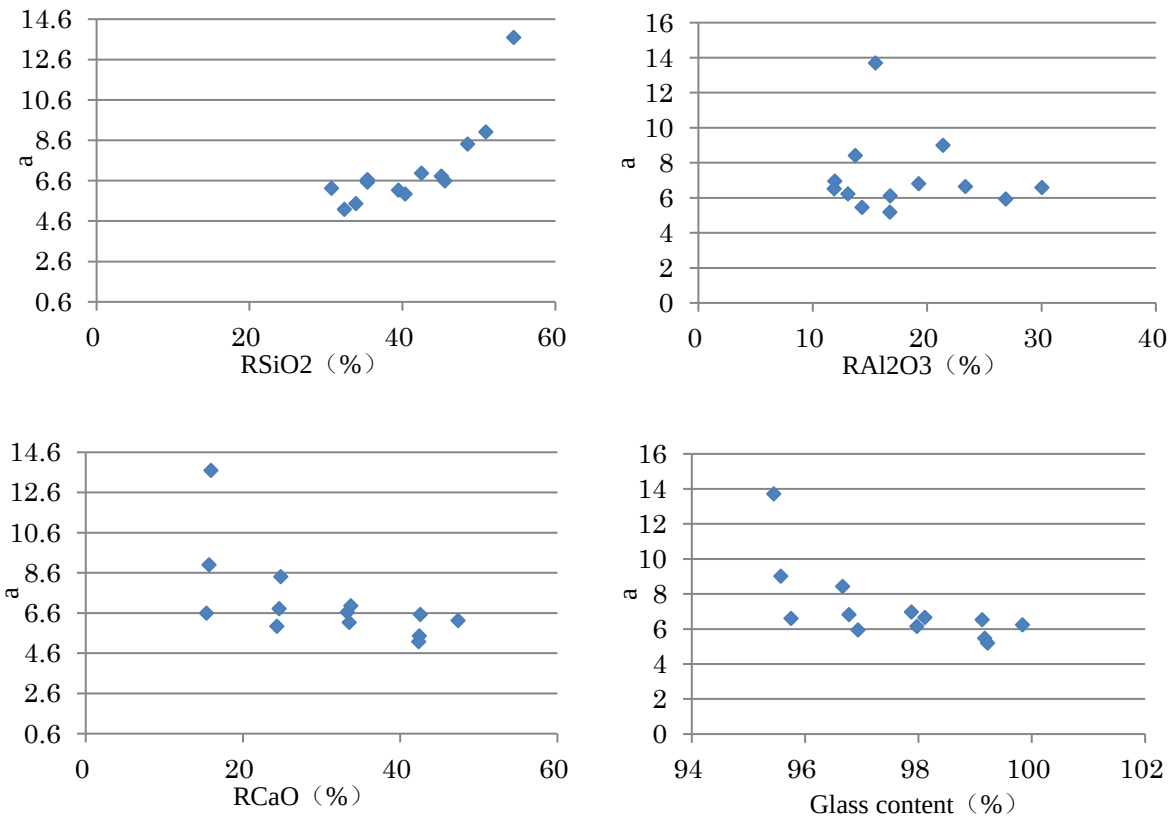

Fig.5.2.12 Relationship between a value and $RSiO_2$, RAl_2O_3, RCaO content and glass content.

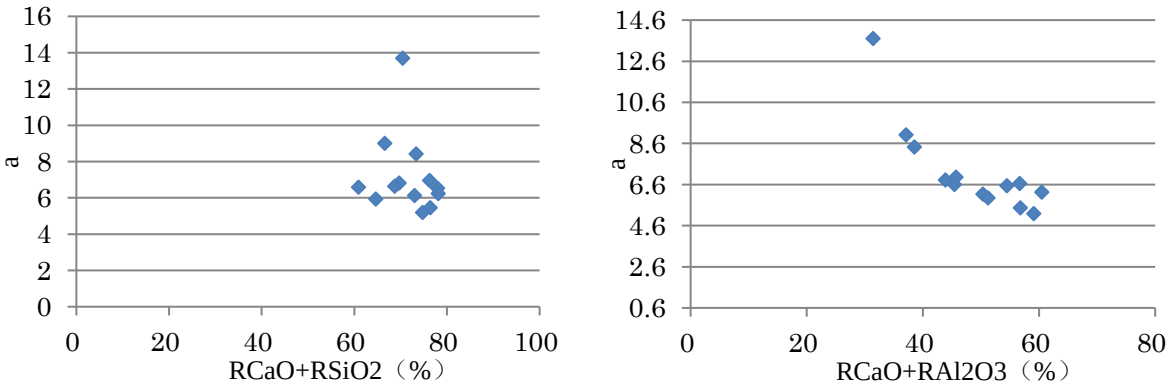

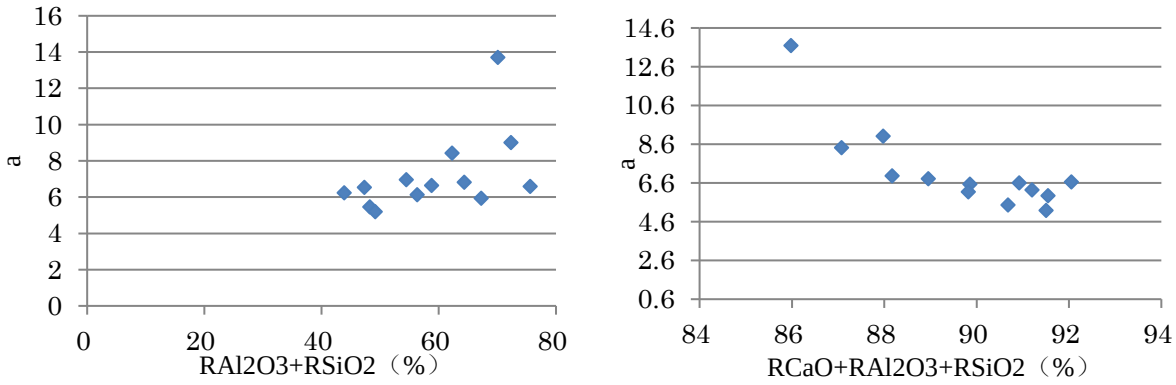

Fig.5.2.13 The relationship between a value and (C+S), (C+A), (S+A) and (C+S+A)

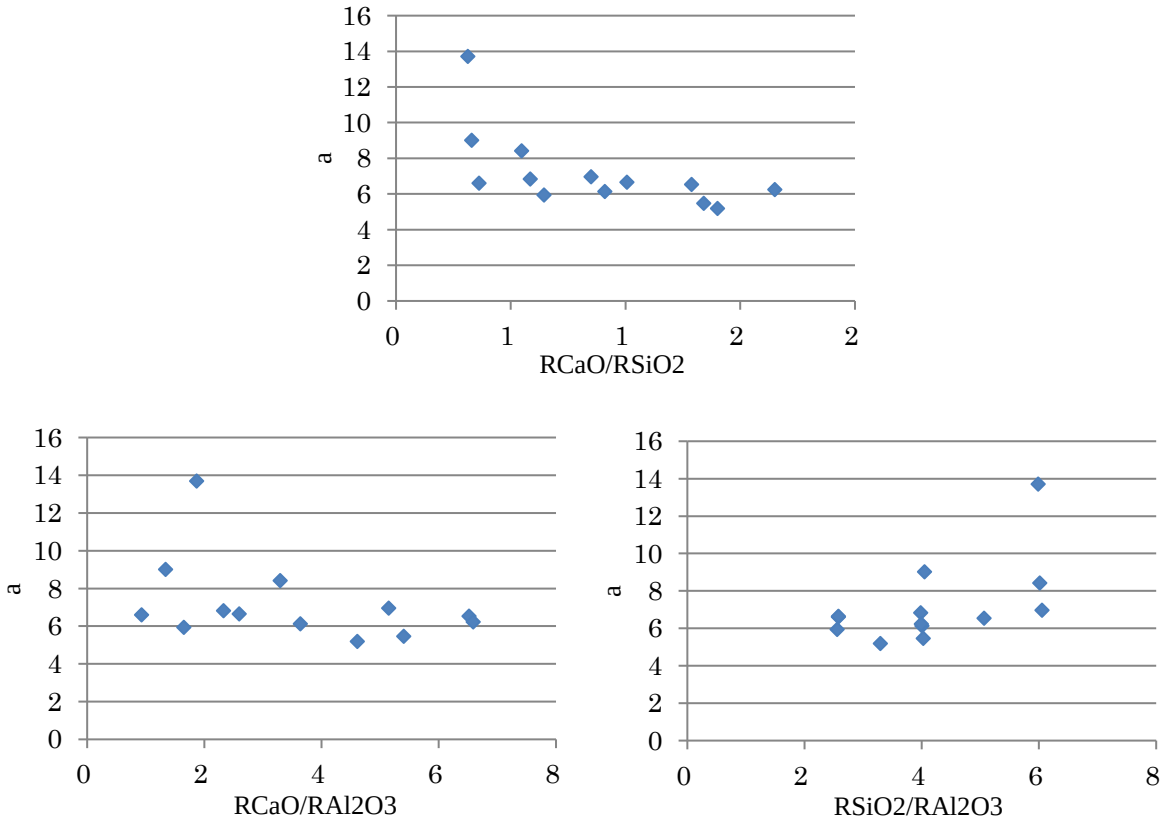

Fig.5.2.14 The relationship between a value and $CaO\text{-}SiO_2\text{-}Al_2O_3$ molar ratio

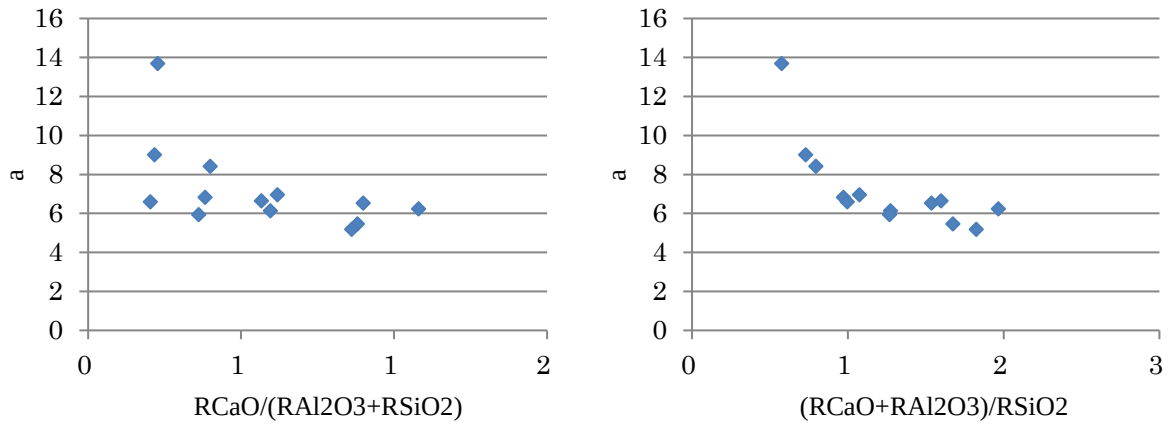

Fig.5.2.15 The relationship between a value and C/(A+S), (C+A)/S molar ratio

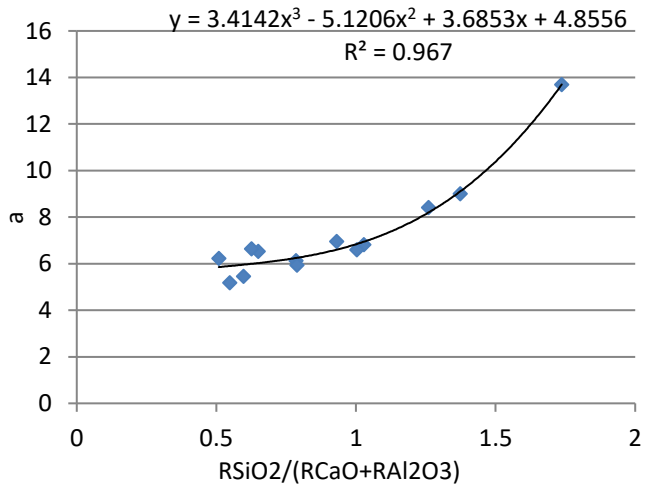

Fig.5.2.16 The relationship between a value and S/(C+A)

a value has the highest correlation (R^2=0.967) with S/(C+A), which can be approximated by a cubic function as follows.

$$a = 3.4142x^3 - 5.1206x^2 + 3.6853 + 4.8556 \quad (0.5 < x < 1.8)$$

x: S/(C+A) (%)

The greater the S/(C+A) molar ratio, the greater the value of a. Compared with CaO and Al_2O_3, the dissolution speed of SiO_2 is slower. Therefore, the higher the SiO_2 content, the slower the reaction rate and the larger the value of a. Therefore, as long as the percentage of $RSiO_2$, RCaO and RAl_2O_3 contained in zero-cement is determined, the strength development of zero-cement mortar can be predicted.

Fig.5.2.17 show the relationships between the measured value and the prediction values calculated by the zero-cement model (Eq. (6) and Eq. (5)). (a) is when a and b are regarded as linear correlation. (b) is to consider a and b uncorrelated. Compared to the ACI model, the prediction interval is narrower, the zero-cement model can predict the compressive strength more accurately. (a) compared with (b), there is no significant change in the relationship between the predicted value and the measured value, Therefore, considering a and b as a linear relationship can also better predict the development of compressive strength of zero-cement mortar.

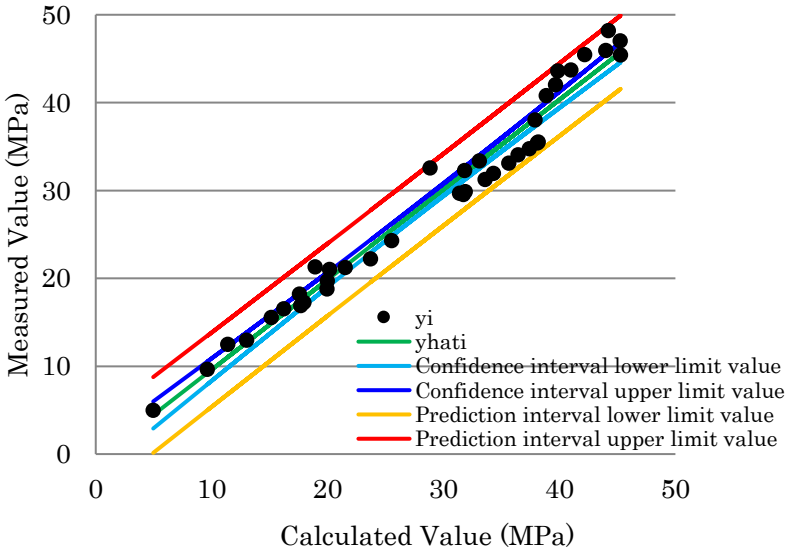

(a) Linear relationship between a and b.

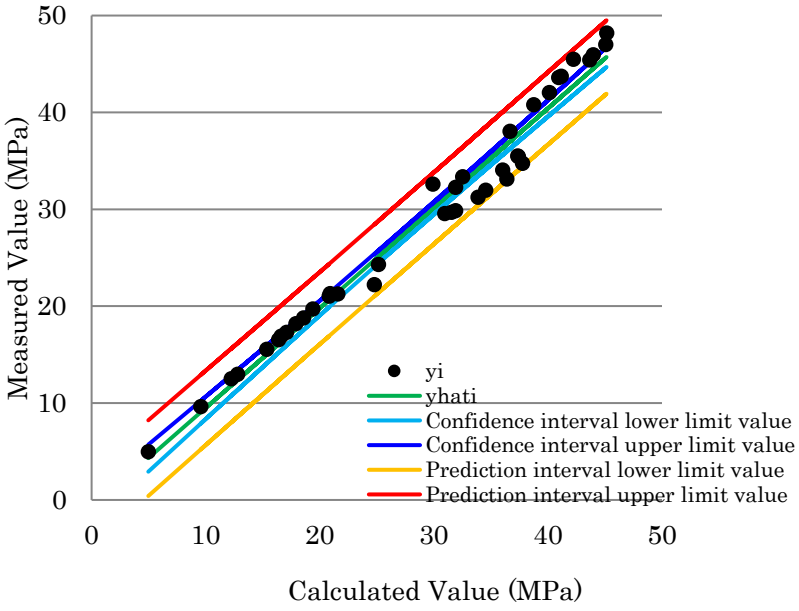

(b) No relationship between a and b.

Fig.5.2.17 Relationship between calculation value (by zero-cement model) and experimental value.

For OPC concrete, with respect to function of compressive strength and cement–water ratio, compressive strength is a linear function of cement–water ratio [(2)]. Unlike OPC concrete, only glass phase in zero-cement participate in the reaction, so the strength is not determined by the C/W ratio, but by the G/W ratio. Fig.5.2.18 show the relationship between 28days mortar strength and glass content/water ratio. Similar to OPC concrete, compressive strength of zero-cement mortar and G/W can be approximated by the following linear functions:

$$f_{cm} = m(G/W)+\mathrm{n} \qquad (7)$$

f_{cm} : Mean tested compressive strength of mortar at the age of 28days;

m and n: constant.

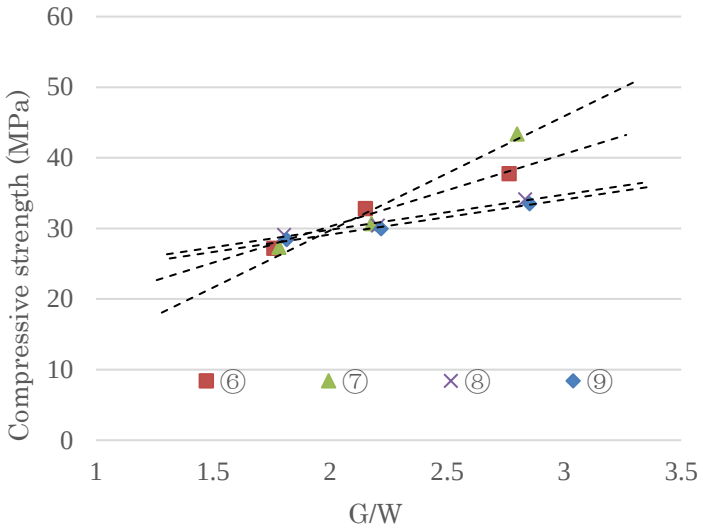

Fig.5.2.18 The relationship between 28days mortar strength and glass content/water ratio

Regarding why the 28 days compressive strength and G/W satisfy the linear approximation relationship, in the concept of the strength index proposed in Chapters 3 and Chapters 4, the strength index has a linear relationship with the compressive strength, and it is determined by the amount and type of gel formation and the pore structure, and G and W correspond to the amount of gel formation and porosity, respectively. Therefore, the 28 days compressive strength and G/W also satisfy the linear approximation relationship.

Then, substituting Eq. (7) into Eq. (6), we can get Eq. (8), the estimation equation for the strength development of zero-cement mortar is expressed as follow:

$$f_c(t) = [\frac{fcm}{exp(\frac{a}{t} - 0.0279 \cdot a - 0.1193)}] \cdot f_{cm}(\frac{G}{W}) \qquad (8)$$

$f_c(t)$ = compressive strength at t days (N/mm^2),

a: is dependent on the zero-cement's RCaO, RAl_2O_3 and RSiO_2 content,

G = Glass content (kg/m^3),

W = unit water content (kg/m^3),

t = age (t days),

Note：This equation is suitable for 1.6＜G/W＜3, curing temperature at 20℃.

Eq. (8) accurately expresses the strength development of zero-cement mortar. This equation is capable of explaining the strength change due to the change in the proportion of RCaO, RAl_2O_3 and $RSiO_2$ content, the relationship between the glass content/water ratio and strength in zero-cement mortar.

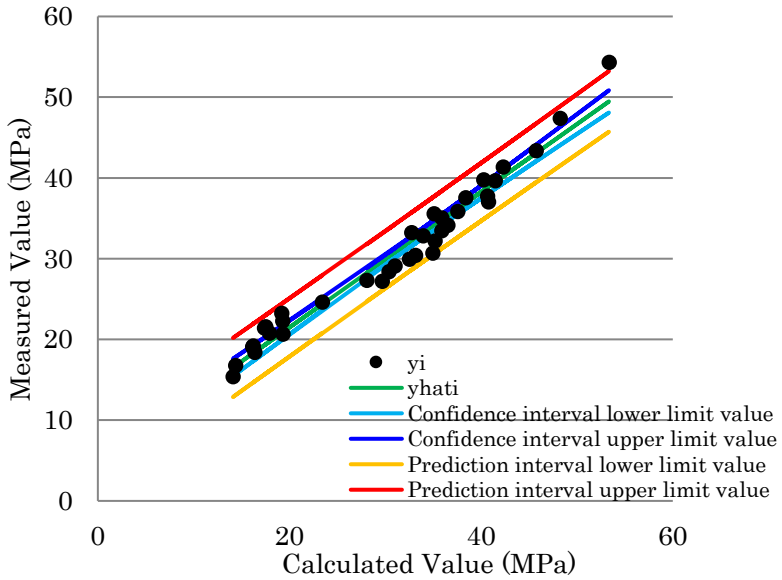

Fig.5.2.19 Relationship between calculation value (by zero-cement model) and experimental value.

Fig5.2.19 show the relationships between the measured value and the prediction values calculated by the zero cement model (Eq. (8)). It is considered useful as an estimation equation for strength development of zero-cement mortar.

5.2.3 Prediction model validation

5.2.3.1 Low-alkali activation

The purpose of this study is to verify the applicability of zero-cement model in the case of different ratios, different type of raw materials and different particle sizes. Fig.5.2.20 shows the $RCaO\text{-}RAl_2O_3\text{-}RSiO_2$ ternary diagram. There are 10 samples, the molar ratios of $RSiO_2/RAl_2O_3$ are close to 4. Mixture 1～3 use same materials, but different proportions. Type II shirasu, metakaolin and the blast furnace slag fine powder 8000 were used. Mixture 4～6 use different type of raw material. Type I fly ash, metakaolin and the blast furnace slag fine powder 8000 were used. Mixture 7～10 use same materials, but different particle size. Type I fly ash, metakaolin and the blast furnace slag fine powder 4000 were used.

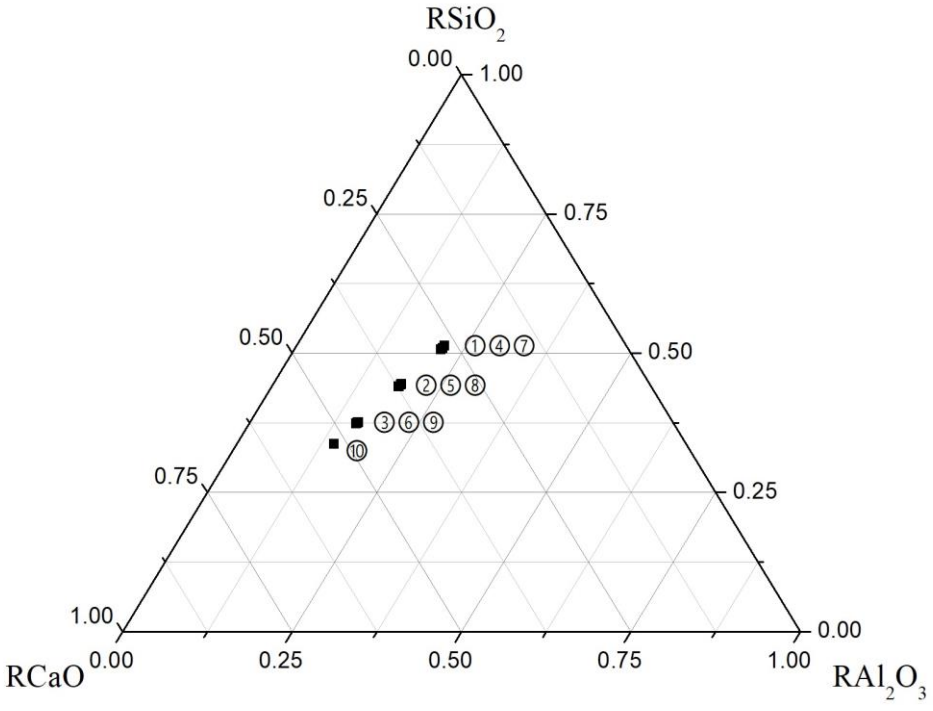

Fig.5.2.20 the $RCaO\text{-}RAl_2O_3\text{-}RSiO_2$ ternary diagram.

Table.5.2.3, Table.5.2.4 and Table.5.2.5 show the mixture proportion. The mass ratio of low

alkali activator CaO to binder was 6%. The mass ratio of water to binder in mortar were 45%.The mass ratio of fine aggregate sand to binder in mortar was 1.4: 1.

Table.5.2.3 Mix proportion (series 1) for zero-cement model validation

Sample	Metakaolin (%)	Shirasu (%)	Slag (%)	CaO (%)	W/G
Mixture 1	24.3	33.2	40	6	45%
Mixture 2	16	20.2	60		
Mixture 3	7.6	7.3	80		

Table.5.2.4 Mix proportion (series 2) for zero-cement model validation

Sample	Metakaolin (%)	Fly ash (%)	Slag (%)	CaO(%)	W/G
Mixture 4	14	53	39	6	45%
Mixture 5	9.5	33	59		
Mixture 6	5	12	80		

Table.5.2.5 Mix proportion (series 3) for model validation

Sample	Slag (%)	Metakaolin (%)	Shirasu (%)	CaO (%)	W/B
Mixture 7	40	23	31	6	45
Mixture 8	60	15	19		
Mixture 9	80	7	7		
Mixture 10	91	3	0		

Fig.5.2.21, Fig.5.2.22 and Fig.5.2.23 shows the relationship between prediction curve and measured value, from series 1 to series 3, respectively. Verification results shows that the prediction curve of compression strength is in good agreement with the measured value. It shows that the application of zero-cement model to predict the strength development of zero-

cement mortar is accurate and effective.

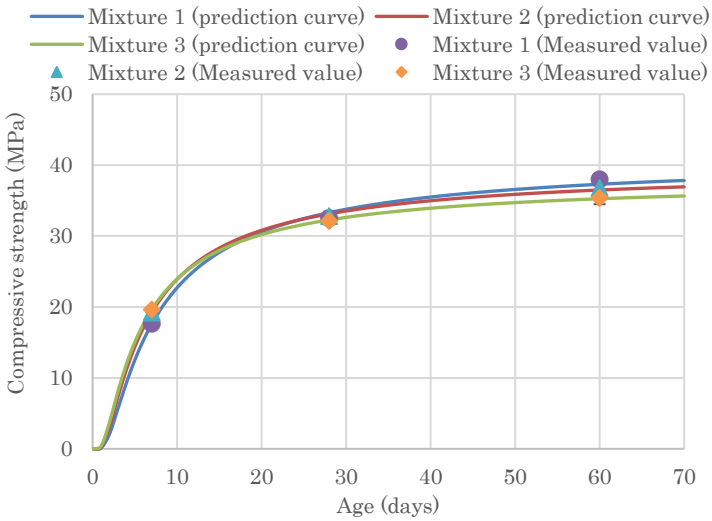

Fig.5.2.21 Relationship between prediction curve and measured value

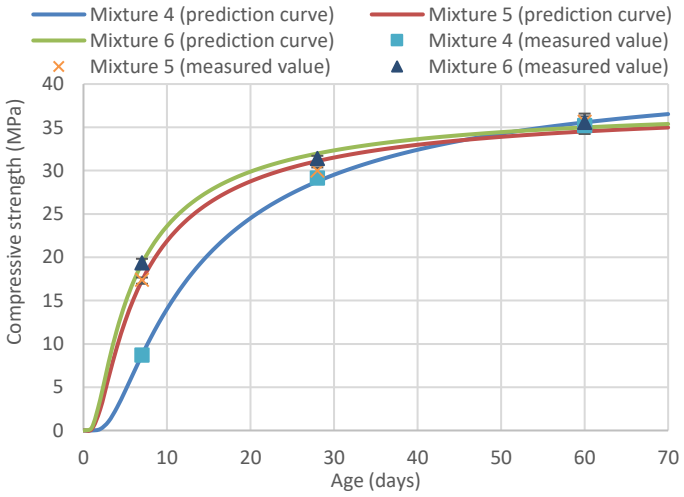

Fig.5.2.22 Relationship between prediction curve and measured value

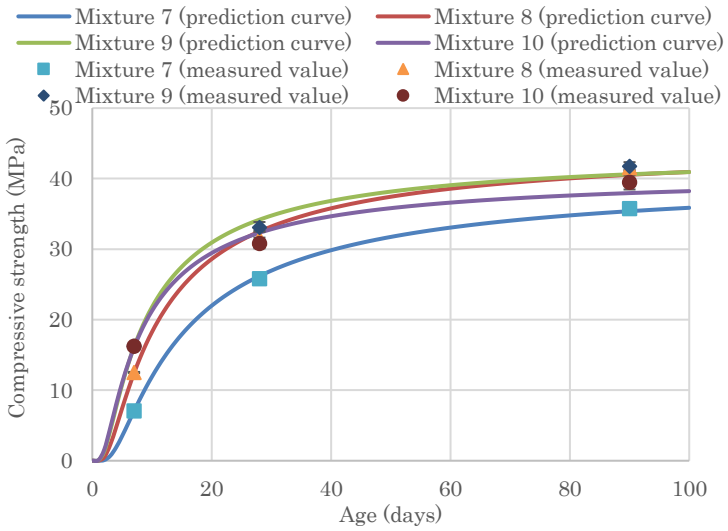

Fig.5.2.23 Relationship between prediction curve and measured value

Fig.5.2.24 shows the relationship between a value and b value. When different types or different particle sizes of raw material are used, a and b always satisfy the linear correlation. It can be approximated by the following linear functions (Eq. (9)).

$$b = A \cdot a + B \qquad (9)$$

a and b: are dependent on the zero cement's RCaO, RAl_2O_3 and $RSiO_2$ content;

A and B: constant.

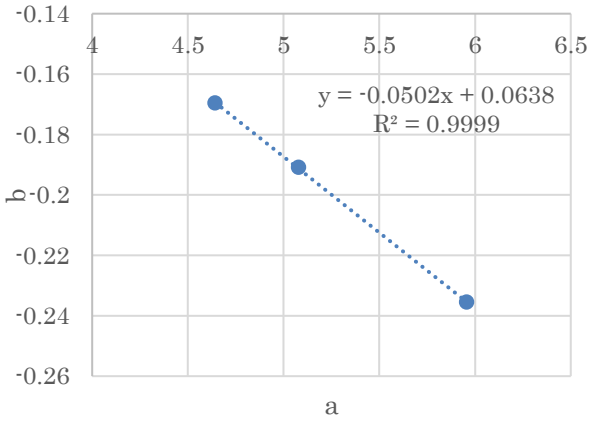

(a) Series 1

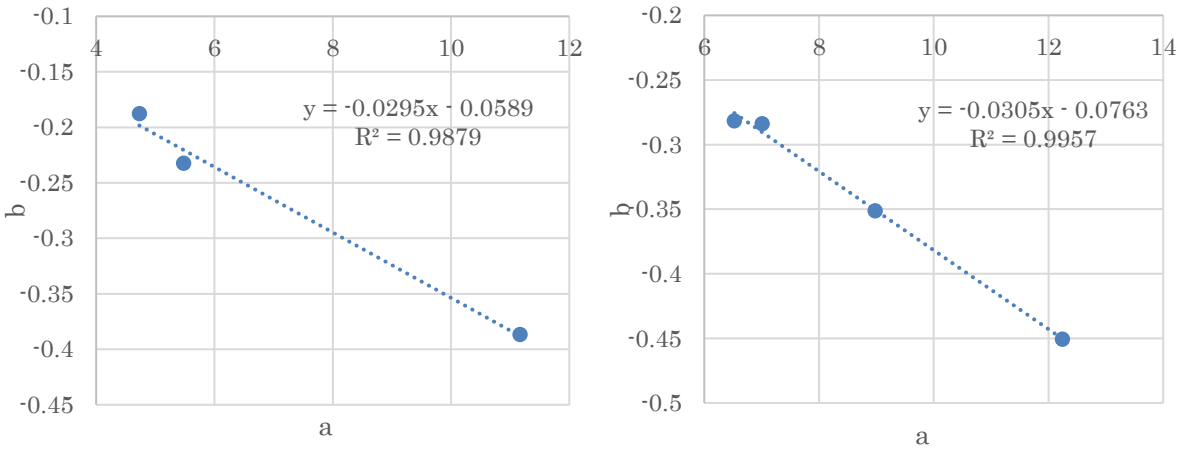

(b) Series 2 (c) Series 3

Fig.5.2.24 Relationship between a value and b value.

Therefore, it is possible to study only the relationship between a value and S/(C+A) molar ratio. When the type of material or the particle size of the raw material changes, the dissolution speed of the active constituents also changes, resulting in a change in the functional relationship between the a value and the S/(C+A) molar ratio. Therefore, when different type or different particle sizes of raw materials are used, as long as the relationship between a value and the S/(C+A) molar ratio is obtained, the compressive strength development of zero-cement can be well predicted.

When using the raw material with slower dissolution speed or with coarser particle size distribution, a value will increase, while the b value will slowly decrease. When using the raw material with faster dissolution speed or with finer particle size distribution, the value of a will decrease, while the value of b will increase rapidly. Regarding its specific functional relationship, further research is needed.

5.2.3.2 High-alkali activation

In section 4.2, fly ash, granulated blast furnace slag and silica fume were used as raw materials,

and NaOH solution was used as the high-alkali activator. Table.5.2.6 shows the mix proportion of high-alkali activated zero-cement. The compressive strengths of 3 days, 7 days, 14 days and 28 days were measured respectively. Here, the results are used to test whether the high-alkali activated zero-cement is suitable for the strength prediction model of the low-alkali activated zero-cement.

Table.5.2.6 Mix proportion

Sample	W/B[%]	B mass ratio (SF:FA:BF)	FNS/B	Concentration of NaOH (mol/L)
2-2	20	1.5 : 2.5 : 6	1.6 : 1	12M
2-3	20	1.5 : 3 : 5.5	1.6 : 1	12M
2-4	20	1.5 : 3.5 : 5	1.6 : 1	12M

Fig.5.2.25 shows the relationship between (fcm/fcm(t)) and 1/t. It shows that (fcm/fcm(t)) and 1/t do not satisfy the exponential function relationship. It is an approximate linear relationship, but some points deviated from the linear relationship.

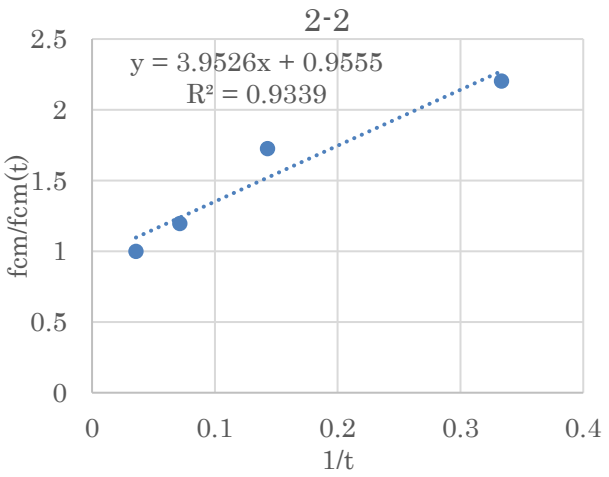

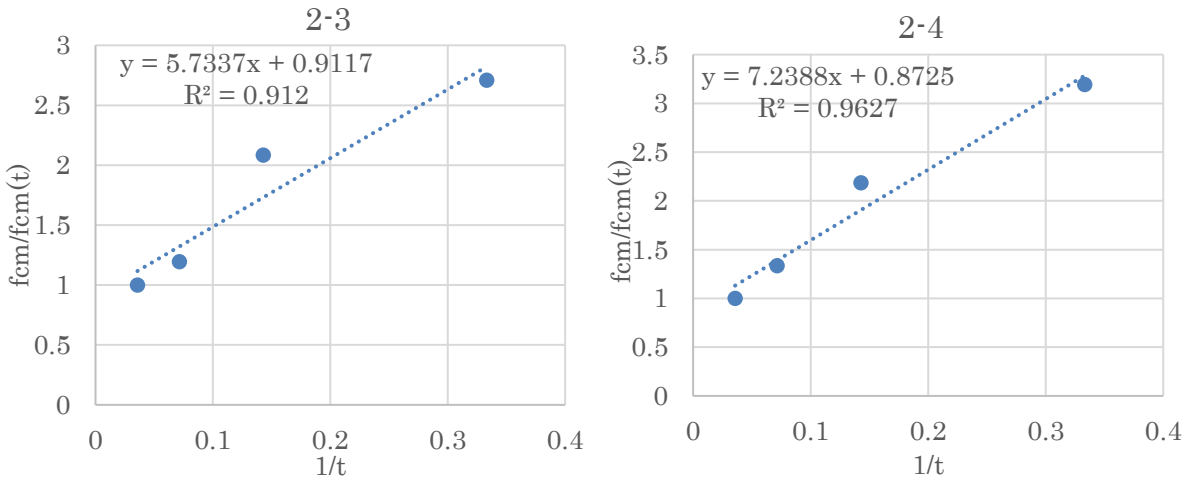

Fig.5.2.25 Relationship between ($f_{cm}/f_{cm}(t)$) and 1/t.

The ACI model is applied to predict the compressive strength, and the results are shown in Fig.5.2.26. It shows that the development of compressive strength seems to have two different stages of development trends. Perhaps one equation is difficult to express the development of compressive strength of high-alkali system. The first stage is at 3 days and 7 days, the compressive strength increases rapidly, the second stage is at 14 days and 28 days, once again, the 14 days compressive strength suddenly increases rapidly, which has a different compressive strength growth trend than the first stage, may indicate the formation of new reaction products. In the highly alkaline environment, the chemical reaction mechanism is more complicated, and it has different strength development from the low-alkali activation. FA-BF blended binder system usually presents coexisting N-A-S-H and C-(A)-S-H type gels [3]. Chemical reactions can be presented as follows [4]:

$Ca^{+2} + SiO_2(OH)_2^{2-}$ or $SiO(OH)_3^{-1} + Al(OH)_4^- \Rightarrow$ CASH gel (1)

$Na^{+} + SiO_2(OH)_2^{2-}$ or $SiO(OH)_3^{-1} + Al(OH)_4^- \Rightarrow$ NASH gel (2)

As CASH gel is stable at high pH (＞12) environments and reaction (1) is dominant at early age. The pH of the system decreases with time, due to the consumption of OH- during hydrolysis to further form silicate and aluminate species. The low pH and limited Ca^{+2} environments facilitate the polymerization reaction between silicate and aluminate species producing NASH gel. The reaction (2) becomes feasible at lower pH (9–12) where NASH is stable. Therefore reaction (2) becomes secondary in these systems which is mainly responsible for strength development at later age. This can explain why there are two different stages of strength development trend in high-alkali systems.

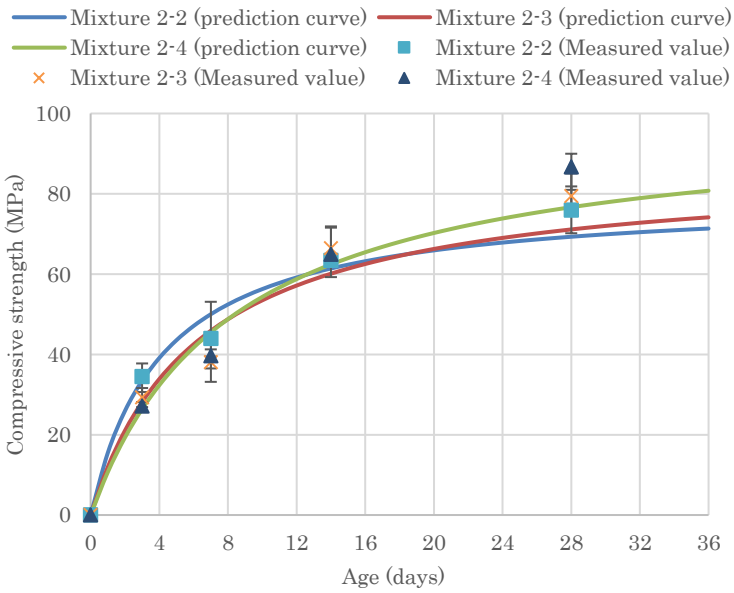

Fig.5.2.26 Relationship between prediction curve and measured value

5.3 Relationship between compressive strength of zero-cement and active constituents.

In order to investigate which active constituent has the highest correlation with compressive strength of zero-cement, and to clarify the relationship between the molar ratio of three active constituents and compressive strength. This section studies the relationship between

compressive strength of zero-cement and C, A, S, (C+S), (C+A), (S+A) and (C+S+A), S/A, C/S, C/A, C/(S+A) respectively, And according to the relationship between the active constituents to predict the compressive strength of zero-cement.

Fig.5.3.1, Fig.5.3.2 and Fig.5.3.3 shows the relationship between 7days, 28days and 140days strength and RCaO, RAl_2O_3 and $RSiO_2$ content, respectively.

The correlation between the 7 days strength and the RCaO content is relatively high. Overall, the higher the RCaO content, the greater the compressive strength. However, the specimen with the same RCaO content show different compressive strength, indicating that the contents of RAl_2O_3 and $RSiO_2$ also affected the development of compressive strength at early age. With the increase of age, the correlation between RCaO content and compressive strength is getting higher and higher, indicating that RCaO content has a crucial influence on the final strength of the zero-cement.

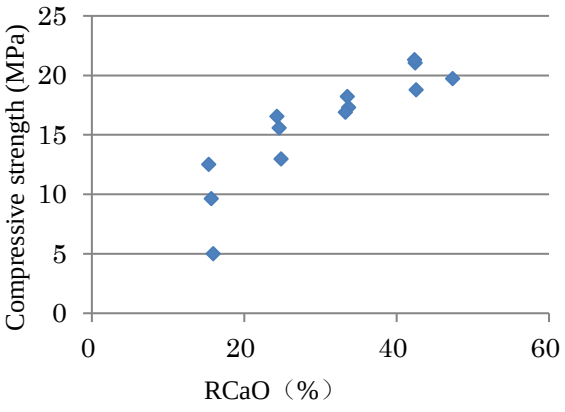

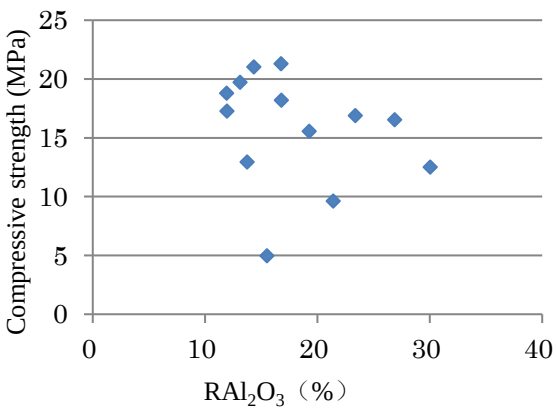

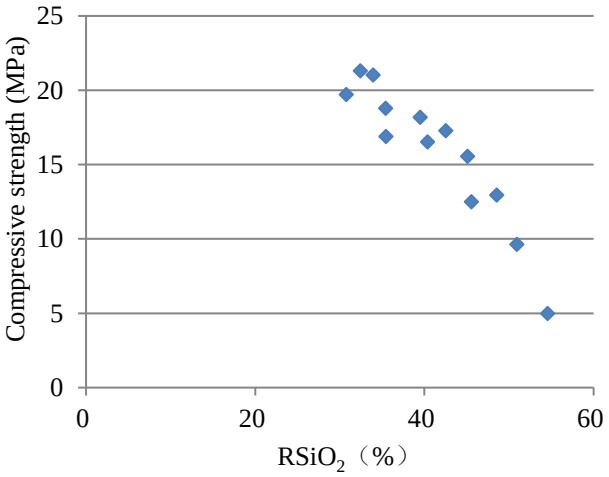

Fig.5.3.1 The relationship between 7days strength and RCaO, RAl_2O_3 and $RSiO_2$ content.

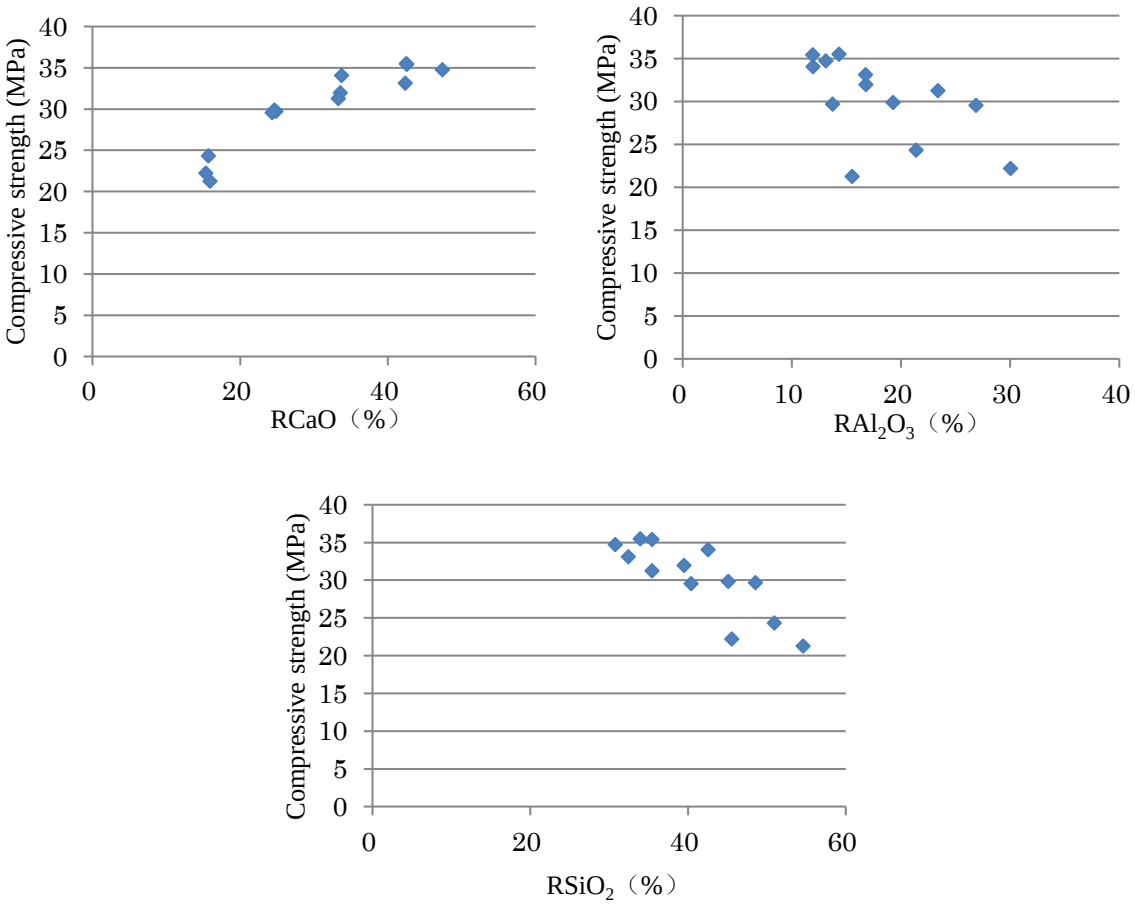

Fig.5.3.2 The relationship between 28days strength and RCaO, RAl_2O_3 and $RSiO_2$ content.

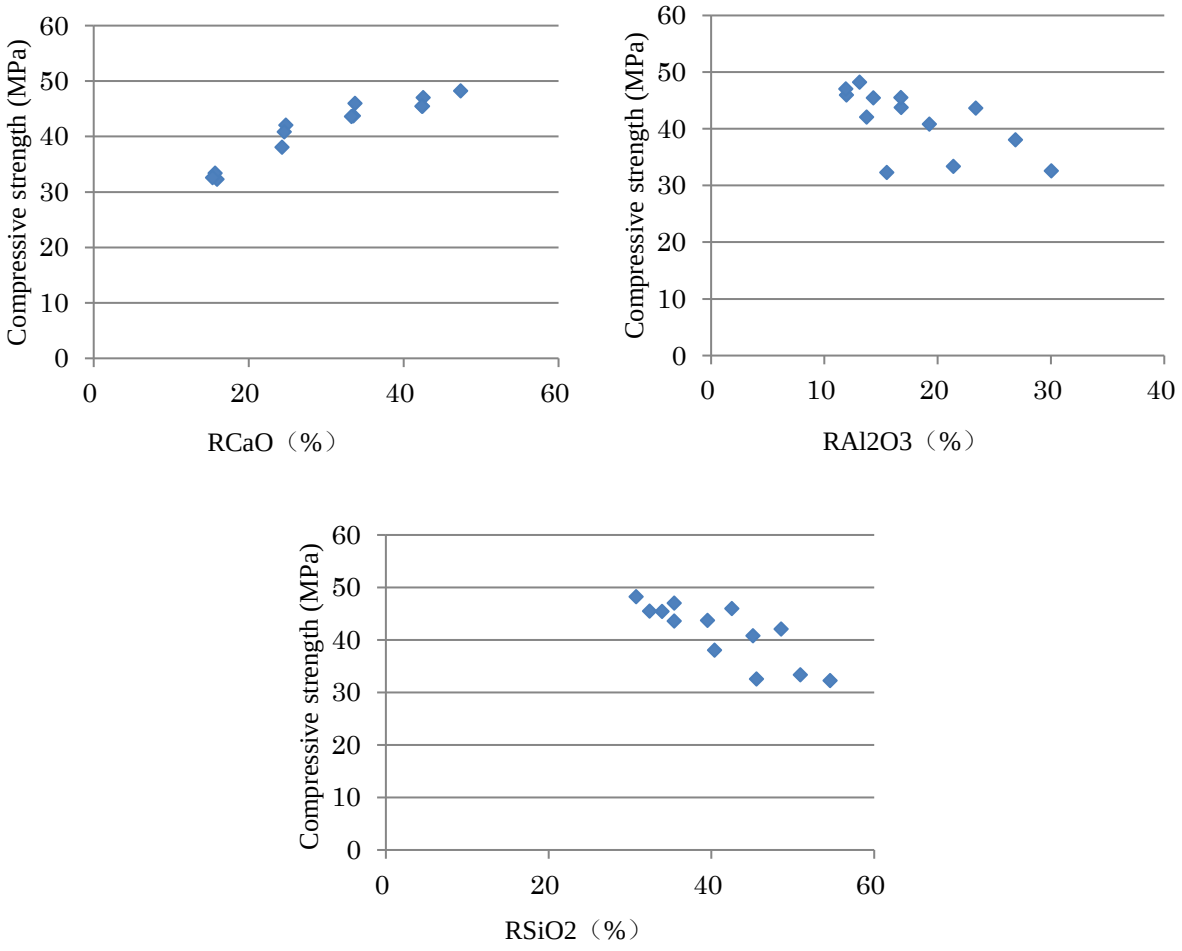

Fig.5.3.3 The relationship between 140 days strength and RCaO, RAl_2O_3 and $RSiO_2$ content.

Fig.5.3.4, Fig.5.3.5 and Fig.5.3.6 shows the relationship between 7days, 28days and 140days strength and (C+S), (C+A), (S+A) and (C+S+A). It can be seen from the figure that only (C+A) content has the high correlation with compressive strength at 7 days, the higher the content of RCaO and RAl_2O_3, the greater the 7days compressive strength.

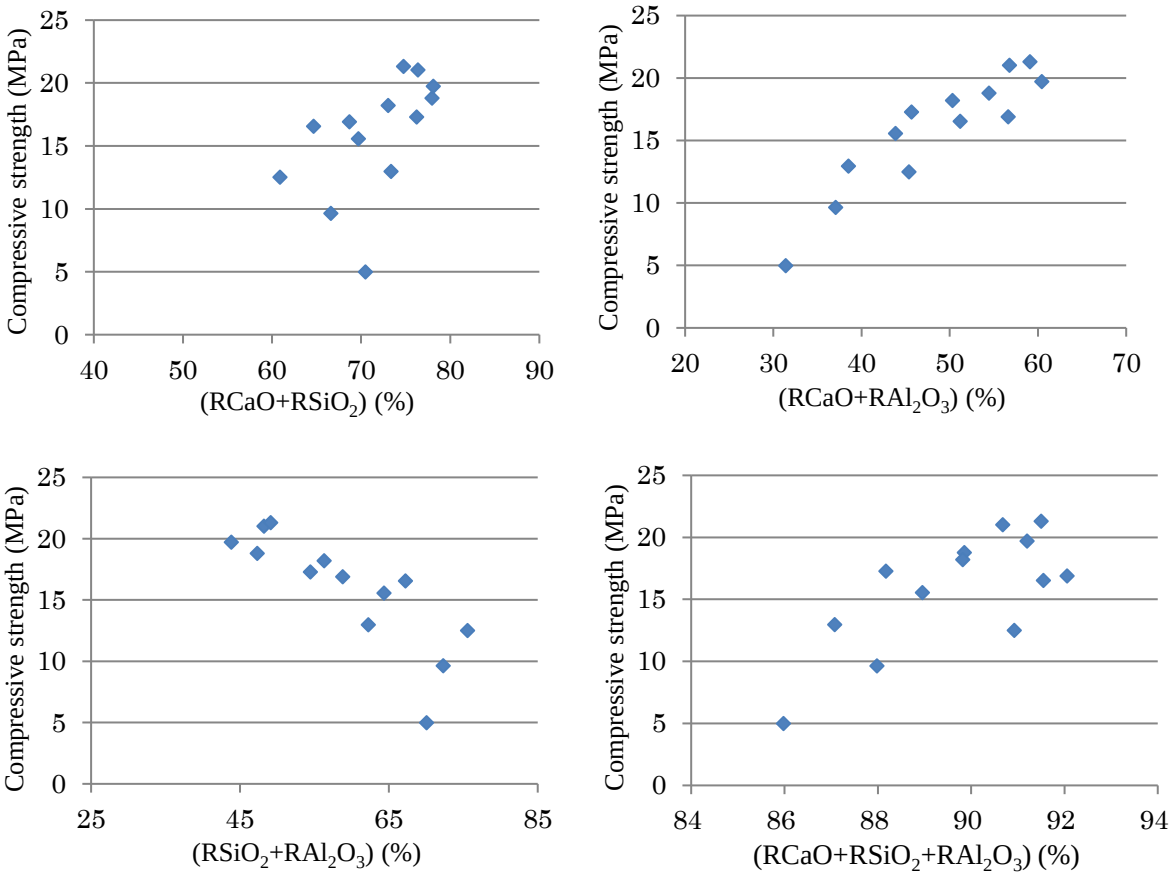

Fig.5.3.4 The relationship between 7days strength and (C+S), (C+A), (S+A) and (C+S+A)

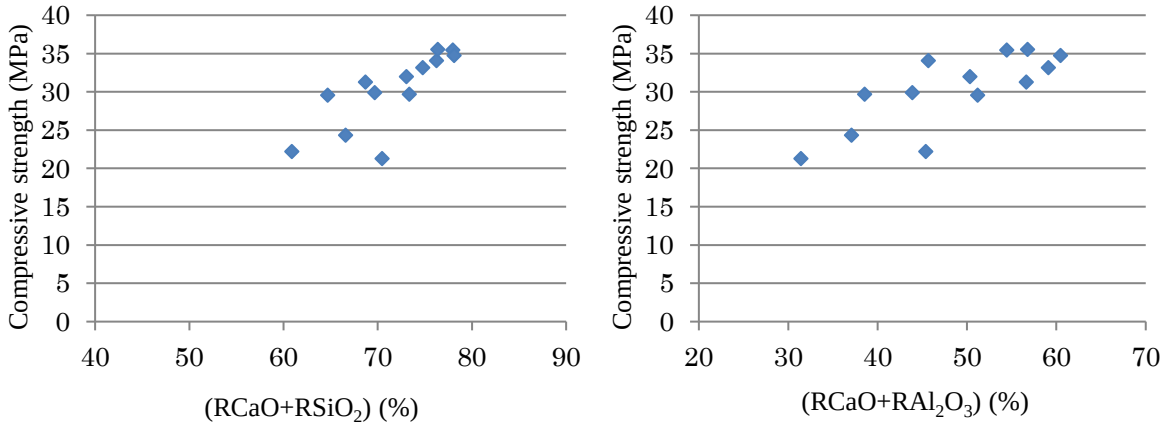

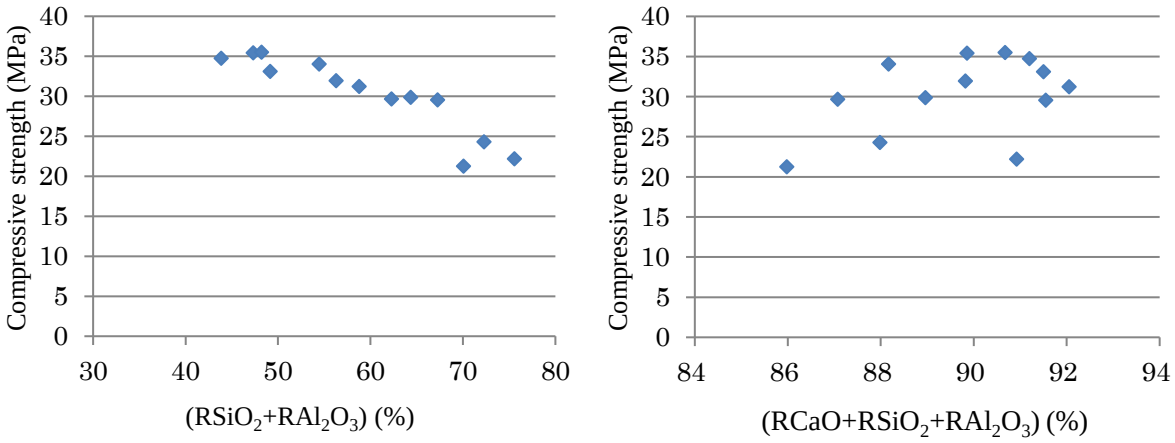

Fig.5.3.5 The relationship between 28days strength and (C+S), (C+A), (S+A) and (C+S+A)

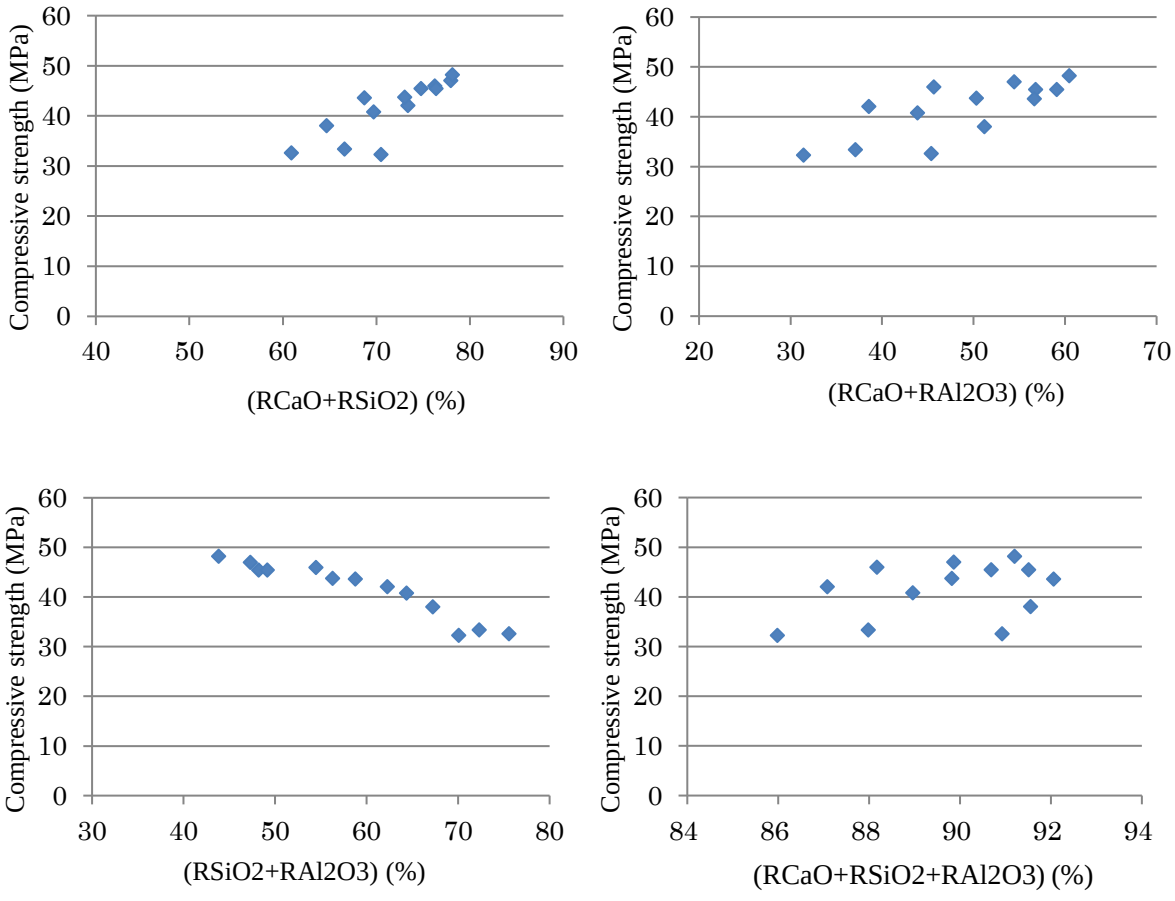

Fig.5.3.6 The relationship between 140 days strength and (C+S), (C+A), (S+A) and (C+S+A)

Fig.5.3.7, Fig.5.3.8 and Fig.5.3.9 shows the relationship between 7days, 28days and 140days mortar strength and CaO-SiO_2-Al_2O_3 molar ratio, respectively. It can be seen from the figure that regardless of curing age, CaO/SiO_2 has the high correlation with compressive strength.

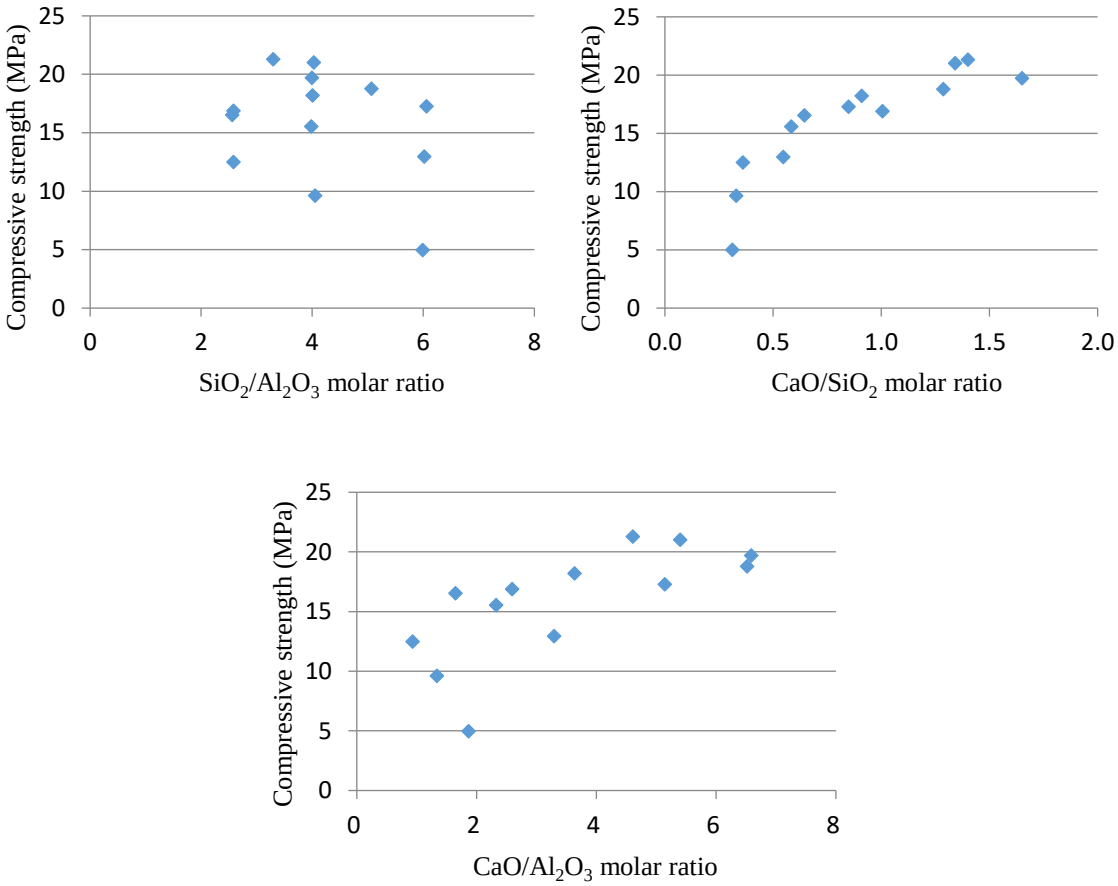

Fig.5.3.7 The relationship between 7days strength and CaO-SiO_2-Al_2O_3 molar ratio

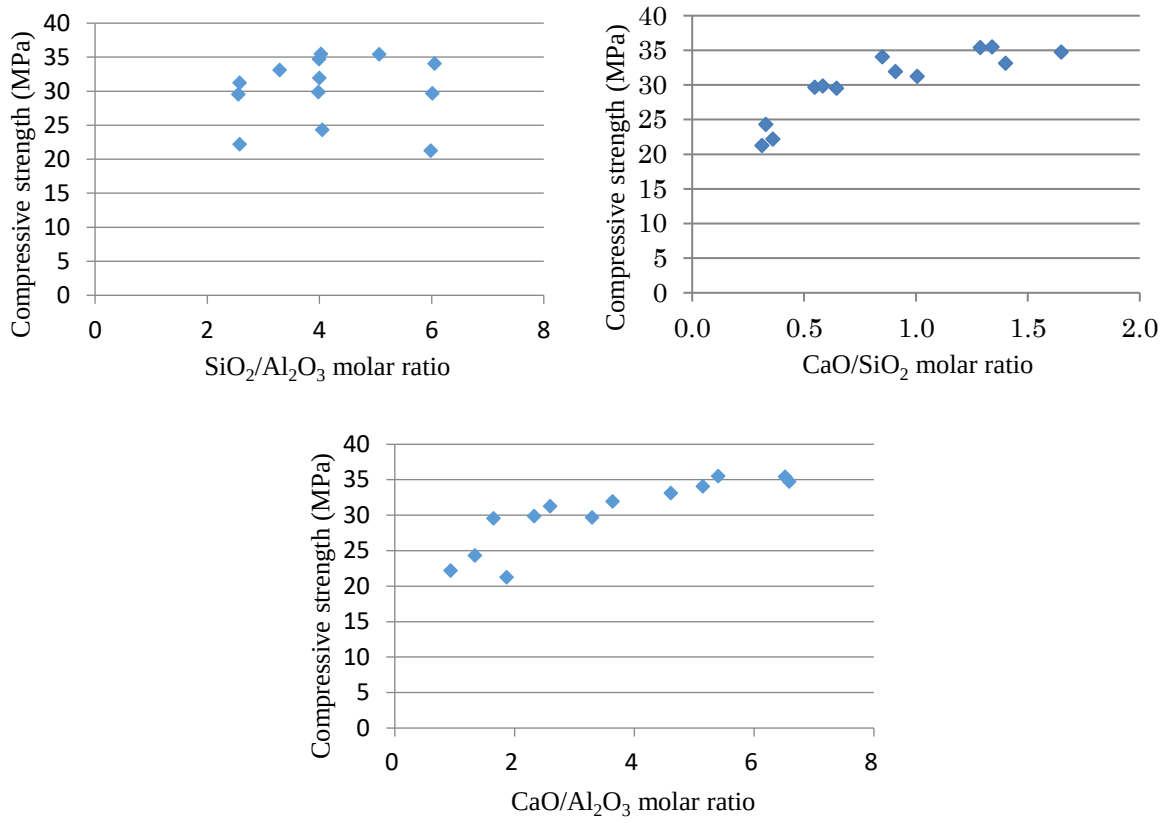

Fig.5.3.8 The relationship between 28days strength and $CaO\text{-}SiO_2\text{-}Al_2O_3$ molar ratio

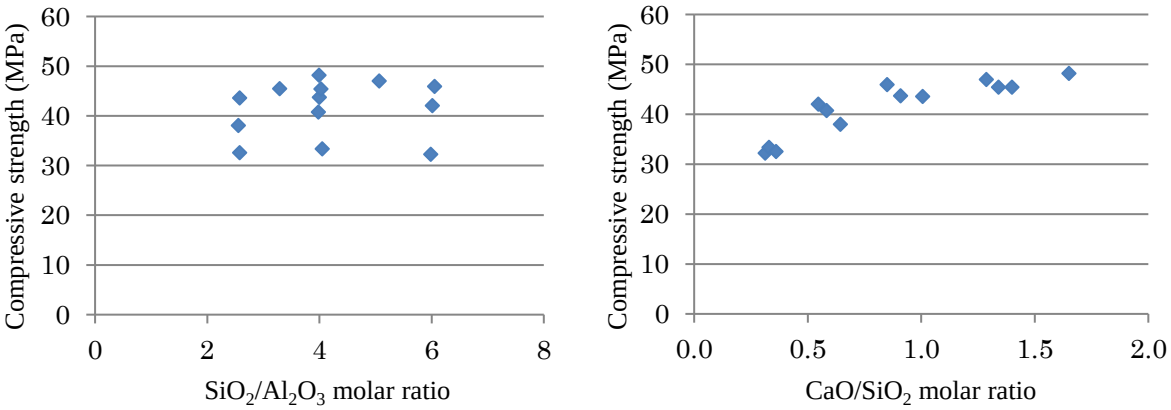

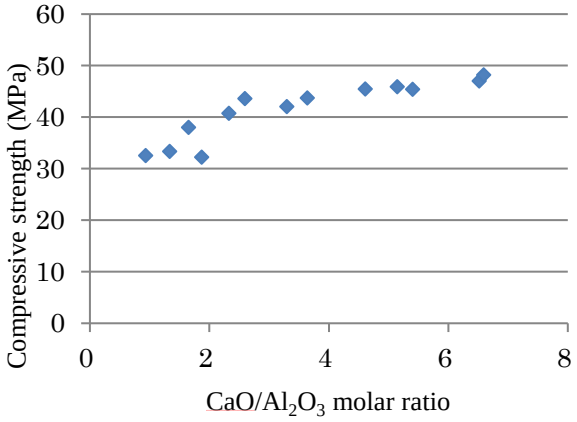

Fig.5.3.9 The relationship between 140days strength and CaO-SiO_2-Al_2O_3 molar ratio

According to the existing literature, in the case of C-S-H, the compressive strength is related to the Ca/Si ratio. Compressive strength increases with decreasing Ca/Si ratio. It is believed that this is because the amount of C-S-H interaction increases as the Ca/Si ratio decreases.

Kunther W et al. [5] demonstrates that the compressive strengths of the C–S–H pastes increase for decreasing Ca/Si ratio for all synthesized samples and testing ages. The molar volumes of the C–S–H phase decrease with decreasing Ca/Si ratio, which along with the related higher surface areas may partly explain the differences in strength development.

However, Li S et al. [6] found that the strength of the materials with C/S molar ratio of 1.5 is comparatively higher than that of the others, after curing from 1 day to 28 days. The preferable C/S ratio is 1.4-1.5, because of the apparently higher bonding capability of the C-S-H having this composition.

In the case of zero-cement, the main reaction product is C-A-S-H. In terms of chemical structure, it is often the case that Al replaces Si and enters to form the skeleton of the chemical structure. Kalousek [7] shows that Al enters into calcium silicate hydrate structure and suggested that it occurs primarily in the tetrahedral position substituting for Si. Diamond et al. [8] demonstrated

that it is possible to replace up to 15% of silicon by aluminium in tobermorite. A kinetic study [9] showed that the Al insertion in C-S-H is a fast reaction, typically less than one day. The characterization of the solid samples by XRD and EDX (TEM) indicates that pure C-A-S-H is obtained only if the Ca/Si ratio of the initial C-S-H is below 1.

Therefore, in this study, consider C/(S+A) molar ratio in the same way as C-S-H. Fig.5.3.10 shows the relationship between 7days, 28days and 140days mortar strength and C/(S+A) molar ratio. C/(S+A) molar ratio has the low correlation with 7days compressive strength (R^2=0.7772), but high correlation with 28 days and 140 days compressive strength (R^2=0.9067 and R^2=0.9352).

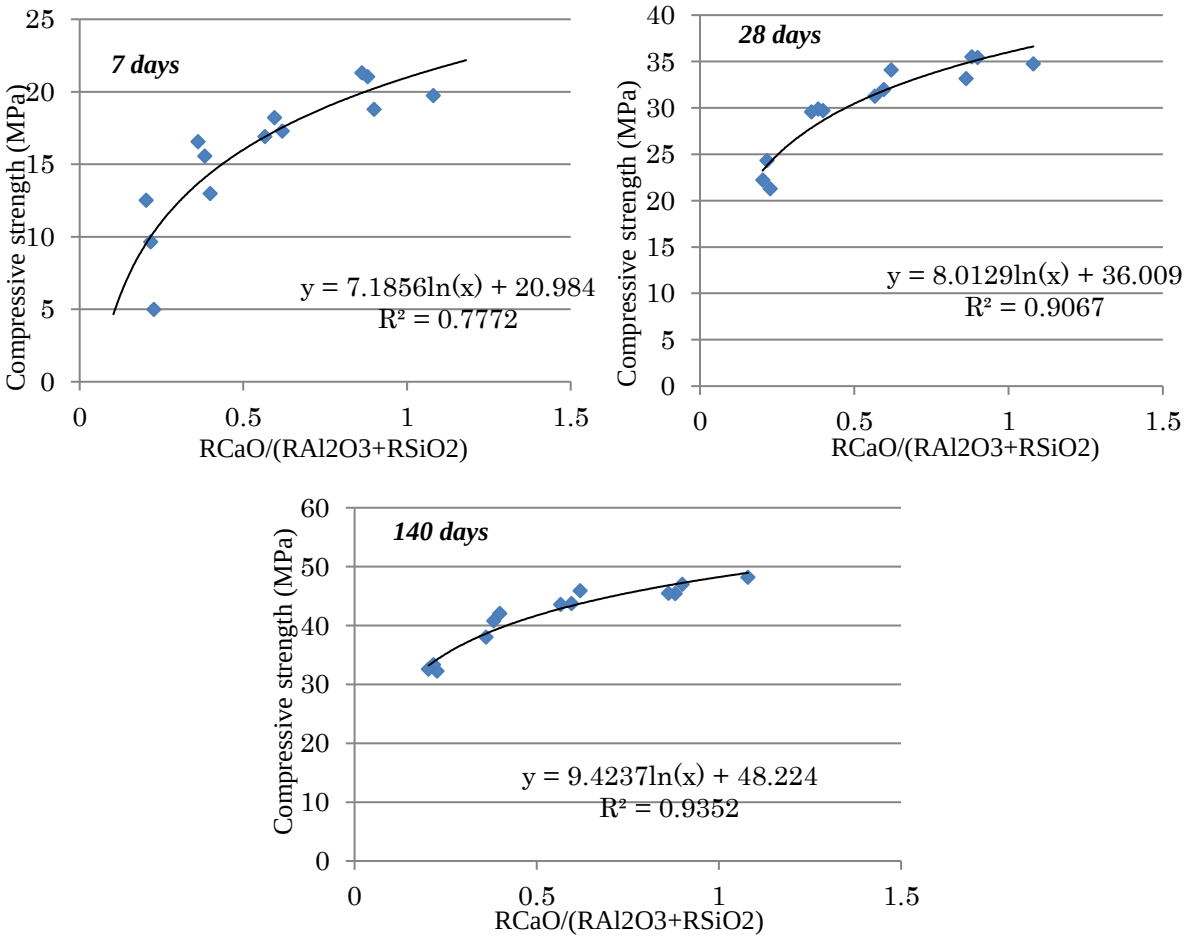

Fig.5.3.10 The relationship between mortar strength and C/(S+A) molar ratio

7 days compressive strength:

$$F_{7days}=7.1856\ln(x) + 20.984 \ (R^2=0.7772)$$

28 days compressive strength:

$$F_{28days}=8.0129\ln(x) + 36.009 \ (R^2=0.9067)$$

140 days compressive strength:

$$F_{140days}==9.4237\ln(x) + 48.224 \ (R^2=0.9352)$$

x: C/(S+A) molar ratio

Generally, compressive strength and C/(S+A) molar ratio can be approximated by a logarithmic function as follows.

$$F = a \cdot ln(x) + b \qquad (0.2 < x < 1.1)$$

In this study, as the curing age increase, the pozzolanic reaction proceed, and the correlation between compressive strength and C/(S+A) molar ratio is getting higher and higher. It has increased from $R^2 = 0.7772$ to $R^2 = 0.9352$. At later age, the reaction of SiO_2 and Al_2O_3 in raw materials depends on the concentration and content of $Ca(OH)_2$ supply. The higher the $Ca(OH)_2$ concentration, the higher the rate of pozzolanic reaction. At late ages, the higher the $Ca(OH)_2$ content, the longer that the pozzolanic reaction of lasts[10]. It can explain that the high correlation between the 28 days and 140 days strength and C/(S+A) molar ratio (R^2=0.9067 and R^2=0.9352).

The compressive strength has a logarithmic relationship with C/(S+A). It is possible to predict the development of compressive strength simply by C/(S+A) molar ratio. The applicable range is 0.2< C/(S+A) <1.1.

Fig.5.3.11 shows the relationship between strength (high-alkali activation) and C/(S+A) molar ratio. Compressive strength of 7 days and 28 days has a high correlation with C/(S+A). From the overall trend, the greater the C/(S+A), the higher the compressive strength.

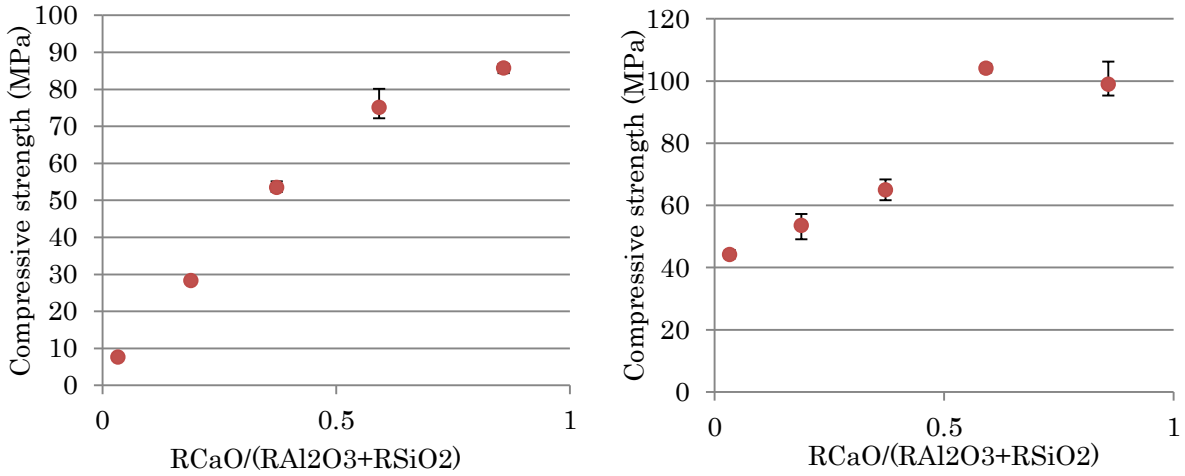

Fig.5.3.11 The relationship between strength (high-alkali activation) and C/(S+A) molar ratio

Fig.5.3.12 shows the relationship between relative strength and C/(S+A) molar ratio. Regardless of high-alkali activation or low-alkali activation, the relative compressive strength of 7 days and 28 days has a high correlation with C/(S+A). From the overall trend, the greater the C/(S+A), the higher the relative compressive strength. When the molar ratio exceeds 0.9, the increase in relative compressive strength gradually stabilizes. Therefore, when designing ultra-high-strength zero-cement mortar, proper C/(S+A) is crucial.

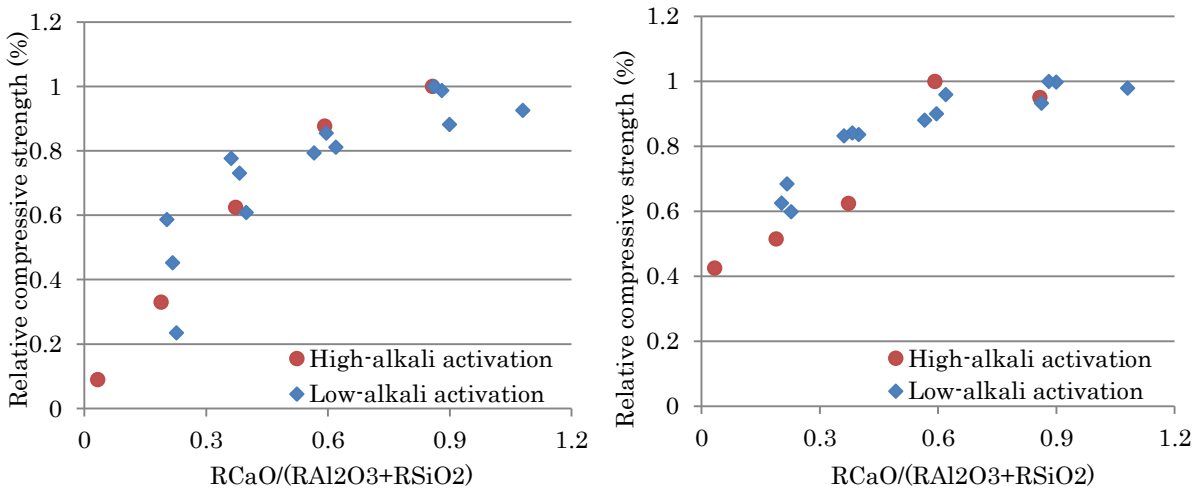

(a) 7days (b) 28days

Fig.5.3.12 The relationship between relative strength and C/(S+A) molar ratio

5.4 Conclusions

Based on the results conducted in this chapter, the following conclusions can be inferred:

(1) Compared to the ACI model, the zero cement model can predict the compressive strength of zero-cement mortar more accurately. For zero cement, a value and b value have a high linear correlation.

(2) a value is dependent on the zero-cement's RCaO, RAl_2O_3 and $RSiO_2$ content. It can approximately represent the reaction rate of zero-cement binder. The larger a value, the slower the reaction rate.

(3) The value of a have the highest correlation with S/(C+A) molar ratio. With the increase of S/(C+A) molar ratio, a value also increases. Therefore, as long as the percentage of RCaO, $RSiO_2$ and RAl_2O_3 contained in zero-cement is determined, the strength development of zero-cement mortar can be predicted.

(4) This prediction model can expresses a value, in the form of a function of age, glass content/water ratio. It is considered useful as an estimation equation for strength development

of zero-cement mortar.

(5) When different types or different particle sizes of raw material are used, a and b always satisfy the linear correlation.

(6) It is also possible to predict the strength development of zero-cement simply by C/(S+A) molar ratio. Regardless of high-alkali activation or low-alkali activation, the relative compressive strength of 7 days and 28 days has a high correlation with C/(S+A). From the overall trend, the greater the C/(S+A), the higher the relative compressive strength. When the molar ratio exceeds 0.9, the increase in relative compressive strength gradually stabilizes.

References

(1) Videla C, Carreira D J, Garner N. Guide for modeling and calculating shrinkage and creep in hardened concrete[J]. ACI report, 2008, 209.

(2) Hwang K, Noguchi T, Tomosawa F. Prediction model of compressive strength development of fly-ash concrete[J]. Cement and Concrete Research, 2004, 34(12): 2269-2276.

(3) Gao X, Yu Q L, Brouwers H J H. Apply 29Si, 27Al MAS NMR and selective dissolution in identifying the reaction degree of alkali activated slag-fly ash composites[J]. Ceramics International, 2017, 43(15): 12408-12419.

(4) Chindaprasirt P, De Silva P, Sagoe-Crentsil K, et al. Effect of SiO2 and Al2O3 on the setting and hardening of high calcium fly ash-based geopolymer systems[J]. Journal of Materials Science, 2012, 47(12): 4876-4883.

(5) Kunther W, Ferreiro S, Skibsted J. Influence of the Ca/Si ratio on the compressive strength of cementitious calcium–silicate–hydrate binders[J]. Journal of Materials Chemistry A, 2017, 5(33): 17401-17412.

(6) Li S, Roy D M. Preparation and characterization of high and low CaO/SiO 2 ratio “pure” C–S–H for chemically bonded ceramics[J]. Journal of Materials Research, 1988, 3(2): 380-386.

(7) G.L. Kalousek, Crystal chemistry of hydrous calcium silicates: I, substitution of aluminum in lattice of tobermorite, J. Am. Ceram. Soc. 40 (1957) 74–80.

(8) S. Diamond, W. Dolch, J. White, Effects of Isomorphous Substitution in Hydrothemal Synthesized Tobermorite : Technical Paper, 1964.

(9) Pardal X, Pochard I, Nonat A. Experimental study of Si–Al substitution in calcium-silicate-hydrate (CSH) prepared under equilibrium conditions[J]. Cement and Concrete Research, 2009, 39(8): 637-643.

(10) H. Uchikawa, Effect of blending compressive strength on the hydration structure formation of blended cement, Cement Science and Concrete Technology, vol. 484, Japan Cement Association, 1987.

6. Environmental performance evaluation

6.1 Introduction

Compared with OPC, the reported CO_2 emissions values of alkali activated materials has a wider range. Some researchers [1-2] reported that its CO_2 emissions can be reduced by as high as 80%, and some other researchers [3-7] believe that its CO_2 emissions can only be reduced by 26–45%. The purpose of this chapter is to confirm the CO_2 emissions of ultra-high strength zero-cement mortar made in low-alkali or high-alkali conditions, compared to cement mortar made in normal conditions.

6.2 Comparison of CO_2 emissions between ultra-high strength OPC mortar and zero-cement mortar.

The CO_2 emissions is usually calculated as the sum of the CO_2 emissions of each raw material in unit volume of concrete. In order to compare different ultra-high strength mortar made with OPC and zero-cement binders. It is first necessary to determine the mix proportion, and then according to the CO_2 emissions generated by various raw materials in the mixture used, the CO_2 emissions produced $1m^3$ of concrete can be calculated.

Common 100 MPa mortar made with OPC mixtures and 100 MPa mortar made with zero-cement mixtures in this study summarized in Table.6.2.1.

Considering that CO_2 emissions value is highly related to the raw materials used and the mix proportion of mortar or concrete. In this study, the evaluation is based on three high-alkali activated zero-cement mortar mixtures and one low-alkali activated zero-cement mortar mixtures, and a Portland cement based mortar is used as a reference.

Table.6.2.1 Mixture proportions for 100 MPa mortar

Material	OPC based mortar[8] (kg/m^3)	High alkali activated zero-cement (kg/m^3)			low alkali activated zero-cement (kg/m^3)
		Mixture 1	Mixture 2	Mixture 3	
Free water	137.5	234.1	266.7	246.5	95
Superplasticizer	4.7	/	/	/	11.6
OPC	495	/	/	/	/
Silica fume	55	/	/	/	133.2
Slag	/	679.5	354.2	445.7	532.9
Fly ash	/	226.5	531.3	445.7	222
Expanding material	/	/	/	/	30
Sodium hydroxide	/	52.9	55.4	53.5	/
Sodium silicate	/	166.1	120.7	145.7	/
Fine aggregates	711.2	906	885.5	891.3	1421
Curing	Moist curing	20℃ curing	20℃ curing	20℃ curing	20℃ curing

Table.6.2.2 shows the emission factor of manufacture of each raw materials used in the calculation, these data obtained from [9] [10] [11]. Sodium hydroxide has the highest emission factor of 1.915 kg CO_2-e/kg, followed by sodium silicate with an emission factor of 1.514 kg CO_2-e/kg. It is much larger than the emission factor of cement of 0.82 kg CO_2-e/kg, indicating that for manufacturing 1 kg of sodium hydroxide and sodium silicate, the carbon dioxide emissions are 2.3 times and 1.8 times compared with cement, respectively. Other waste by-products and fine aggregates have smaller emission factors, while the emission factor of silica fume (0.461 kg CO_2-e/kg) was estimated from a life cycle analysis performed by VTT (EU F7th project, ProMine internal report) [12]. It is important to note that the emission factor of silica fume shown here is an average European industrial case scenario, without making use of the heat that is generated during the production of silica fume, once this part of energy is reused, the carbon emission will be further reduced. In addition, the main component of the expansive material is CaO, which can be approximately regarded as cement. Therefore, in this calculation,

the emission factor of the expansive material is considered to be approximately equal to the emission factor of cement.

Table.6.2.2 Emission factor of manufacture of each raw materials (obtained from [9] [10] [11])

Materials	Emission factor	Unit
OPC	0.82	kg CO_2-e/kg
Silica fume	0.461	kg CO_2-e/kg
Slag	0.143	kg CO_2-e/kg
Fly ash	0.027	kg CO_2-e/kg
Expanding material*	0.82	kg CO_2-e/kg
Sodium hydroxide	1.915	kg CO_2-e/kg
Sodium silicate	1.514	kg CO_2-e/kg
Fine aggregates	0.0139	kg CO_2-e/kg

*Note: Similar to OPC, the emission factor is approximately 0.82.

The contribution to CO_2 emissions from sourcing raw materials to the manufacture and construction of 1 m^3 of mortar, is summarized in Fig.6.2.1. The total CO_2 emissions from the OPC based mortar were estimated as 441.1 kg CO_2-e/m^3. Portland cement was by far the most significant contributor to emissions; contributing 92% of CO_2 emissions for OPC based mortar. The total CO_2 emissions from the low alkali activated zero-cement mortar were estimated as 188.0 kg CO_2-e/m^3. Compared with cement based mortar, the CO_2 emissions of low alkali activated zero-cement mortar decreased by 57.4%. The total CO_2 emissions from three high alkali activated zero-cement mixture used in this report were estimated as 468.7 kg CO_2-e/m^3, 366.1 kg CO_2-e/m^3 and 411.2 kg CO_2-e/m^3, respectively. The CO_2 emissions value is highly related to the proportions of Sodium silicate and Sodium hydroxide used in the mix proportion, which can be largely varied. Compared with cement based mortar, the CO_2 emissions of high alkali activated zero-cement mortar increased by 6.2% and decreased by 17% and 6.8%,

respectively. In order to reduce CO_2 emissions by a large amount, it is crucial to optimize the design of the mix proportion and minimize the use of Sodium silicate and Sodium hydroxide, but the reduction in the amount of alkali content will also bring about reducing of compressive strength, therefore, an optimal balance between CO_2 emissions and performance must be found.

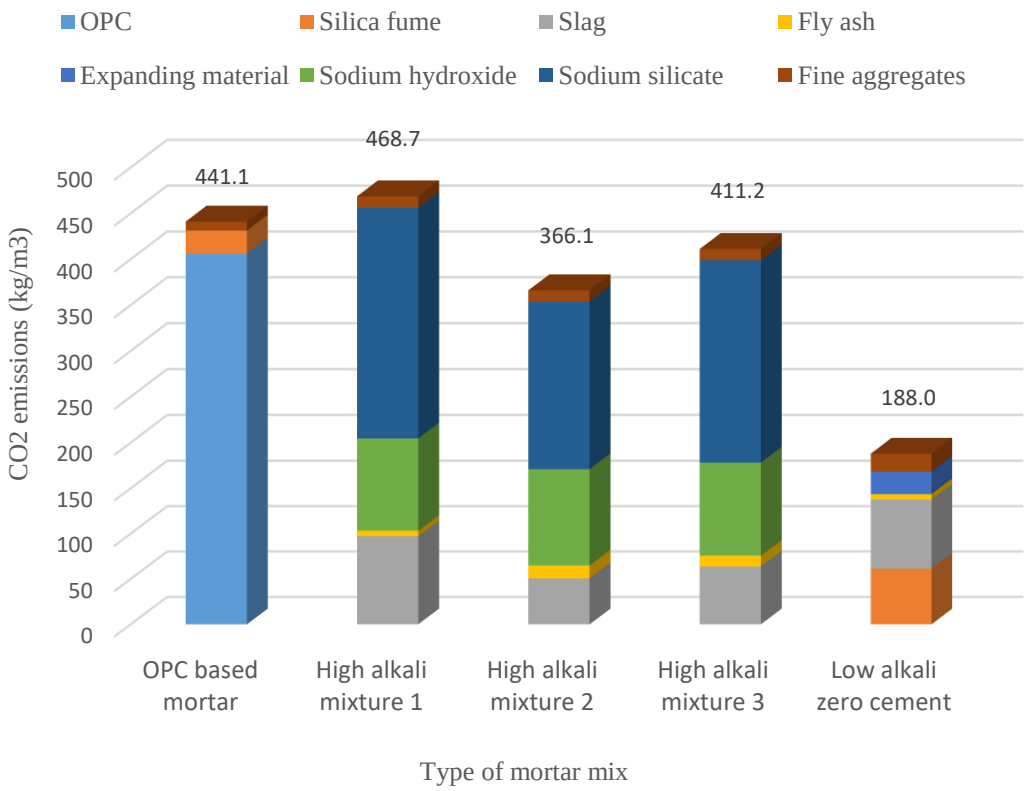

Fig.6.2.1 Calculation of CO_2 emissions based on the mortar mix (kg/m^3).

6.3 Conclusions

This chapter confirmed the CO_2 emissions based on 1 m^3 of mortar mix. The CO_2 emissions generated by ultra-high strength mortar comprising zero-cement binders and OPC based binder were compared. The CO_2 emissions of 1m^3 low alkali activated zero-cement mortar was approximately 57.4% less than 1m^3 OPC based mortar.

For high alkali activated zero-cement mortar, the CO_2 emissions value is highly related to the proportions of Sodium silicate and Sodium hydroxide used in the mix proportion, which can be largely varied. Compared with $1m^3$ cement based mortar, the CO_2 emissions of $1m^3$ high alkali activated zero-cement mortar increased by 6.2% and decreased by 17% and 6.8%, respectively.

References

(1) Van Deventer JSJ, Provis JL, Duxson P, Brice DG. Chemical research and climate change as drivers in the commercial adoption of alkali activated materials. Waste Biomass Valor 2010;1:145–55.

(2) Duxson P, Provis JL, Lukey GC, van Deventer JSJ. The role of inorganic polymer technology in development of 'green concrete'. Cem Concr Res 2007;37:1590–7.

(3) Stengel T, Reger J, Heinz D. LCA of geopolymer concrete – what is the environmental benefit? In: Proceedings Concrete 09, 24th Biennial Conf Australian Concrete Institute, Sydney, Concrete Institute of Australia; 2009. p.54–62.

(4) Witherspoon R, Wang H, Aravinthan T, Omar T. Energy and emission analysis of fly ash based geopolymers. In: Proceedings SSEE int conf – solutions for a sustainable planet, Melbourne. Society for Sustainability and Environmental Engineering; 2009. p. 1–11.

(5) Habert G, d'Espinose de Lacaillerie JB, Lanta E, Roussel N. Environmental evaluation for cement substitution with geopolymers. In: Proceedings 2nd int conf sustainable construction materials and technologies, Ancona, Italy; 2010.p. 1–9.

(6) Habert G, d'Espinose de Lacaillerie JB, Roussel N. An environmental evaluation of geopolymer based concrete production: reviewing current research trends. J Clean Prod 2011;19:1229–38.

(7) McLellan BC, Williams RP, Lay J, van Riessen A, Corder GD. Costs and carbon emissions for geopolymer pastes in comparison to ordinary portland cement. J Clean Prod 2011;19:1080–90.

(8) Bahri S, Mahmud H B. Rice Husk Ash–An Alternative Material to Silica Fume For Production Of 100 MPa Mortar [J]. Electronic Journal of Structural Engineering, 2013, 13(1): 31-35.

(9) F. Collins, Inclusion of carbonation during the life cycle of built and recycled concrete: influence on their carbon footprint, Int. J. Life Cycle Assess. 15 (2010) 549–556.

(10) Gao X, Yu Q L, Lazaro A, et al. Investigation on a green olivine nano-silica source based activator in alkali activated slag-fly ash blends: Reaction kinetics, gel structure and carbon footprint [J]. Cement and Concrete Research, 2017, 100: 129-139.

(11) Turner L K, Collins F G. Carbon dioxide equivalent (CO2-e) emissions: A comparison between geopolymer and OPC cement concrete [J]. Construction and Building Materials, 2013, 43: 125-130.

(12) EU FP7 project ProMine: Nanoparticle products from new mineral resources in Europe (Grant agreement No. 228559).

7. Conclusion and further research outlook

7.1 Conclusion

Based on the results conducted in this study, the following conclusions can be inferred:

Chapter 3

(1) The optimum combination is achieved by 50 wt% Slag8000, NaOH concentration of 10 M and silica modulus M=2, the compressive strength reach up to 113.3 MPa. NaOH concentration (M/L) have the highest contribution to compressive strength.

(2) Crystallization occurred in Solutions of modulus 0.4−1.0. Therefore, when preparing the alkali activator, the solutions of modulus should be avoided within the range of 0.4−1.0.

(3) As the substitution rate of blast furnace slag increases, the workability of mortar increases first and then decreases. Specimen FA50BF50 showed the best workability. Even if each mortar was given 15 falling movements, each specimen increased only about 20 mm, which showed high viscosity.

(4) At 7 days, the compressive strength tended to increase as the substitution rate of ground granulated blast furnace slag increased. The 7 days compressive strength of the specimen BF100 was 86 MPa. At 28 days, the specimen FA25BF75 showed the highest strength instead of the specimen BF100, and its compressive strength reached up to 104 MPa.

(5) The total pore volume tended to decrease as the substitution rate of ground granulated blast furnace slag increased. Compared with 7 days, the total pore volume of all the specimens decrease at 28 days. The compressive strengths of the specimens FA100 and FA75BF25 increased by about 483% and 90% from 7 days, respectively. Consistent with that, the shift from the large pore diameter to the smaller pore diameter is considered to have led to a significant increase in the compressive strength.

(6) Unlike cement mortar, the compressive strength of high alkali activated zero-cement mortar

showed a low correlation with the pore volume of more than 50 nm, and it was considered that it was related to the reaction products of high alkali activated zero-cement.

(7) Hardened paste of high alkali activated zero-cement is mainly composed of the amorphous phase indicated by a halo peak of 18 to 35°(2θ) and unreacted crystal phase.

(8) Specimen FA75BF25 and FA50BF50 had the highest gel content, but not the highest strength. The compressive strength of zero-cement is not simply determined by the gel content, the type of gel also has a huge effect on the strength.

(9) The strength and strength index have a high correlation (R^2=0.9533), so it is effective to use the strength index to evaluate the compressive strength of the zero-cement.

Chapter 4

(1) The longer the curing age, the higher the compressive strength. The specimens 1-2 (SF: FA: BF = 1.5: 2.5: 6) are optimal. The compressive strength at 3 days increased to 35 MPa and the compressive strength at 28 days increased to 95 MPa.

(2) At 20℃ curing, the more low alkali activator content, the greater the compressive strength. The maximum strength at 7 days is 70.2 MPa, and the maximum strength at 28 days is 79.8 MPa. At 90℃ heat curing, as the amount of low-alkali activator increases, the compressive strength increases first and then decreases. When the amount of low-alkali activator is 80kg/m^3, the maximum compressive strength in 7 days reaching up to 136 MPa.

(3) The higher the content of RCaO and RAl_2O_3, the greater the 7days compressive strength. The higher the RCaO content, the greater the 28days and 140days compressive strength.

(4) The change of Young's modulus is consistent with the change of compressive strength. The larger the Young's coefficient, the higher the compressive strength.

(5) Compressive strength has a correlation with saturated water content. The lower the saturated water content, the greater the compressive strength.

(6) The XRD analysis shows that the main reaction product of low alkali zero-cement is composed of a glass phase (gel) indicated by a halo peak of 18 to 35°(2θ) and a crystal phase of Hemicarbonate ($C_4Ac_{0.5}H_{12}$), Straetlingite (C_2ASH_8) and Portlandite ($Ca(OH)_2$). As the content of RCaO increases, the amount of Straetlingite produced gradually decreases. Regardless of the $RSiO_2/RAl_2O_3$ molar ratio, when the RCaO content is low, low-alkali activated zero-cement tends to form Straetlingite.

(7) When $RSiO_2/RAl_2O_3$ is consistent, the compressive strength and strength index have a very high liner correlation (R^2 is 0.9749, 0.9799 and 0.9894). It is possible to use the strength index to evaluate the compressive strength. At the same strength index, The smaller the $RSiO_2/RAl_2O_3$ ratio, the greater the compressive strength, indicating that the generated CASH gel with lower $RSiO_2/RAl_2O_3$ ratio contributes more to the strength. The compressive strength can be predicted by the dehydration amount at 105 to 300°C and the percentage of saturated water content.

(8) The bigger the binder/water ratio, the greater the compressive strength, and it showed an approximate linear function correlation. The strength is determined by the combined effect of the degree of pozzolanic reaction and the distance between the particles.

(9) The finer the particle size of BF, the higher the compressive strength of the mortar at early age. Higher fineness BF and higher specific surface area can increase the speed of pozzolanic reaction. However, the compressive strength of some BF4000 samples even exceed BF8000 samples at later age. The difference in compressive strength between the type Ⅱ SR group and the typeⅢ SR group is very small, while the type Ⅰ SR group with the largest specific surface area has the highest compressive strength.

(10) Regardless of W/B=45% or W/G=45%, when the amount of SR or FA used is small, the compressive strength of the SR group and the FA group is very close. However, when the

content of SR or FA increase, the compressive strength of the FA group is smaller than that of the SR group, especially in the early age. In the later age, the gap between the compressive strength of the FA group and the SR group gradually decreased.

Chapter 5

(1) Compared to the ACI model, the zero cement model can predict the compressive strength of zero-cement mortar more accurately. For zero cement, a value and b value have a high linear correlation.

(2) a value is dependent on the zero-cement's RCaO, RAl_2O_3 and $RSiO_2$ content. It can approximately represent the reaction rate of zero-cement binder. The larger a value, the slower the reaction rate.

(3) The value of a have the highest correlation with S/(C+A) molar ratio. With the increase of S/(C+A) molar ratio, a value also increases. Therefore, as long as the percentage of RCaO, $RSiO_2$ and RAl_2O_3 contained in zero-cement is determined, the strength development of zero-cement mortar can be predicted.

(4) This prediction model can expresses a value, in the form of a function of age, glass content/water ratio. It is considered useful as an estimation equation for strength development of zero-cement mortar.

(5) When different types or different particle sizes of raw material are used, a and b always satisfy the linear correlation.

(6) It is also possible to predict the strength development of zero-cement simply by C/(S+A) molar ratio. Regardless of high-alkali activation or low-alkali activation, the relative compressive strength of 7 days and 28 days has a high correlation with C/(S+A). From the overall trend, the greater the C/(S+A), the higher the relative compressive strength. When the molar ratio exceeds 0.9, the increase in relative compressive strength gradually stabilizes.

Chapter 6

This chapter confirmed the CO_2 emissions based on 1 m^3 of mortar mix. The CO_2 emissions generated by ultra-high strength mortar comprising zero-cement binders and OPC based binder were compared. The CO_2 emissions of $1m^3$ low alkali activated zero-cement mortar was approximately 57.4% less than $1m^3$ OPC based mortar.

For high alkali activated zero-cement mortar, the CO_2 emissions value is highly related to the proportions of Sodium silicate and Sodium hydroxide used in the mix proportion, which can be largely varied. Compared with $1m^3$ cement based mortar, the CO_2 emissions of $1m^3$ high alkali activated zero-cement mortar increased by 6.2% and decreased by 17% and 6.8%, respectively.

7.2 Further research outlook

The present work studied essential factors which have considerable effect on the compressive strength of zero-cement. At the same time, the mechanism of ultra-high-strength zero-cement mortar was also studied. Besides, a design method for ultra-high strength zero-cement mortar was proposed as well. But there are still many problems to be further studied as below:

(1) Effect of dissolution speed of raw materials:

The dissolution speed of the active constituent in the raw materials has a crucial influence on the development of strength. The nature of the raw materials is different, and dissolution speed of the RCaO, RAl_2O_3 and $RSiO_2$ contained in them are different, which may lead to changes a value and b value, and affect the strength development of zero-cement. It is crucial to study what determines the dissolution speed of raw materials, and establish the function relationship between dissolution speed, a value and b value.

(2) Effects of the type of gel produced on the strength contribution rate;

The compressive strength of zero-cement is not simply determined by the gel content. The type

of gel also has a huge effect on the strength. Study of the contribution rate of CASH gel with different Ca/Si ratio and different Si/Al ratio to compressive strength is crucial.

(3) Strength diagram of quaternary components considering the influence of Na:

It is necessary to systematically study the effect of Na amount on compressive strength. When the amount of Na used is 5%, 10%, 15% and 20%, in the $RCaO\text{-}RAl_2O_3\text{-}RSiO_2$ ternary diagram, how will the compressive strength of zero-cement change? How will the reaction products change? How will the pore structure change?

(4) Influence of trace elements:

In addition to the above influencing factors, the presence of trace elements such as Mg, K, Fe, Cu and C also has a considerable effect on strength. Some trace elements play a positive role in the development of strength, while other trace elements will lead to a decrease in strength. The influence of trace elements on strength needs further study.

Acknowledgement

Lu Xun, a famous Chinese writer, wrote an article commemorating his teacher, "Fujino-sensei." The image of Fujino-sensei made me naturally think of Professor Noguchi immediately. Professor Noguchi is a teacher with profound knowledge, rigorous scientific research attitude, and noble personality charm. As a scientific researcher, he often teaches us to do "Shuhari" [守 •破 •離] in scientific research. I have always borne this motto in mind. During the three years of the Ph.D., Professor Noguchi often took time out of his busy schedule to discuss the problems I encountered in scientific research, patiently answered my doubts, and helped me find my own shortcomings in time. At the same time, Professor Noguchi has devoted a lot of effort to the conception, modification and finalization of my thesis, and has put forward many valuable opinions to benefit me for life. Here, I would like to pay high respect and heartfelt thanks to Professor Noguchi.

"Sensei's virtue, high as mountains and long as rivers" [先生の徳.山高く水長く], which is most vividly reflected in Professor Noguchi. Among the teachers I know, Professor Noguchi is the one I am most grateful for and most respectful of. I hope that in the future I will become someone like Professor Noguchi.

Professor Maruyama put forward many valuable opinions in the revision of my thesis, which has benefited me a lot. His rigorous attitude towards scientific research will inspire me all my life. Here, I would like to extend my heartfelt thanks to Professor Maruyama.

In the research process of this topic, I also have received the selfless help from Kitagaki-sensei, Tomoyose-sensei, Tamura-san, Kanematsu-sensei and Matsuda-san. Here, I would like to express my most sincere gratitude to them.

Thanks to Wang Dianchao, Sun Bochao, Chen Qingkai, Xu Zheng, Wang Wei, Zhou Biao, Xu Liuyun, Cheng Luge, Mu Ang, Kong Yanhui, Yan Yajie, Ren Yuqi, Sawa-san, Ishita-san, Nakata-san, Kusumoto-san and others for their help. What I have experienced study and life in Japan will always be incomparably precious in my entire life. Thanks to classmates and friends who grew up with me.

Thank my family for their silent contribution. It is precisely because of their care, support, and encouragement that I have my current achievements.

Finally, thank for the valuable comments from reviewing teachers. This is an opportunity for me to further improve my level of scientific research and make my thesis more perfectible.

July 1, 2020

Liao Gaoyu